(12)

WT-1639(EX)
EXTRACTED VERSION

OPERATION HARDTACK—PROJECT 6.5

Radar Determination of Fireball Phenomena

E. Baker
T. Viars
W. S. McAfee
I. A. Balton
U.S. Army Signal Research and Development Laboratory
Fort Monmouth, NJ

AD-A995 347

DTIC
ELECTE
FEB 0 6 1986
S D
D

16 May 1960

NOTICE:
This is an extract of WT-1639, Operation HARDTACK, Project 6.5.

Approved for public release;
distribution is unlimited.

DTIC FILE COPY

Extracted version prepared for
Director
DEFENSE NUCLEAR AGENCY
Washington, DC 20305-1000

1 September 1985

DISCLAIMER NOTICE

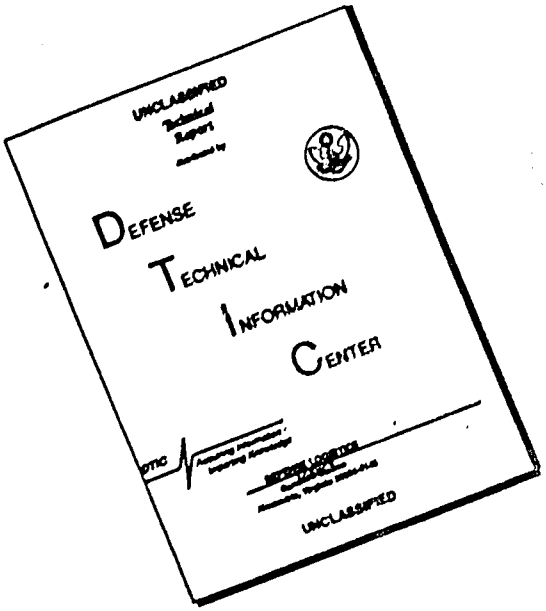

THIS DOCUMENT IS BEST QUALITY AVAILABLE. THE COPY FURNISHED TO DTIC CONTAINED A SIGNIFICANT NUMBER OF PAGES WHICH DO NOT REPRODUCE LEGIBLY.

UNCLASSIFIED

SECURITY CLASSIFICATION OF THIS PAGE

AD-A195 347

REPORT DOCUMENTATION PAGE

1a. REPORT SECURITY CLASSIFICATION UNCLASSIFIED	1b. RESTRICTIVE MARKINGS
2a. SECURITY CLASSIFICATION AUTHORITY N/A since Unclassified	3. DISTRIBUTION/AVAILABILITY OF REPORT Approved for public release; distribution is unlimited.
2b. DECLASSIFICATION/DOWNGRADING SCHEDULE N/A since Unclassified	
4. PERFORMING ORGANIZATION REPORT NUMBER(S)	5. MONITORING ORGANIZATION REPORT NUMBER(S) WT-1639 (EX)
6a. NAME OF PERFORMING ORGANIZATION U.S. Army Signal Research and Development Laboratory 6b. OFFICE SYMBOL (If applicable)	7a. NAME OF MONITORING ORGANIZATION Defense Atomic Support Agency
6c. ADDRESS (City, State, and ZIP Code) Fort Monmouth, NJ	7b. ADDRESS (City, State, and ZIP Code) Washington, DC
8a. NAME OF FUNDING/SPONSORING ORGANIZATION 8b. OFFICE SYMBOL (If applicable)	9. PROCUREMENT INSTRUMENT IDENTIFICATION NUMBER
8c. ADDRESS (City, State, and ZIP Code)	10. SOURCE OF FUNDING NUMBERS PROGRAM ELEMENT NO. / PROJECT NO. / TASK NO. / WORK UNIT ACCESSION NO.

11. TITLE (Include Security Classification) OPERATION HARDTACK—PROJECT 6.5, Radar Determination of Fireball Phenomena, Extracted Version

12. PERSONAL AUTHOR(S)
Baker, E.; Viars, T.; McAfee, W.S.; and Balton, I.A.

13a. TYPE OF REPORT	13b. TIME COVERED FROM ____ TO ____	14. DATE OF REPORT (Year, Month, Day)	15. PAGE COUNT
		600516	70

16. SUPPLEMENTARY NOTATION This report has had sensitive military information removed in order to provide an unclassified version for unlimited distribution. The work was performed by the Defense Nuclear Agency in support of the DoD Nuclear Test Personnel Review Program.

17. COSATI CODES			18. SUBJECT TERMS (Continue on reverse if necessary and identify by block number)			
FIELD	GROUP	SUB-GROUP	Hardtack	Cactus Shot	Butternut Shot	Teak Shot
18	3		Nuclear Fireball	Fir Shot	Wahoo Shot	
17	9		Radar	Koa Shot	Holly Shot	

19. ABSTRACT (Continue on reverse if necessary and identify by block number)

The objectives of this project were to investigate the nature of radar echoes from the fireball produced by atomic detonations, and to determine the feasibility of finding ground zero, height-of-burst, and yield by means of radar echoes.

It was concluded that no radar echoes were received from the fireballs of any Hardtack detonations. For surface shots, radar techniques can be used to determine ground zero to an accuracy of ± 140 feet. The proportionality between maximum target size and yield of the device indicated that maximum size might be used as a rough measure of yield.

20. DISTRIBUTION/AVAILABILITY OF ABSTRACT ☒ UNCLASSIFIED/UNLIMITED ☐ SAME AS RPT ☐ DTIC USERS	21. ABSTRACT SECURITY CLASSIFICATION UNCLASSIFIED
22a. NAME OF RESPONSIBLE INDIVIDUAL MARK D. FLOHR	22b. TELEPHONE (Include Area Code) (202) 325-7559 22c. OFFICE SYMBOL DNA/ISCM

DD FORM 1473, 84 MAR — 83 APR edition may be used until exhausted. All other editions are obsolete.

SECURITY CLASSIFICATION OF THIS PAGE

UNCLASSIFIED

FOREWORD

Classified material has been removed in order to make the information available on an unclassified, open publication basis, to any interested parties. The effort to declassify this report has been accomplished specifically to support the Department of Defense Nuclear Test Personnel Review (NTPR) Program. The objective is to facilitate studies of the low levels of radiation received by some individuals during the atmospheric nuclear test program by making as much information as possible available to all interested parties.

The material which has been deleted is either currently classified as Restricted Data or Formerly Restricted Data under the provisions of the Atomic Energy Act of 1954 (as amended), or is National Security Information, or has been determined to be critical military information which could reveal system or equipment vulnerabilities and is, therefore, not appropriate for open publication.

The Defense Nuclear Agency (DNA) believes that though all classified material has been deleted, the report accurately portrays the contents of the original. DNA also believes that the deleted material is of little or no significance to studies into the amounts, or types, of radiation received by any individuals during the atmospheric nuclear test program.

Accesion For
NTIS CRA&I ☑
DTIC TAB ☐
Unannounced ☐
Justification
By
Distribution /
Availability Codes
Dist | Avail and/or Special
A-1

UNANNOUNCED

QUALITY INSPECTED

OPERATION HARDTACK—PROJECT 6.5

RADAR DETERMINATION of FIREBALL PHENOMENA

E. Baker, Project Officer
T. Viars, Project Officer
W.S. McAfee
I.A. Balton

U.S. Army Signal Research and
Development Laboratory
Fort Monmouth, New Jersey

FOREWORD

This report presents the final results of one of the projects participating in the military-effect programs of Operation Hardtack. Overall information about this and the other military-effect projects can be obtained from ITR-1660, the "Summary Report of the Commander, Task Unit 3." This technical summary includes: (1) tables listing each detonation with its yield, type, environment, meteorological conditions, etc.; (2) maps showing shot locations; (3) discussion of results by programs; (4) summaries of objectives, procedures, results, etc., for all projects; and (5) a listing of project reports for the military-effect programs.

ABSTRACT

The objectives of this project were to investigate the nature of radar echoes from the fireball produced by atomic detonations, and to determine the feasibility of finding ground zero, height of burst, and yield by means of radar echoes.

The operations of this project were conducted on Eniwetok and Rongelap Atolls for the Eniwetok tests, using Radar Sets AN/MPG-1 and SCR-584 (9,000 and 2,800 Mc, respectively), and on U.S. Navy destroyers for the Johnston Island tests using Radar Set SRb (200 Mc). Photos were taken of the radarscope presentations.

Data was obtained for Shots Cactus, Fir, Butternut, Koa, Wahoo, Holly, and Teak. Data analysis was performed on a magnifying viewer with movable crosshairs accurate to 0.001 inch. Actual photos of the physical event were studied side by side with the time-equivalent scope photos. This report presents representative photos for each of the shots that yielded data.

The B- and PPI-scope displays established identifying characteristics of a nuclear detonation according to four discrete time intervals: (1) the sporadic occurrence of a bright-point return; (2) a 2-second delay for S- and X-band radar returns (surface shots), and a 1-minute delay for VHF radar returns (Shot Teak); (3) maximum growth of the symmetrical scope pattern occurred at 7 to 15 seconds after time zero; and (4) the nondescript pattern associated with the decay stage remained on the radar screen from 1 to 8 minutes. The data correlated with that from previous tests on a number of points.

Analysis of the data indicated that radar returns were not received from the fireball. However, the data indicates that ground zero for surface shots can be determined to an accuracy of ± 140 feet. The proportionate growth of maximum dimensions for a burst indicated that maximum size might be used as a rough measure of yield. The results seem to point out that accurate height information cannot be obtained with the techniques used by this project.

PREFACE

The project officers of Project 6.5, Operation Hardtack, wish to express their appreciation to the officers and men of the USS Cogswell and De Haven for their splendid cooperation and assistance in making the shipboard radar sets SRb available to the project. The efforts of these Navy personnel were greatly instrumental in making the project a success.

CONTENTS

FOREWORD ---------- 4

ABSTRACT ---------- 5

PREFACE ---------- 6

CHAPTER 1 INTRODUCTION ---------- 11

1.1 Objectives ---------- 11
1.2 Background ---------- 11
1.3 Theory ---------- 12
1.3.1 General ---------- 12
1.3.2 Ultra High-Altitude Explosion ---------- 13
1.3.3 Sea-Level Shots ---------- 14

CHAPTER 2 PROCEDURE ---------- 16

2.1. Operations ---------- 16
2.1.1 Stations ---------- 16
2.1.2 Shot Participation ---------- 16
2.2 Instrumentation ---------- 16
2.2.1 Radar Set AN/MPG-1 ---------- 16
2.2.2 Flight Research Recording Camera, Model 4C ---------- 16
2.2.3 Radar Set SCR-584 ---------- 18
2.2.4 Automax Recording Camera, Model GIR ---------- 18
2.2.5 High-Speed Oscilloscope Recording Camera ---------- 19
2.2.6 Modified A Scope ---------- 19
2.2.7 General Radio Strip Camera ---------- 19
2.2.8 Radar Set SRb ---------- 19
2.2.9 Pulse-Stretcher Adapter ---------- 19
2.2.10 Magnetic-Tape Recorder ---------- 20
2.3 Data Requirements ---------- 20
2.4 Methods of Recording Data ---------- 20
2.4.1 A Scope, SCR-584 ---------- 20
2.4.2 PPI Scope, SCR-584 ---------- 21
2.4.3 B Scope, AN/MPG-1 ---------- 21
2.4.4 A Scope, SRb ---------- 21
2.5 Data Reduction ---------- 21
2.5.1 Film Data ---------- 21
2.5.2 Magnetic-Tape Data ---------- 21
2.6 Requirements from Other Projects ---------- 21

CHAPTER 3 RESULTS AND DISCUSSION ---------- 22

3.1 Shot Yucca ---------- 22
3.2 Shot Cactus ---------- 22
3.2.1 Radar Set AN/MPG-1 ---------- 22
3.2.2 Radar Set SCR-584 ---------- 23
3.3 Shot Fir ---------- 23

3.3.1 Radar Set SCR-584, PPI Scope, Rongelap ---------- 23
3.3.2 Radar Set SCR-584, A Scope, Rongelap ---------- 23
3.3.3 Radar Set SCR-584, PPI Scope, Eniwetok ---------- 28
3.3.4 Radar Set SCR-584, A Scope, Eniwetok ---------- 28
3.3.5 Radar Set AN/MPG-1, Eniwetok ---------- 32
3.4 Shot Butternut ---------- 32
3.4.1 Radar Set AN/MPG-1, Eniwetok ---------- 32
3.4.2 Radar Set SCR-584, PPI Scope, Eniwetok ---------- 32
3.5 Shot Koa ---------- 37
3.5.1 Radar Set SCR-584, A Scope, Eniwetok ---------- 37
3.5.2 Radar Set SCR-584, PPI, Eniwetok ---------- 40
3.5.3 Radar Set AN/MPG-1 ---------- 45
3.6 Shot Wahoo ---------- 46
3.6.1 Radar Set AN/MPG-1, B Scope ---------- 46
3.6.2 Radar Set SCR-584, A Scope ---------- 46
3.7 Shot Holly ---------- 46
3.7.1 Radar Set SCR-584, PPI, Eniwetok ---------- 46
3.7.2 Radar Set SCR-584, A Scope ---------- 46
3.7.3 AN/MPG-1, Local B Scope ---------- 54
3.8 Shot Teak ---------- 54
3.9 Discussion of Results ---------- 61
3.9.1 Interpretation of the Data ---------- 61
3.9.2 Reliability of the Data ---------- 62
3.9.3 Correlations With Data From Previous Tests ---------- 63
3.9.4 Estimate of Satisfaction of the Objectives ---------- 63
3.9.5 Effectiveness of the Instrumentation ---------- 64

CHAPTER 4 CONCLUSIONS AND RECOMMENDATIONS ---------- 65
4.1 Conclusions ---------- 65
4.2 Recommendations ---------- 65
4.2.1 Surface Shots ---------- 65
4.2.2 High-Altitude Shots ---------- 66

REFERENCES ---------- 67

APPENDIX MINIMUM DETECTABLE TARGET AREA ---------- 69

FIGURES

2.1 Van-installed radar sets AN/MPG-1 on left and SCR-584 on right ---------- 17
2.2 Shipboard radar set SRb ---------- 17
3.1 Shot Cactus, AN/MPG-1 B-scope returns, Fred radar site ---------- 24
3.2 Shot Cactus, AN/MPG-1 B-scope returns, Fred radar site ---------- 25
3.3 Shot Cactus, AN/MPG-1 B-scope returns, Fred radar site ---------- 26
3.4 Shot Cactus, AN/MPG-1 B-scope returns, Fred radar site ---------- 27
3.5 Graph of returns from Shot Cactus, B scope ---------- 28
3.6 Shot Fir, SCR-584 PPI-scope returns, Rongelap radar site ---------- 29
3.7 Shot Fir, SCR-584 A-scope returns, Rongelap Site ---------- 30
3.8 Shot Fir, SCR-584 PPI-scope returns, Fred radar site ---------- 31
3.9 Shot Butternut, AN/MPG-1 B-scope returns, Fred radar site ---------- 33
3.10 Shot Butternut, AN/MPG-1 B-scope returns, Fred radar site ---------- 34
3.11 Shot Butternut, AN/MPG-1 B-scope returns, Fred radar site ---------- 35
3.12 Shot Butternut, AN/MPG-1 B-scope returns, Fred radar site ---------- 36

3.13 Graph of returns from Shot Butternut, B scope ---------- 37
3.14 Shot Butternut, SCR-584, PPI-scope returns, Fred radar site ---------- 38
3.15 Shot Butternut, SCR-584, PPI-scope returns, Fred radar site ---------- 39
3.16 Shot Butternut, SCR-584, PPI-scope returns, Eniwetok Site ---------- 40
3.17 Shot Koa, SCR-584 A-scope returns, Eniwetok Site ---------- 41
3.18 Shot Koa, SCR-584, PPI-scope returns, Fred radar site ---------- 42
3.19 Shot Koa, SCR-584, PPI-scope returns, Fred radar site ---------- 43
3.20 Shot Koa, SCR-584, PPI-scope returns, Fred radar site ---------- 44
3.21 Shot Koa, SCR-584, PPI-scope returns, Fred radar site ---------- 45
3.22 Shot Wahoo, AN/MPG-1 B-scope returns, Fred radar site ---------- 47
3.23 Shot Wahoo, AN/MPG-1 B-scope returns, Fred radar site ---------- 48
3.24 Shot Wahoo, AN/MPG-1 B-scope returns, Fred radar site ---------- 49
3.25 Shot Wahoo, SCR-584 A-scope returns, Eniwetok Site ---------- 50
3.26 Shot Holly, SCR-584, PPI-scope returns, Fred radar site ---------- 51
3.27 Shot Holly, SCR-584, PPI-scope returns, Fred radar site ---------- 52
3.28 Shot Holly, SCR-584, PPI-scope returns, Eniwetok Site ---------- 53
3.29 Shot Holly, SCR-584 A-scope returns, Eniwetok Site ---------- 54
3.30 Shot Holly, AN/MPG-1 B-scope returns, Fred radar site ---------- 55
3.31 Shot Teak, SRb PPI-scope returns, USS Cogswell ---------- 56
3.32 Shot Teak, SRb PPI-scope returns, USS Cogswell ---------- 57
3.33 Shot Teak, SRb PPI-scope returns, USS Cogswell ---------- 58
3.34 Graphs of equal electron density in the upper atmosphere ---------- 59
3.35 Graphs of equal electron density in the upper atmosphere ---------- 60
3.36 Graphs of equal electron density in the upper atmosphere ---------- 60
3.37 Graph of maximum diameter of radar returns versus yield of device ---------- 62

TABLES

2.1 Shot Information ---------- 18
2.2 Characteristics of Radar Set AN/MPG-1 ---------- 18
2.3 Characteristics of Radar Set SCR-584 ---------- 19
2.4 Characteristics of Radar Set SRb ---------- 20
3.1 Table of Values for Graph of Fore and Back Radial Growth, Figure 3.5, Shot Cactus ---------- 23
3.2 Table of Values for Graph of Fore and Back Radial Growth, Figure 3.13 Shot Butternut ---------- 32
3.3 Chronological Development of Significant Returns ---------- 61
A.1 Characteristics of the Radars Used in Project 6.5 ---------- 69

Chapter I
INTRODUCTION

1.1 OBJECTIVES

The objectives of this project were to investigate the nature of radar echoes from the fireball produced by atomic detonations, and to determine the feasibility of finding ground zero, height of burst, and yield by means of radar echoes. In the case of high-altitude bursts, achievement of the second objective (which is the military objective) is dependent upon achievement of the first one. The primary reason for participating in the low-altitude series of shots was to ascertain whether the radar echoes could be sufficiently resolved to enable accurate determination of burst point and yield, and to determine, if possible, whether any component of the echoes could be attributed solely to the fireball.

1.2 BACKGROUND

Previous AFSWP projects, with the use of S-, Q-, and X-band air-borne equipment, have yielded many radar observations of phenomena produced by nuclear detonations (References 1 through 11). Air-borne radar reflections possessed characteristics such as horseshoe, annular, and cloud-shadow patterns, and the dimensions of the reflections were commensurate with those of the shock wave rather than of the fireball. The radarscope presentations displayed the coordinates of ground zero (slant range and azimuth), and in many cases also displayed a known landmark that aided greatly in determining ground zero. In general the participating projects had common objectives, namely, radar fireball observation and determination of yield and ground zero. However, these objectives were sought for varying purposes, such as bomb scoring, bomb efficiency, indirect bomb damage assessment, and development of data-gathering techniques. The published reports contain much data and many recommendations.

Although oscilloscope data obtained during previous tests show great uniformity, such presentations allowed only approximate measurements of ground zero for two reasons: (1) there was a 2-second delay in signal reception, and (2) the detonation grew rapidly within this 2-second interval. This growth placed ground zero hundreds of feet distant from the periphery of the shot configuration displayed as the radar target.

However, previous investigators did not have unanimity of opinion on the theory of the returns. Many of these authors, realizing that radar was being used in a new role for fast-time resolution of a short-lived event, introduced new techniques to be used in obtaining the data. The literature indicates that this new radar role is a growing field.

With reference to recommendations, authors contributed valuable suggestions that in large measure formed the bases and guidelines in employing radar as a diagnostic device in nuclear weapons phenomenology. Some of these recommendations were: the use of fast-scan radars for study of the burst area, the use of high-speed photography to obtain more frames of data per second, and the application of high-information content study to radarscope photography. Knowledge of this background assisted the personnel of Operation Hardtack 6.5 in achieving project objectives. Realization of these objectives would have a number of military implications. First, if radar can determine (from slant-height measurements) that the fireball touched or nearly

touched the ground, then approximate bomb-damage assessments can be made, and contamination in the area can be estimated. This estimate would establish the time-safety margin for troops entering the area. Second, if radar can detect the growth of the nuclear detonation, this information can be an approximate measure of yield for bomb-damage assessments. Third, if radar can detect ground zero of a burst, this technique can be employed in an observation post to evaluate the efficiency of bomb emplacements and pattern-laying of atomic warheads.

1.3 THEORY

1.3.1 General. Phenomena which accompany a nuclear explosion are strongly dependent on the yield and the altitude of detonation of the bomb. Although several such phenomena may affect the propagation of radio waves, the most important of these is the ionization of the atmosphere. Radio waves propagating through a region in which a nuclear explosion occurs may be unaffected or may experience varying combinations of absorption, refraction, and reflection. The results will depend on the density of ionization (mainly the number-density of electrons), and on the local temperature and particle density of the air. (The equation of state relates the pressure to the last two quantities.) Further, the result will depend on the frequency of the wave since ionized media are dispersive.

Other observable effects on radio waves may arise which are not related to the degree of local ionization. For example, particulate matter may be carried aloft or water droplets may condense to form scattering centers. The observability of these objects as radar targets will also show a frequency dependence. Results may also be observed which arise from mainly hydrodynamic effects as, for example, reflection of radio waves at the shock front or scatter of radio waves by turbulence in the region of the detonation.

The propagation of radio waves through an ionized medium may be described by the complex propagation constant

$$k = \frac{2\pi}{\lambda}(\alpha + i\beta) \tag{1.1}$$

In Equation 1.1, λ is the wave length of the radio waves and

$$\alpha = \left\{ \tfrac{1}{2}\left[\left(\epsilon^2 + \frac{\omega_p^4 \nu^2}{\omega^2(\omega^2+\nu^2)^2} \right)^{1/2} + \epsilon \right] \right\}^{1/2}$$

$$\beta = \left\{ \tfrac{1}{2}\left[\left(\epsilon^2 + \frac{\omega_p^4 \nu^2}{\omega^2(\omega^2+\nu^2)^2} \right)^{1/2} - \epsilon \right] \right\}^{1/2}$$

Where: $\omega_p^2 = 4\frac{\pi N e^2}{m}$

$\omega = 2\pi \times$ radio frequency

ν = collision frequency of electrons with heavy atoms or ions

$\epsilon = 1 - \frac{\omega_p^2}{\omega^2 + \nu^2}$

N = number of electrons/cm^3

e = the charge of the electron, esu

m = the mass of the electron, grams.

The phase velocity of the waves is given by

$$v = \frac{\omega\lambda}{2\pi\alpha} \tag{1.2}$$

which, through α, depends on the electron density. In principle one could obtain information concerning refraction by applying Fermat's Principle or its equivalent to rays traversing a medium for which the electron density has been determined as a function of position. Since measurement of refraction was not undertaken in the present program, no estimates of refraction have been made here.

The absorption index is given by

$$\kappa = \frac{2\pi\beta}{\lambda} \tag{1.3}$$

The amplitude attenuation in decibels is given by the expression

$$20 \log e^{-\int \kappa(s)\,ds}$$

where the integration is taken along the line-of-sight between two points. (For greater accuracy, the integral should be evaluated along a ray path, but the difference is trivial for the estimates made here.)

1.3.2 Ultra High-Altitude Explosion. A considerable amount of numerical work has been done to give estimates of the electron density as a function of position and time following the 3.8-Mt VHA and UHA detonations. The curves given in the Rand report (Reference 12) as Figures 13 through 16 have been employed to determine contours of equal electron density at particular instants after shot time. The distributions adopted herein correspond to the larger electron attachment cross section given in Reference 12. The contours are plotted for t = 1, 10, and 100 seconds, and are given as Figures 3.34 to 3.36 of this report. The collision frequencies have been calculated according to the work of Nicolet, although recent studies indicate that his values may be too high by a factor of 2 or 3 (Reference 12a).

Attenuation has been determined for a radio frequency of 2×10^8 cps, which represents the situation expected for Radar Set SRb following Shot Teak. For most of the range of interest

$$\omega \gg \nu$$

and (at least in the heavily attenuating regions)

$$\omega \gg \omega_p$$

Thus, to a fairly good approximation

$$\beta \approx \tfrac{1}{2} \frac{\omega_p^{\,2}\,\nu}{\omega^3}$$

and

$$\kappa = \frac{\omega}{c}\,\beta \approx \frac{1}{2c}\,\frac{\omega_p^{\,2}}{\omega^2}\,\nu$$

or

$$\kappa \approx 3.2 \times 10^{-15}\, N\nu \text{ km}^{-1} \tag{1.4}$$

The value of $\int \kappa(s)\,ds$ along the line-of-sight from the radar has been obtained essentially by taking small intervals in which the electron density may be assumed constant and equal to the value near the center of the interval. Where the intervals were large or charge density varied rapidly with height, closer interpolation of the Rand curves was made. The results are as follows:

(a) t + 1 sec
Total one-way attenuation to within 20 km of the point of detonation: 320 db

(b) t + 10 sec
As above: 195 db

(c) t + 100 sec
As above: 12 db

The lower collision frequencies (Reference 12a) would reduce these values by a factor of one-half or one-third. Also, although the values of N are not available near the point of detonation, it is clear that a charge density great enough to reflect the radio waves must exist for a considerable time after t + 0. For this, one must have $\omega \approx \omega_p$ or $2 \times 10^8 \approx 9 \times 10^3 \sqrt{N}$, which gives $N \approx 5 \times 10^8$ electrons/cm^3. Thus it seems reasonable that echoes from high-altitude detonations should not be received during the earliest times at a frequency of 200 Mc. However, after some seconds the heavily attenuating layer should be dissipated (by attachment and recombination) to such an extent that echoes become possible. Ultimately the density of the reflecting region must become too low, or, because of motion, be removed beyond effective radar range. (The Rand curves do not include the effect of motion.)

1.3.3 Sea-Level Shots. For explosions at low altitudes the released energy is trapped in a few meters of air, thus causing a rapid rise in temperature. At the earliest times (less than 10^{-4} sec) there is no need to distinguish between thermally induced ionization and ionization due to nuclear radiations, since the dissipation of the energy of nuclear radiation contributes to the initial rise of temperature. At these high temperatures (several hundred thousand degrees to perhaps a few million), ionization of all atomic levels of the atmospheric gases is practically complete. Heavy atoms of the bomb materials will have most of the outer electrons removed. During the early stages the temperature is essentially uniform throughout the spherical ball of fire. The spherical mass cools by expansion and by radiation as well as by loss of energy to the shock wave. The measured effective temperatures are determined by the (optically thick) surface layer from which the radiation arrives without further re-emission.

These high temperatures determine the ion densities and cause an increase in the electron collision frequency. One may employ the equilibrium equations for an assembly of atoms, ions, and electrons in order to determine the degree of ionization of the various constituents (Reference 12b). (Relaxation times are quite short here, so that equilibrium at each temperature is not a bad approximation.)

The numerical work required for such an assembly is considerable. A survey of the problem might be made by considering the situation where T ≈ 15 or 30 thousand degrees. For this range one may neglect multiple ionization and write

$$\frac{X_1^2}{1 - X_1} \approx \frac{0.664}{p} \quad T^{5/2} \, e^{-X_0/kT} \tag{1.5}$$

Where: X_1 = fractions of atoms ionized

p = total pressure, dynes/cm^2

X_0 = ionization potential of gas

and T = absolute temperature.

If $p \approx 250$ atmospheres[1] (this accounts approximately for the increase due to atoms from bomb material, dissociation of O_2 and N_2 into atoms, and the temperature contribution), and $X_0 \approx 14$ ev (for atomic oxygen and nitrogen), one gets

$$X_1 = 0.53$$

This clearly understimates the fraction of heavy atoms (bomb material) ionized. For example, iron has a first ionization potential of 7.83 volts, and its second ionization potential is only slightly greater than the value for X_0 used above. This procedure is admittedly crude. However, it does give an order-of-magnitude estimate of the electron density of some 10^{18} cm^{-3}. At the lower temperatures mentioned, the number may be as low as 10^{17} cm^{-3}.

[1] Actually the electron pressure is included in arriving at Equation 1.5. Using $p \approx 400$ atmospheres reduces X_1 to 0.46 which is not considered significant.

The values of β for electron densities of the order 10^{17} to 10^{19} with $T \approx 3 \times 10^4$, and $\omega = 2\pi \times 10^{10}$ sec^{-1} (i.e. radio frequency = 10 k Mc) fall within the range of 10 to 100. (The effect of the temperature on the collision frequency has been included.) This range of β values represents an absorption coefficient, κ, of 21 to 210 cm^{-1}. Thus, one should expect complete attenuation of radio waves by a fireball in an extremely short distance, even for such a high frequency, at temperatures of a few thousand degrees.

Unfortunately it is not possible on the basis of the above considerations to set a time scale for the attenuation. Once the temperature is too low to maintain ionization, recombination is extremely rapid and the attenuation becomes negligible even for the lowest frequencies. Residual nuclear radiations produce ionization several orders of magnitude less than that considered here and should have an inappreciable effect on centimeter waves.

Chapter 2
PROCEDURE

2.1 OPERATIONS

2.1.1 Stations. Stations used for this project were both shore- and ship-based. The shore-based stations were at Eniwetok and Rongelap Atolls. The ship-based stations were located aboard U.S. Navy destroyers located 75 and 150 miles from Johnston Island, on a bearing of 020 degrees (with respect to true north) from the island. Since Shot Teak was detonated almost directly above the launch site, Johnston Island is considered to be ground zero in this report. The shore-based stations were horizontally levelled to establish accurate antenna-elevation angles and surveyed so that range and azimuth readings could establish the geographical ground zero of the shots. Map measurements gave predicted range and azimuth values that formed a basis of comparison for actual values obtained. All stations were manned and placed in operation several hours before shot time to allow for equipment adjustments and warmup.

2.1.2 Shot Participation. Project 6.5 participated in Shots Yucca, Cactus, Fir, Butternut, Koa, Wahoo, Holly, and Teak (Table 2.1). The Rongelap station participated only in Shots Yucca and Fir; the destroyer stations participated only in Shot Teak.

2.2 INSTRUMENTATION

Radar Sets AN/MPG-1 and SCR-584, operated at 9,000 and 2,800 Mc, respectively, were used at the shore-based stations (Figure 2.1). The Eniwetok station used both radars, whereas the Rongelap station used only the SCR-584. Radar Sets SRb, operated at 205 and 220 Mc, were used for Shot Teak at the ship-based stations (Figure 2.2).

2.2.1. Radar Set AN/MPG-1. This set was a 3.3-cm, mobile, fire-control radar designed for use with seacoast artillery batteries. It had two modes of operation: the plan-position-indicator (PPI) mode and the B mode. To achieve best results, plans were made to use only B mode. Chief characteristics of the AN/MPG-1 are listed in Table 2.2, and additional information can be found in Reference 13.

On B operation, the antenna feed horn sprayed a focal line of radio-frequency (r-f) energy 16 times per second across the reflector. This process had the effect of an electrical scan, 10 degrees in azimuth. The horizontal sweep of the B scope was synchronized with the azimuthal sweep of the antenna and gave 16 looks per second (at any target).

The B scope showed 10 degrees of azimuth horizontally and 2,000 yards of range vertically. The horizontal grid lines of the scope represented 1,000-yard range separations, the middle horizontal line being preset by the range dials to represent a given range. The vertical grid lines were 1-degree azimuth markers, the middle vertical line being preset by the azimuth dials.

2.2.2 Flight Research Recording Camera, Model 4C. This camera was used to photograph the B-scope displays of the AN/MPG-1. The camera was synchronized to the horizontal sweep circuit of the B scope. This synchronization was achieved by using the (B scope) blanking pulse to trigger a relay circuit that closed the camera shutter and advanced the next film frame during scope-blanking time.

A flash bulb scored the film and designated time zero on the passing frame. A photographed clock, plus the accurate camera rate of 16 frames/sec, afforded a precise time reference for each film frame.

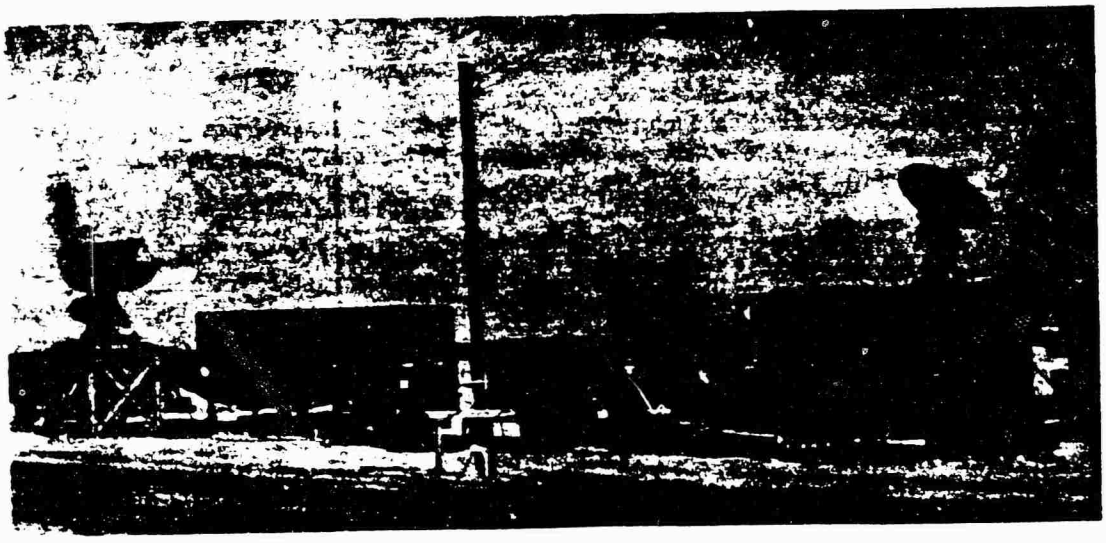

Figure 2.1 Van-installed radar sets AN/MPG-1 on left and SCR-584 on right, with their accompanying antennas. Power Unit PU-26 is in the center.

Figure 2.2 Shipboard radar set SRb, used aboard destroyers DeHaven and Cogswell.

2.2.3 Radar Set SCR-584. The SCR-584 was a 10-cm, mobile, fire-control radar set with a maximum range of 70,000 yards. This set had PPI- and J-scope displays. Plans were to photograph the PPI scope and a modified A scope. The chief characteristics of the SCR-584 are listed in Table 2.3, and additional information is available in Reference 14. The original design

TABLE 2.1 SHOT INFORMATION

Shot	Date	Map Range	Radar Range	Azimuth	Angle of Evaluation	Estimated Yield
		yd	yd	deg	deg	kt
Yucca	28 April 1958	176,176	—	32	9.15	
Cactus	6 May 1958	24,833	24,782	4	0	16.7
Fir	12 May 1958	402,340 *	399,740 *	84.5 *	0	
		231,120 †	232,000 †	58 †	0	
Butternut	12 May 1958	23,333	23,250	4	0	
Koa	13 May 1958	42,233	42,220	339	0	1,370
Wahoo	16 May 1958	19,750	19,743	267	0	
Holly	21 May 1958	23,070	23,105	5.5	0	
Teak	31 July 1958	320,000	374,000	198	18.5	

* From Eniwetok.
† From Rongelap.

of the set provided only manual sector scanning. Attempts were made to secure automatic sector scan kits MC-645, but these efforts were unsuccessful. Accordingly, plans were made to use a 3- to 4-second manual scan, whose azimuthal width could be divided into fractions of a second for time-resolution studies.

2.2.4 Automax Recording Camera, Model GIR. This camera was used to photograph the luminous traces of the SCR-584 PPI scope at Eniwetok. The camera was operated manually and

TABLE 2.2 CHARACTERISTICS OF RADAR SET AN/MPG-1

Frequency	9,090 Mc
Power output	35 kw (peak), 35 w (average)
Pulse repetition frequency	4,097 pulses/sec
Pulse width	0.25 μsec
Beam width	0.6 degree horizontal, 3 degrees vertical (at half power points)
Scan rate	16 per second
Transmitter RF oscillator	Magnetron
Receiver bandwidth	10 Mc
Power	60 cps, 3 phase, 115 volts
Tower	Antenna support, about 10 feet high, constructed on site to support pedestal and antenna

photographed each clockwise and counterclockwise sweep in unison with the antenna scan rate. A time-zero marker and an illuminated clock were photographed for time reference. The same type of camera was used at the Rongelap site to photograph the PPI scope. This camera was operated at a speed of 16 frames/sec to show instantaneous range sweep lines as the antenna was gently rocked to either side of the acquired target. A time-zero marker and the constant speed of the camera afforded a basis for time resolution of the documentary film.

2.2.5 High-Speed Oscilloscope Recording Camera. This was a Dumont-321 strip-type camera with a film capacity of 400 feet of 35-mm film and a film speed of 30 in/sec. This camera was used to photograph the modified A scope of the SCR-584 at the Eniwetok site. The film recordings obtained for the A scope gave an integrated effect to amplitude variations as the radar beam swept across the target. Time markers of $^1/_{120}$th of a second scored the film for the purpose of time resolution.

2.2.6 Modified A Scope. The video output of the SCR-584 was applied to the vertical deflection plates of Tetronix Oscillograph Models 511 and 513. The former was used at Eniwetok and the latter at Rongelap. No oscilloscope sweep was employed but a pseudo-sweep was scored on the fast-running film as it continuously photographed the focused electron beam at the center of the scope. Any target return would cause a vertical elongation of the central dot in proportion to the strength of the signal. Such a display scored the film in either of two ways: a dual line or a solid wide line, depending upon the gain-control settings or the strength of the return. Instantaneous variations of signal amplitude, indicative of target size and yield, could be recorded by

TABLE 2.3 CHARACTERISTICS OF RADAR SET SCR-584

Frequency	2,700 to 2,900 Mc
Power output	210 kw (peak), 200 w (average)
Pulse repetition frequency	1,707 pulses/sec
Pulse width	0.8 μsec
Beam width	4 degrees at half power points
Transmitter RF oscillator	Magnetron
Receiver bandwidth	2 Mc
Antenna	Paraboloidal, stored within trailer, and elevated when operating
Power	60 cps, 3 phase, 115 volts

such an arrangement. To assure reception of only target echoes, the main bang of the radar set was cancelled by a blanking pulse applied to the A scope.

2.2.7 General Radio Strip Camera. This camera was used at the Rongelap site to record the amplitude variations appearing on the above-mentioned oscillographs. The film was driven at a speed of 30 in/sec. The camera had a film capacity of 1,000 feet of 35-mm film. Time markers of $^1/_{120}$th of a second scored the film.

2.2.8 Radar Set SRb. The SRb equipment, designed for ship installation, functioned as a searching, ranging, and direction-finding device. As employed by Project 6.5, this set was operated as a ranging and direction-finding device. Two types of target information were obtained by the PPI- and A-scope presentations. The set had the advantageous features of a wide vertical beam and low frequency. The former feature offset the rolling of the ship and the accompanying danger of losing an acquired target; the latter feature extended the spectrum of radar observation of the burst to the lower-frequency region. The chief characteristics of the SRb are listed in Table 2.4, and additional information is available in Reference 15.

2.2.9 Pulse-Stretcher Adapter. This unit was designed to pulse-modify the radar's 4-μsec video output for magnetic-tape recording. The equipment had a fast charge time and a slow discharge time that stretched the trailing edge of the 4-μsec pulse. This effect afforded adequate response for the magnetic-tape recorder and aided in differentiating the main bang from the target echo. Near-range sea-clutter would be seen riding the modified trailing edge of the main bang, whereas absence of clutter from the trailing edge of the target echo, together with its smaller amplitude, would identify the latter.

2.2.10 Magnetic-Tape Recorder. The A-scope input of the SRb radar set was fed to the Ampex Recorder Model 600, in series with the pulse stretcher. The recorder had a tape speed of 7.5 in/sec, a 40-cps to 15-kc frequency response, and separate record and playback amplifiers with level controls.

2.3 DATA REQUIREMENTS

Assuming sufficient radar power output, and a target that is within radar range, radar returns are dependent upon the electromagnetic properties of the target. Hence, if radar returns were to be obtained from the fireball, they would have to reveal in some measure the electromagnetic

TABLE 2.4 CHARACTERISTICS OF RADAR SET SRb

Frequency	175 to 225 Mc
Pulse repetition frequency	120 cps
Pulse width	4 μsec
Power output	200 kw (peak), 100 w (average)
Antenna	Stacked colinear arry, 12 half-wave dipoles. Computed beam-width: 47 degrees elevation, 35 degrees azimuth. (A given SRb antenna is designed to operate in the low, medium or high portion of the frequency range covered by the radar. Coverage of the entire frequency range by one antenna is not possible.)
Height of antenna above waterline	78 feet (USS DeHaven) 90 feet (USS Cogswell)
Frequency control	Push-pull triode oscillator, tuned-plate, tuned-cathode, ringing type. (This is also the RF output stage.)
PPI-scope diameter (repeater)	12 inches
PPI-scope phosphor type	P-7
Receiver noise figure	8 db
Minimum detectable signal	5×10^{-14} watts

properties of the target. In almost every instance of AFSWP's radar investigations of the fireball, no radar returns were received within the first second or two except the bright-point return, which occurred at H + 0.2 seconds. Accordingly, Project 6.5 anticipated bright-point returns and the time of the earliest return. This information placed the requirement of a high time rate of recording data. The actual method of recording data was limited, by the nature of radar outputs, to scope photography, oscillograph tracings, and magnetic-tape recordings, but the time rate of data recording could be increased. This time-rate requirement suggested the use of high-speed cameras, time markers of the order of $^1/_{120}$th of a second, synchronization between scope sweeps and cameras, where possible, and high scan rates of the antenna system, such as in the AN/MPG-1.

Another requirement was that the radar should have the capability of obtaining high resolution of the parameters of range and azimuth that might be indicative of fireball growth and dimensions. The B scope of the AN/MPG-1 was chosen as capable of exhibiting these properties to a greater degree than the PPI scope of the SCR-584.

2.4 METHODS OF RECORDING DATA

2.4.1 A Scope, SCR-584. For A-scope displays, high-speed motion-picture cameras were used in an attempt to resolve individual pulse returns. The documentary films afforded a study of amplitude variations in relation to yield.

2.4.2 PPI Scope, SCR-584. The PPI-scope presentations of the SCR-584 at Eniwetok were photographed at the end of each clockwise and counterclockwise sector scan. Such a scan and its photograph allowed a study to be made of the range and azimuth growth of nuclear detonations at close range. The PPI-scope presentations of the SCR-584 at Rongelap were photographed at a relatively high speed, 16 frames/sec, to ascertain whether nuclear detonations at greater ranges could be acquired as radar targets.

2.4.3 B Scope, AN/MPG-1. The B-scope displays of the AN/MPG-1 were photographed 16 times per second in synchronism with the scope sweep. The data film displayed high resolution in range and azimuth. The film was then used to study the nature of the radar returns.

2.4.4 A Scope, SRb. The data of the A scope of the ship-based SRb was recorded on a magnetic tape. An attempt was made to ascertain whether very high-altitude detonations could be detected by radar techniques, and to resolve each pulse return for a study of amplitude growth as a measure of yield.

2.5 DATA REDUCTION

2.5.1 Film Data. Documentary films were analyzed on a magnifying viewer with measuring devices accurate to $^1/_{1000}$ inch. A frame-by-frame study was made for target characteristics peculiar to a nuclear detonation. Measurements were made of parameters that could establish ground zero and of dimensions commensurate with those of the fireball and its growth.

2.5.2 Magnetic-Tape Data. Data recorded on magnetic tape was played back and fed to an oscilloscope, which was photographed. Studies were then made of distant target acquisitions and amplitude variations of the returns.

2.6 REQUIREMENTS FROM OTHER PROJECTS

Yield and radial-growth measurements of various atomic explosions were obtained from other projects to ascertain whether there was any correlation with the results of Project 6.5. Motion pictures of the physical events were obtained from Edgerton, Germeshausen & Grier. The films were viewed with their time-equivalent radar scope displays in an attempt to extract correct information from the latter and to obtain interpretations of scope displays by comparing them with actual photos of the event.

Chapter 3
RESULTS and DISCUSSION

The main source of data was radar scope photography. Data analysis was performed on a magnifying viewer with movable crosshairs accurate to 0.001 inch. In the frame-by-frame study, the immediate tasks confronting the analysts were the correct interpretation, significance, and reliability of the data. In an attempt to achieve correct interpretation, actual photos of the physical event were studied side by side with the time-equivalent scope photos. Some representative frames of these photos were chosen and are presented in this report so as to give a chronological development of each detonation. (Some photos were retouched to improve reproducibility.)

In Project 6.5, the employment of radar was changed from its normal role of identifying simple targets to one of a research tool commissioned to investigate the nature of fireball returns. Other reports on such uses of radar indicated the need for new techniques of obtaining data to understand fully the observed effects (References 2 and 11).

3.1 SHOT YUCCA

There was no evidence of a radar return from Shot Yucca at any of the Project 6.5 sites. This event, a 85,000-foot-high shot, occurred at a range of 100.1 miles from the Eniwetok site and over 200 miles from the Rongelap site. Failure to obtain a radar reflection was an indication that a burst of this yield, height, and range did not present an area large enough to permit detection by the radars used.

At 3-minute intervals, exact positions of the balloon that carried the nuclear device were telephoned to the Eniwetok radar site from a weather-tracking radar set. This information aided Project 6.5 in orienting the antennas toward the target. The wide-beam pattern assured adequate target coverage at all times.

3.2 SHOT CACTUS

3.2.1 Radar Set AN/MPG-1. During the radar warmup period prior to shot time, Site Yvonne, the known ground zero of the shot, was clearly depicted on the radar screen. The island presentation was placed in an off-center scope position so that the scope grid lines would not interfere with any return that might identify ground zero. At H − 5 seconds the Flight Research Camera was set in operation. This camera was synchronized with each scope sweep and gave 16 looks per second that afforded a high-information-content study of the nuclear detonation. At time zero, a time marker was photographed and this particular frame was designated Frame 1 for the purpose of time reference (Figure 3.1a). Frame 9 (H + 0.56 second) revealed a definite distortion of the island foliage which pinpointed ground zero to a good degree of accuracy (Figure 3.1c). Frame 34 (H + 2.13 seconds) evidenced the first blast return which took the form of a small arc-shaped wave front (Figure 3.2a). The radius of curvature of the arc with reference to the island ground zero measured 723 feet. The radar return grew more semicircular in form until H + 3.69 seconds, at which time it became annular with an intense front edge and a faint back edge (Figures 3.3 and 3.4). The annular pattern grew to a radius of 800 feet with respect to ground zero. The dimensions of range and azimuthal growth are listed in Table 3.1 and plotted in Figure 3.5. At H + 7.94 seconds, the pattern lost its annular shape and became a nondescript growing pattern, the result of particle dispersion, which endured for 77 seconds.

The rather long time interval of 2.13 seconds for the first return agreed with the findings of other projects. The shapes of the returns, semicircular and annular, approximated the horse-

shoe and ring returns of air-borne radars in previous operations. The radial growth was in good agreement with fireball dimensions, and the disappearance of the annular pattern at H + 7.94 seconds agreed with the fireball rate of 300 ft/sec, since the radar beam illuminated a height of 2,400 feet in the vertical plane above ground zero.

3.2.2 Radar Set SCR-584. The antenna-positioning circuit became inoperative at H – 5 minutes; hence no results were obtained. This was the only instance of radar failure in Project 6.5.

3.3 SHOT -FIR

3.3.1 Radar Set SCR-584, PPI Scope, Rongelap. The Rongelap radar site was 231,120 yards from ground zero (Site Charlie of Bikini Atoll). At this distance, the curvature of the earth placed ground zero 7,000 feet below the radar line of sight. Since the atomic cloud rises at a

TABLE 3.1 TABLE OF VALUES FOR GRAPH OF FORE AND BACK RADIAL GROWTH, FIGURE 3.5, SHOT CACTUS

Distance readout measurements correct to ± 9.1 ft.

Time	Fore Radius	Back Radius
sec	ft	ft
2.12	723	—
2.5	733	—
3.0	741	—
3.5	765	760
4.0	756	760
5.0	768	768
6.0	780	776
7.0	786	784
8.0	800	796
9.0	801	800

rate of approximately 350 ft/sec (Reference 16), it was estimated that the atomic cloud would take about 20 seconds to reach the radar horizon and several added seconds to be partially visible above the horizon. The first return occurred at H + 25 seconds, in good agreement with the anticipated time of the earliest return (Figure 3.6).

Upon acquisition of the target, the antenna system was gently swept in azimuth to either side of the target, thus keeping it constantly in view. At the same time, the target was photographed at a rate of 16 frames/sec. Another estimate was made to verify the target as a true return from the nuclear detonation. Because of the great distance involved and the design limitations of the radar set, namely, a maximum range of 70,000 yards for ordinary targets, the return, if any, had to be a third-time-around echo. Such a reflection is unheard of in ordinary radar practice. However, a detonation might offer a large enough target to make this reflection possible (see Appendix). A calculation from the parameters of the set indicated that a target, if received, would appear at 40,410 yards of the third PPI sweep. Figure 3.6 shows the return at the fourth range marker, which represents 40,000 yards of range. The target remained visible on the PPI scope for 75 seconds, as it continued to rise through the area illuminated by the radar beam.

3.3.2 Radar Set SCR-584, A Scope, Rongelap. The first return appeared at H + 22.7 seconds. This return reached maximum intensity within 4 seconds, and slowly faded out (Figure 3.7). The A-scope presentation had good time agreement with the PPI display. The low grazing angle of the antenna brought in clutter, but the signal was discernible by the sudden increased amplitude of the return. The amplitude of the return, which can be compared to the 1-volt calibration input in Figure 3.7A, indicated a small-size target.

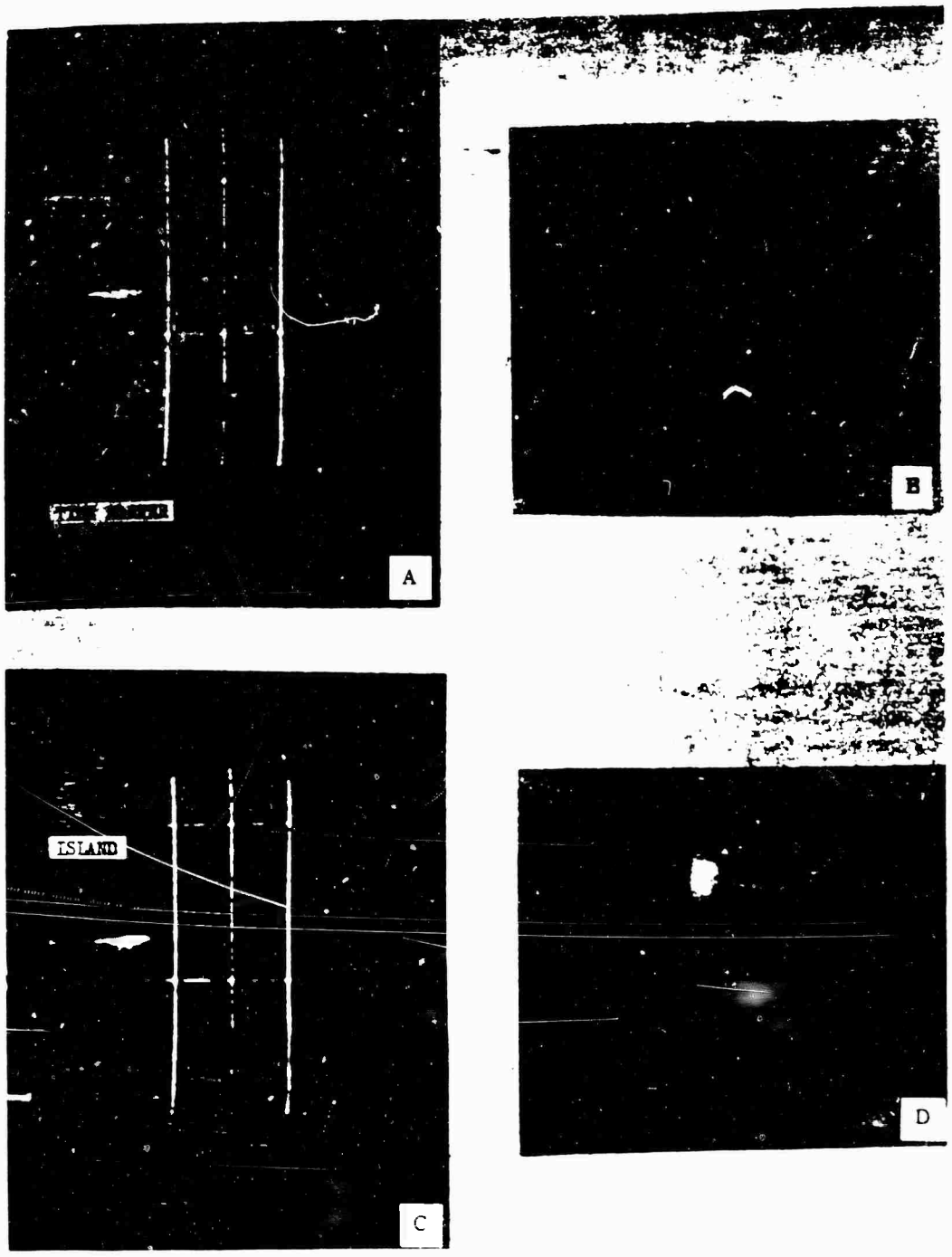

Figure 3.1 Shot Cactus, AN/MPG-1 B-scope returns, Fred radar site. The horizontal grid lines represent 1,000-yard range markers with the center line at a range of 24,500 yards. The vertical grid lines are 1 degree azimuth markers with the center one located at N 6° E. The island is located at a range of 24,782 yards and an azimuth of N 4° E. Photo A shows Site Yvonne at time zero. Photo C shows foliage disturbance on the island at H + 0.56 second. Photos B and D represent views, 3,000 feet wide and at a distance of 24,000 yards, obtained by the actual filming of the event at time zero and H + 0.56 seconds, respectively.

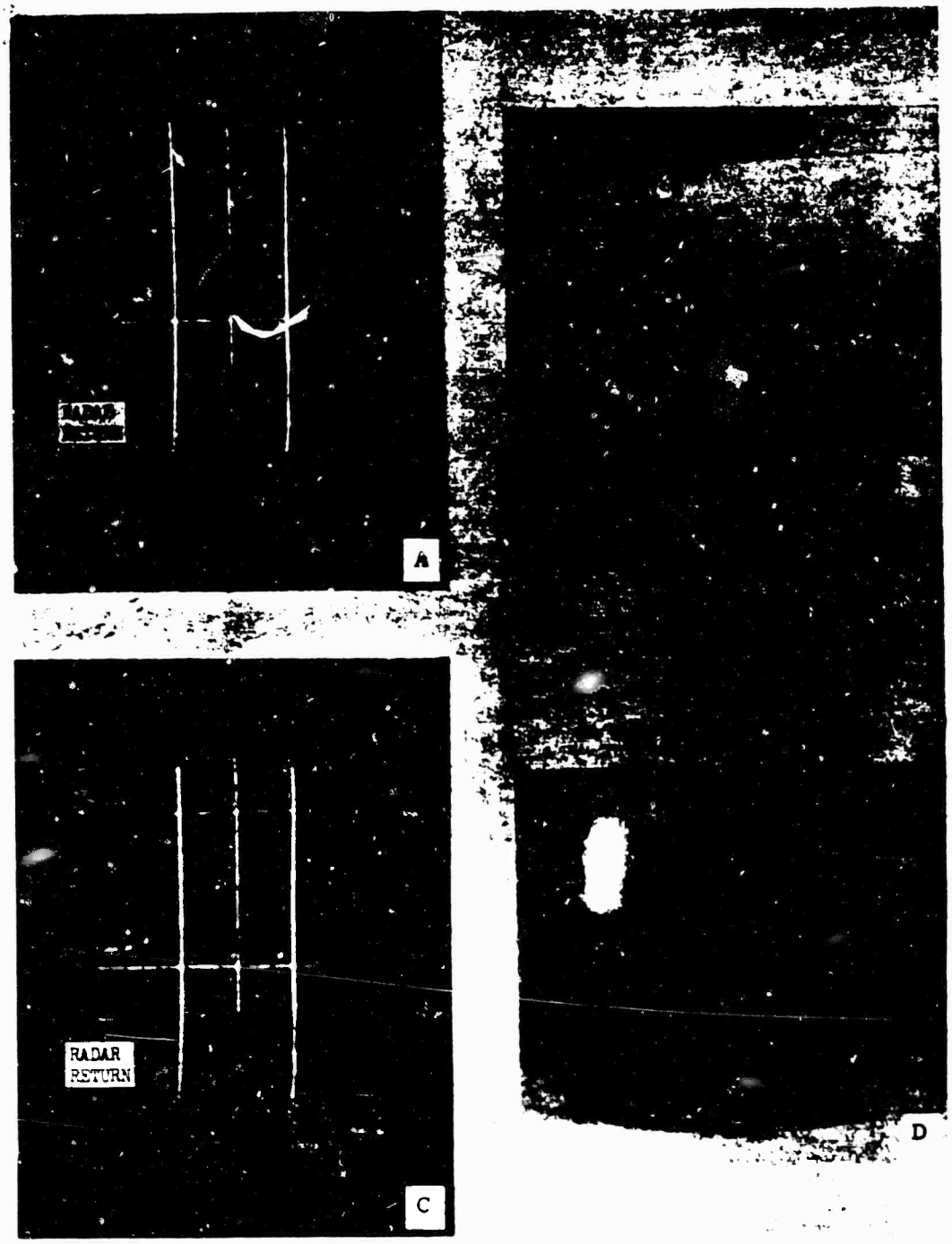

Figure 3.2 Shot Cactus, AN/MPG-1 B-scope returns, Fred radar site. The horizontal grid lines represent 1,000-yard range markers with the center line at a range of 24,500 yards. The vertical grid lines are 1-degree azimuth markers with the center one located at N 6° E. The grid line photos show an arc-shaped radar return growing radially in azimuth and range with respect to the island ground zero point of Figure 3.1. Photo A shows the first return at H + 2.13 seconds. Photo C shows an arc-shaped return at H + 2.75 seconds. Photos B and D represent views, 3,000 feet wide and at a distance of 24,000 yards, obtained by the actual filming of the event at the same instances of time as A and C, respectively.

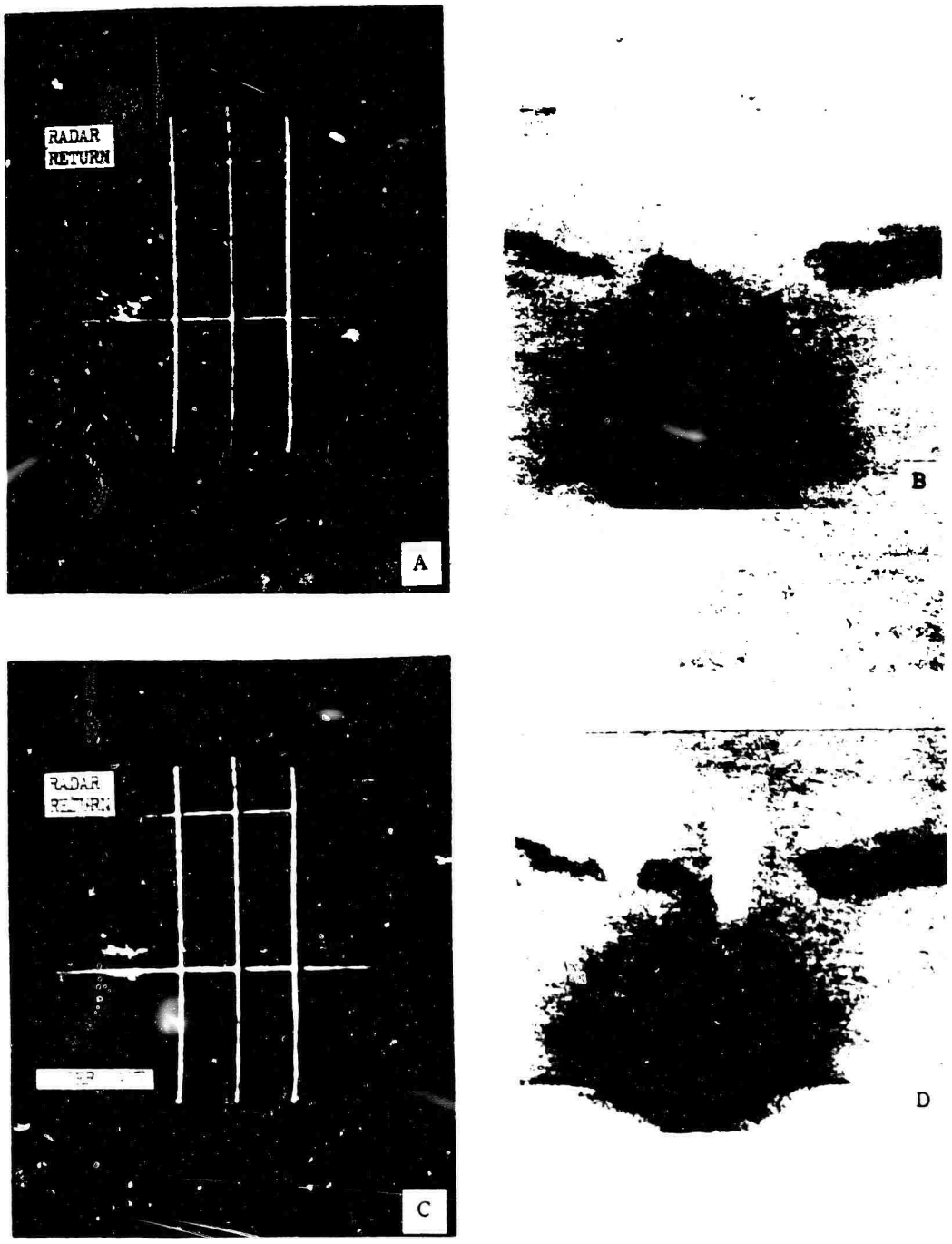

Figure 3.3 Shot Cactus, AN/MPG-1 B-scope returns, Fred Radar site. The area described by the grid lines is explained in Figure 3.1. The grid line photos show the radar return growing more annular with a center approximating the island ground zero point of Figure 3.1 Photo A shows a semicircular return at H + 3.5 seconds. Photo C shows an annular return at H + 5.25 seconds. Photos B and D, the time-equivalent optical views of A and C, respectively, represent a 3,000-foot width at a distance of 24,000 yards. The optical views aid in the physical interpretation of the radar returns.

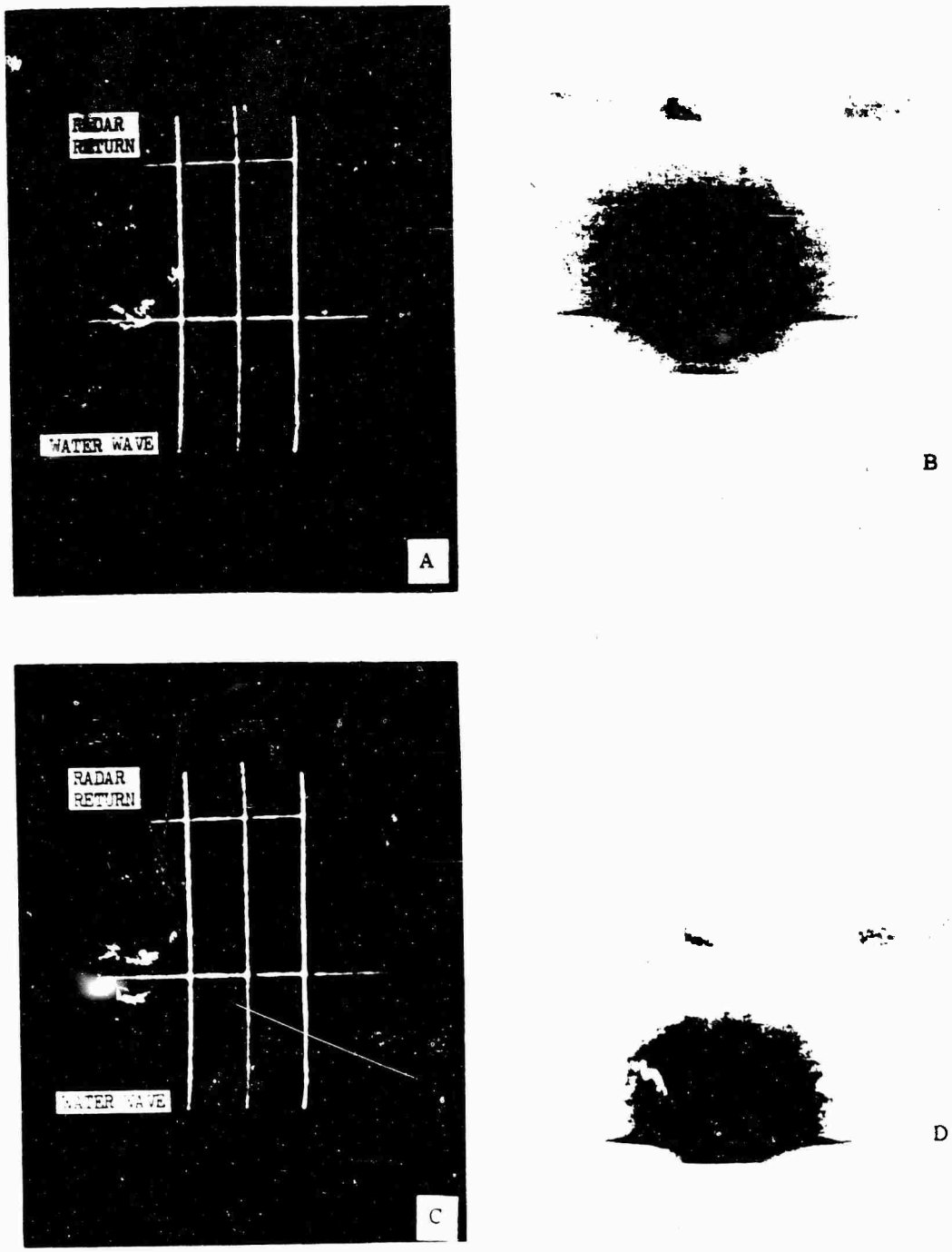

Figure 3.4 Shot Cactus, AN/MPG-1 B-scope returns, Fred radar site. The area described by the grid lines is explained in Figure 3.1. Photos A and C show persistency of the annular returns at H + 6.0 and H + 7.0 seconds, respectively. Photos B and D, time-equivalent motion-picture frames of photos A and C, respectively, represent a 3,000-foot-wide coverage of the event at a distance of 24,000 yards.

3.3.3 Radar Set SCR-584, PPI Scope, Eniwetok. The results of the Eniwetok radar site for Shot Fir substantiated the findings of the Rongelap station in every detail and extended the time study of the event because of the greater distance involved. The Eniwetok station was 402,340 yards from Site Charlie, which placed ground zero 21,200 feet below the radar horizon. The atomic cloud would have to rise above the horizon about 7,200 feet to offer a large enough target for a radar return. The distance to ground zero would then be 28,400 feet. On the basis of a rise rate of 350 ft/sec, it was estimated that the first return could be expected at approximately H + 81.1 seconds. The first return was in fact received at H + 84 seconds (Figure 3.8A). Since

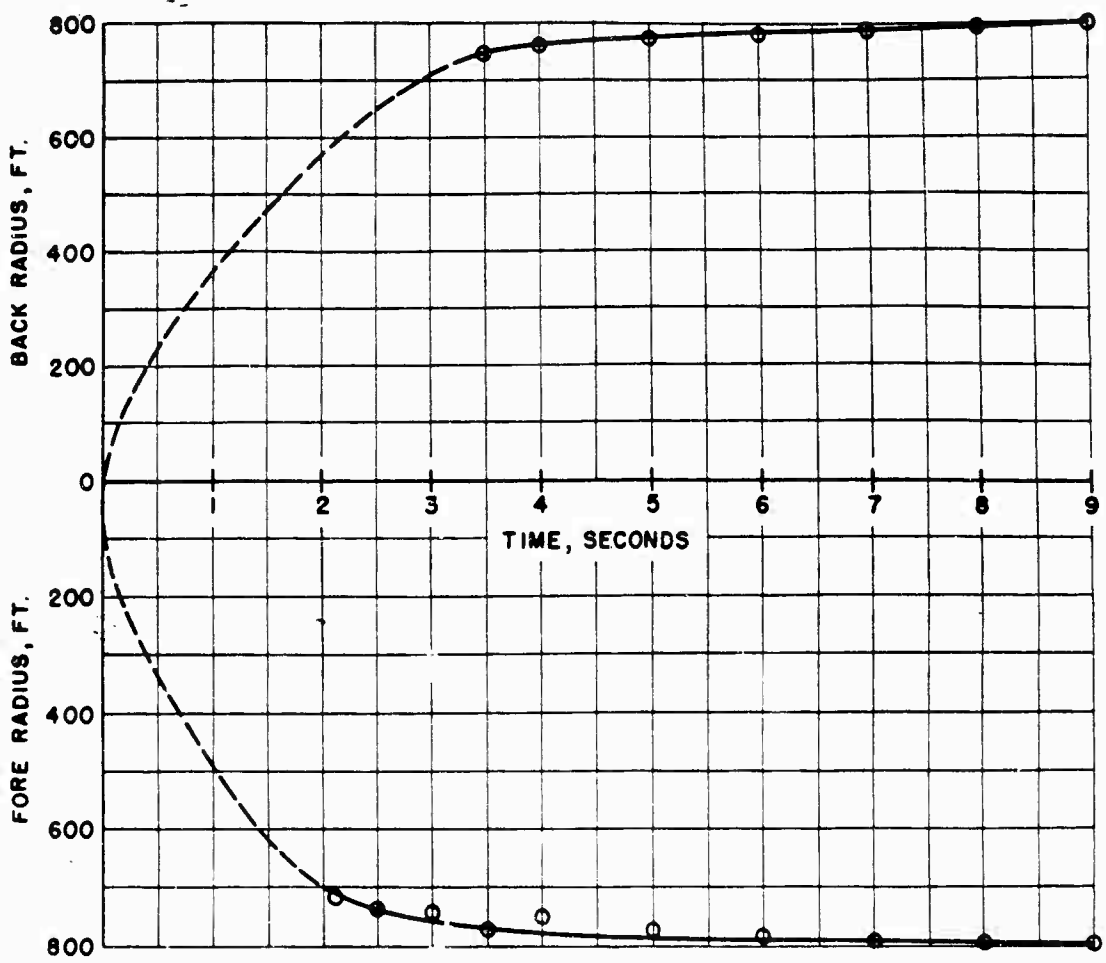

Figure 3.5 Graph of returns from Shot Cactus, B scope, showing fore and back radial growth of the annular return with respect to ground zero (see Figures 3.1 through 3.4).

there was a considerable scope-blanking pulse, a calculation had to be made as to whether the radar return would arrive during the blanking or unblanking portion of the sweep. The calculation showed that the return could be expected at the 17,300-yard position of the fifth-time-around sweep. The reception of this return was even more remarkable than the reception of the third-time-around echo of the Rongelap station and indicated a detonation of

The first return appeared at the 15,270-yard position and progressively advanced along the sweep line, indicating target rise. This rise was not vertical, but a slant-range variation of the moving target. The target was visible on the scope for 20 seconds, which corresponded to H + 104 seconds, compared to H + 100 seconds for the Rongelap station.

3.3.4 Radar Set SCR-584, A Scope, Eniwetok. Since Shot Butternut was scheduled to occur at 25 minutes after Shot Fir, time would not allow all camera magazines to be reloaded. For

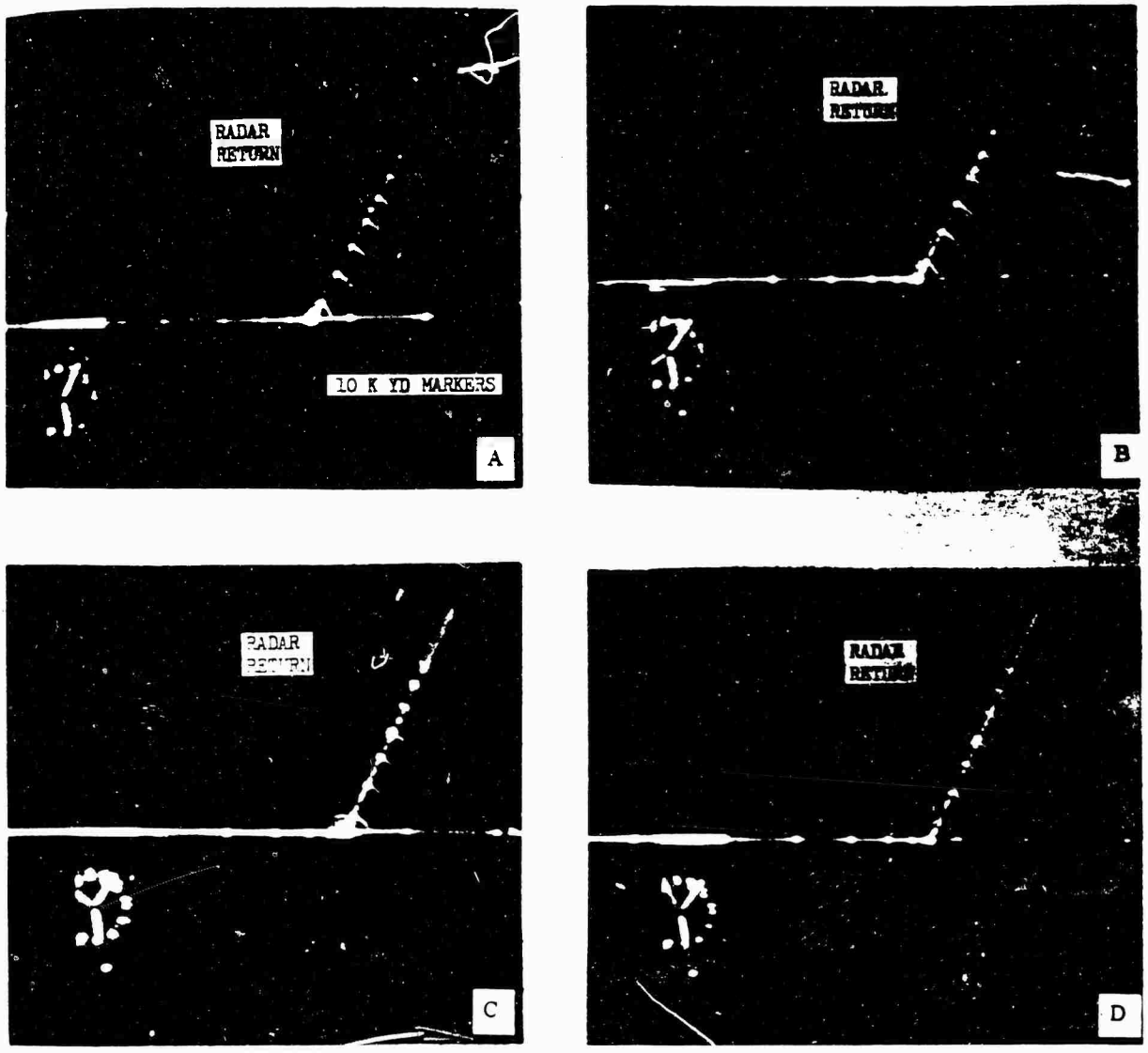

Figure 3.6 Shot Fir, SCR-584 PPI-scope returns, Rongelap radar site. The photos show a slant line which represents 70,000 yards of range, segmented by seven 10,000-yard range markers. The line's length, width, and constant inclination angle of 58 degrees represent a narrow area of interest as the radar antenna looks directly at Site Charlie of Bikini Atoll. The radar return is a third-time-around echo at an actual range of 232,000 yards, when the scope blanking and unblanking time is considered for the three sweeps. Photo A shows the first radar return at H + 25 seconds. Photos B, C, and D show target persistency for H + 57, H + 97 and H + 100 seconds, respectively.

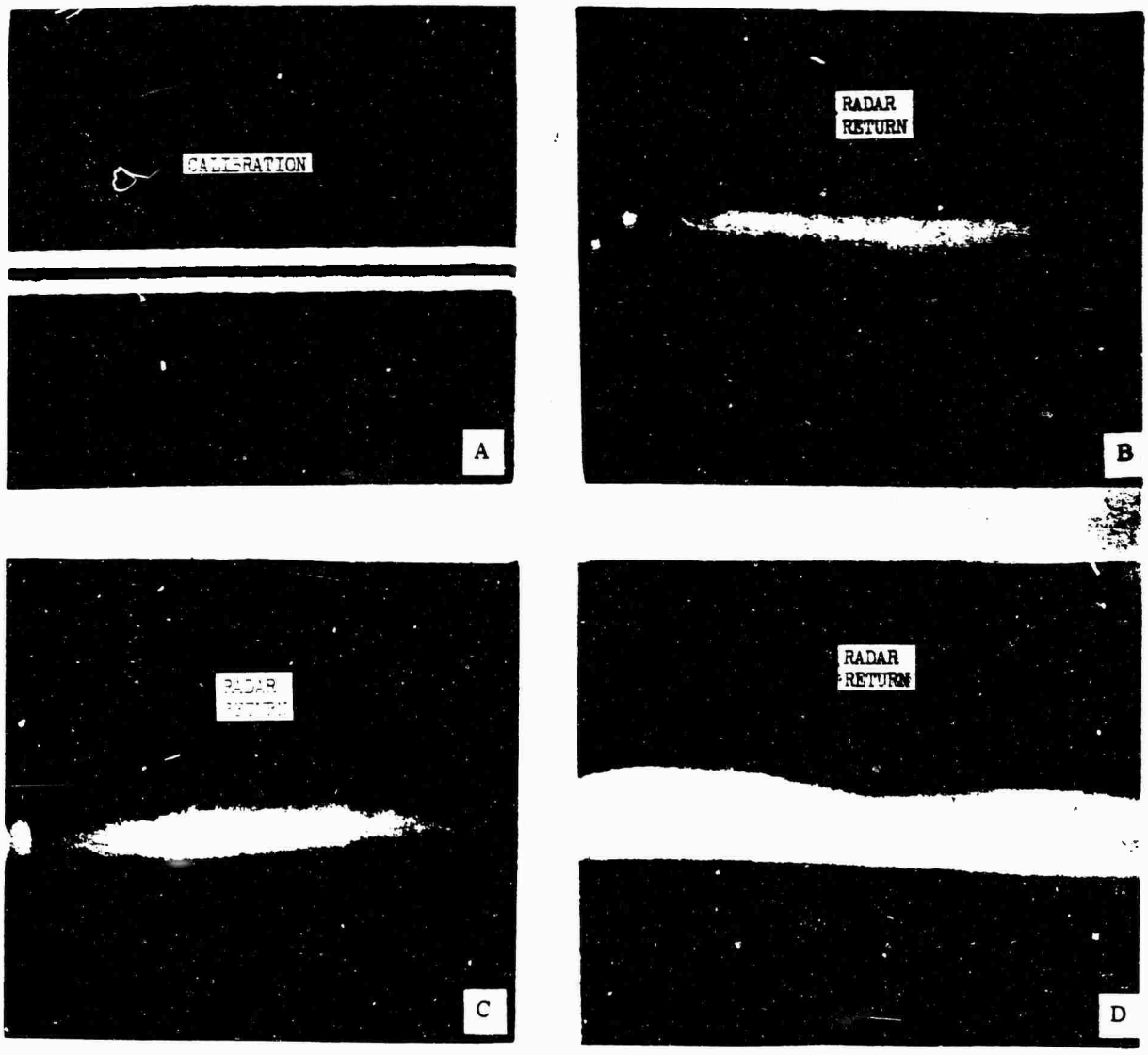

Figure 3.7 Shot Fir, SCR-584 A-scope returns, Rongelap Site. Photo A shows the A-scope's voltage calibration for one volt. Photo B shows target acquisition at H + 22.7 seconds. Photo C shows amplitude growth, and photo D shows maximum amplitude and intensity at H + 26.7 seconds.

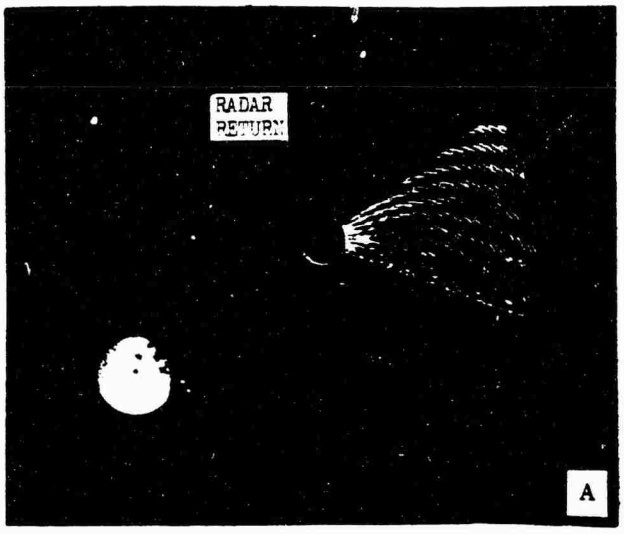

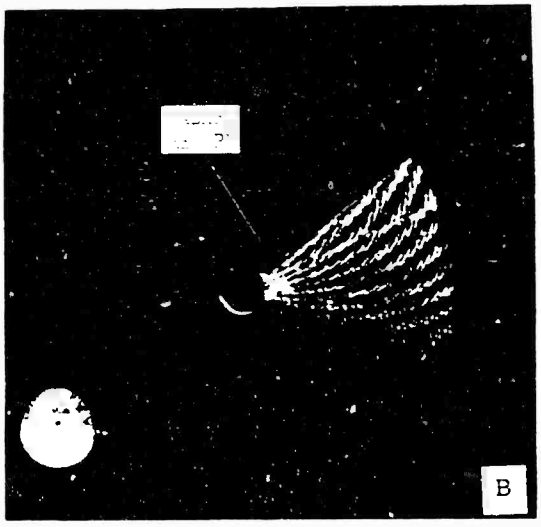

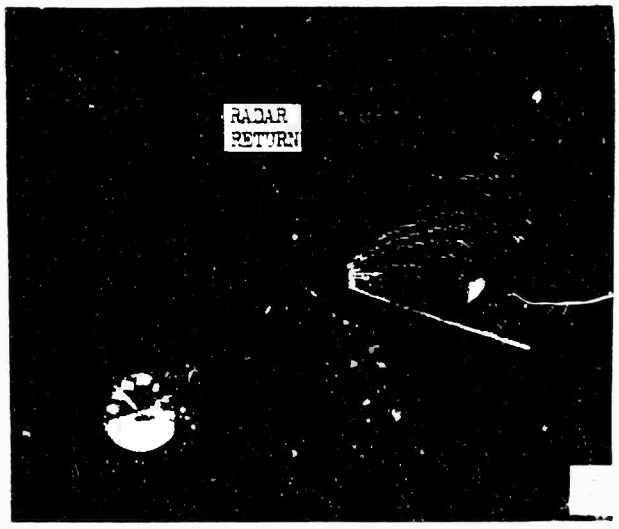

Figure 5.8 Shot Fir, SCR-584 PPI-scope returns, Fred radar site. The photos show a target acquisition within a search area described by a 70,000-yard range line sweeping through a 60-degree angle. At approximately the middle of the sweep, the radar antenna is looking directly at Site Charlie of Bikini Atoll. The radar return is a fifth-time-around echo at an actual range of 399,740 yards, when the scope blanking and unblanking time is considered for the five sweeps radially. Photo A shows target acquisition at H + 84 seconds. Photos B and C show target persistency at H + 87 and H + 91 seconds, respectively. The return faded out at H + 104 seconds.

this reason the high-speed camera film used in photographing the A scope was reserved for Shot Butternut.

3.3.5 Radar Set AN/MPG-1, Eniwetok. The low power output and the inherent range limitations of the radar set when operated B-mode resulted in no target acquisition.

3.4 SHOT BUTTERNUT

3.4.1 Radar Set AN/MPG-1, Eniwetok. During preshot time, the radar screen displayed a barge at 170 yards above the central grid line of the B scope, whose line represented a range of 23,080 yards (Figure 3.9A). At approximately time zero, the radar screen viewed the barge as being violently disturbed and also presented a bright-point return 170 yards south of the barge (Figure 3.9C). This frame identified the barge as the actual shot barge, and pinpointed ground zero to a high degree of accuracy. Ground zero was established at a range of 23,250 yards and

TABLE 3.2 TABLE OF VALUES FOR GRAPH OF FORE AND BACK RADIAL GROWTH, FIGURE 3.13, SHOT BUTTERNUT

Distance readout measurements correct to ± 9.1 ft.

Time	Fore Radius	Back Radius
sec	ft	ft
2.0	849	—
2.5	921	—
3.0	1,029	—
3.5	1,102	1,098
4.0	1,136	1,139
4.5	1,183	1,174
5.0	1,200	1,200
5.5	1,211	1,220
6.0	1,237	1,234
6.5	1,237	1,237
7.0	1,239	1,235

at a bearing of 4 degrees from the geographical site of the radar installation. The bright-point return immediately disappeared, and for the next 2 seconds there was no radar return, although during this time 30 looks were made. On the 32nd look, or at exactly H + 2 seconds, the first return from the detonation was evidenced. The 2-second delay substantiated the similar delay for Shot Cactus.

The target presentation on the B scope followed the same pattern as that for Shot Cactus. The return took the form of a small arc-shaped wave front that grew more semicircular (Figure 3.10). At H + 3.75 seconds it became annular and so remained until H + 6.81 seconds (Figures 3.11 and 3.12). The annular pattern disappeared in shorter time than the annular pattern for Shot Cactus. This pattern gave way to a nondescript scope pattern that grew in size and intensity and finally faded out at H + 100.63 seconds. The size, intensity, and endurance of the latter pattern were greater than for Shot Cactus and indicated a detonation of
The dimensions of range and azimuthal growth are listed in Table 3.2 and graphically represented in Figure 3.13.

3.4.2 Radar Set SCR-584, PPI Scope, Eniwetok. Immediately before time zero, the radar beam swept over ground zero, revealing a barge as a target at a range of 30,400 yards. On the next sweep, the PPI scope presented a bright-point return at approximately time zero (Figure 3.14A). This return appeared as a small dot and allowed range and azimuth to be measured accurately. The low elevation angle of the antenna indicated this to be a water-surface shot. The bright-point return immediately disappeared, and at H + 2 seconds the first persistent re-

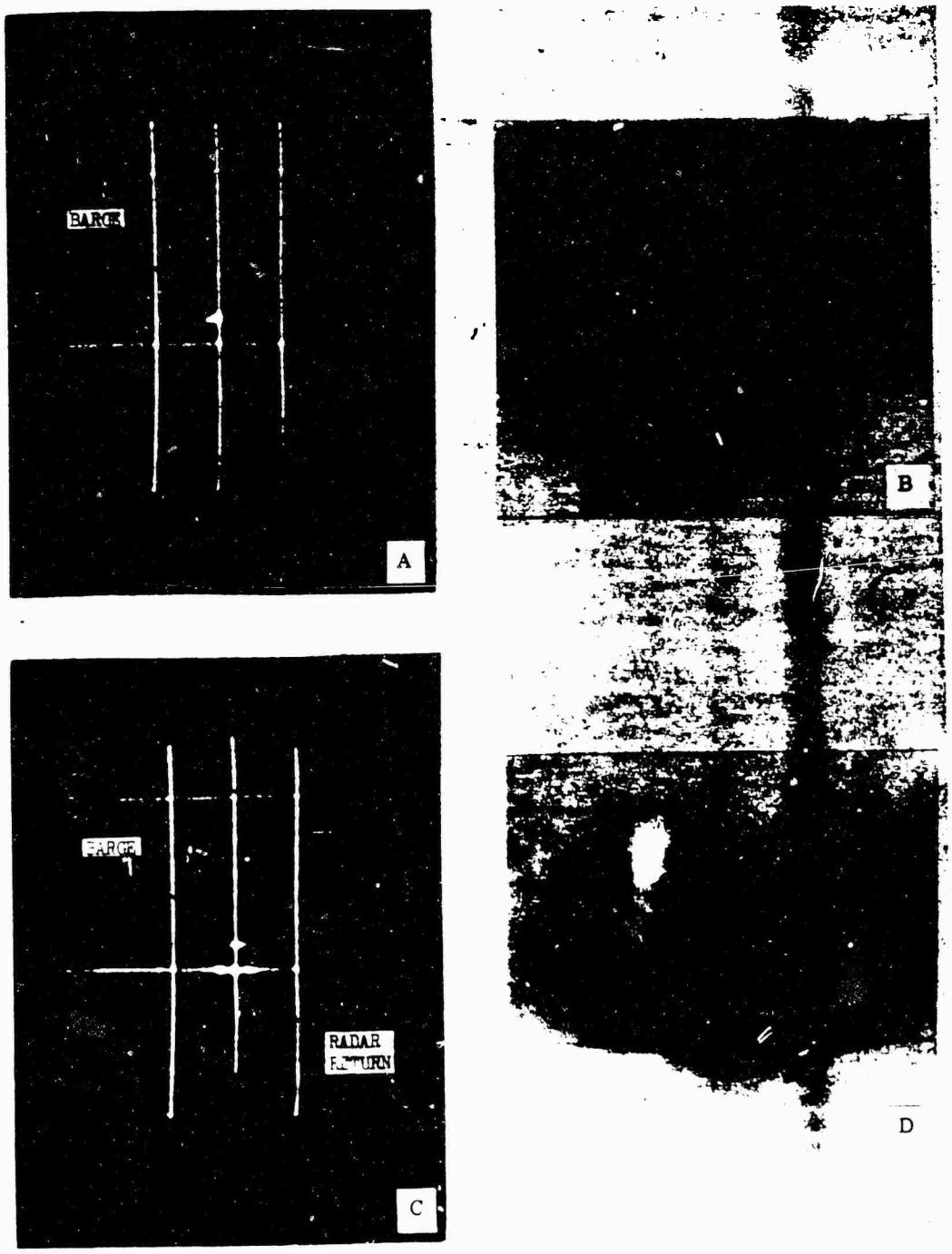

Figure 3.9 Shot Butternut, AN/MPG-1 B-scope returns Fred radar site. The horizontal grid lines represent 1,000-yard range markers with the center line at a range of approximately 23,100 yards. The vertical grid lines are 1-degree azimuth markers with the center one located at N 4° E. The barge is true ground zero of the shot and is geographically pinpointed in azimuth and at a range of 23,250 yards by the radar grid lines. Photo A shows the shot barge before time zero. Photo C shows a radar bright-point return at approximately time zero. Photos B and D represent views, 3,000-feet wide and at a distance of 23,000 yards, obtained by the actual filming of the event at H + 0 and H + 1 seconds, respectively.

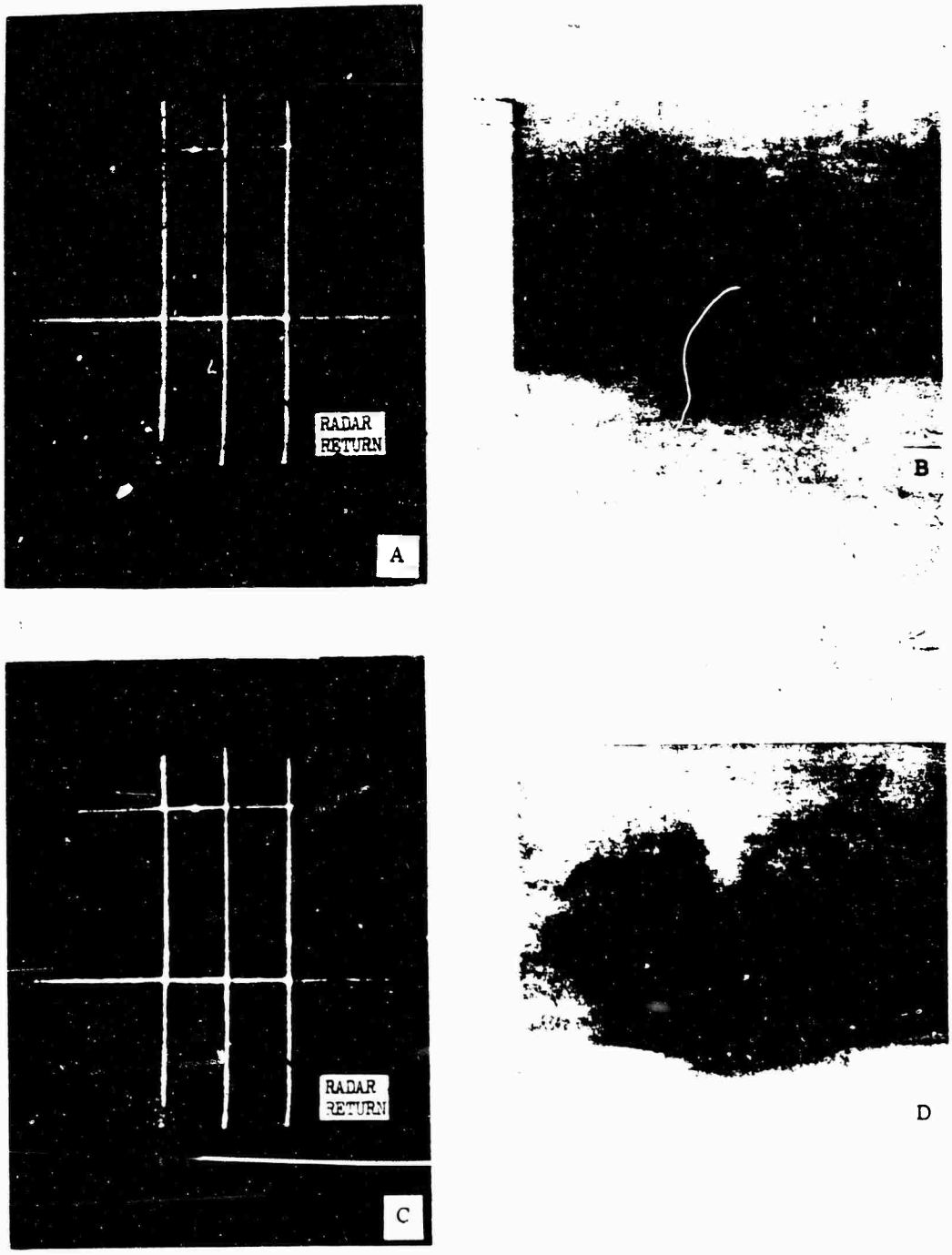

Figure 3.10 Shot Butternut, AN/MPG-1 B-scope returns, Fred radar site. The area covered by the photos is explained in Figure 3.9. Photos A and C show semicircular radar returns at H + 2.5 seconds and H + 3.25 seconds, respectively, with a center of curvature closely approximating the shot barge of Figure 3.9. Photos B and D are motion-picture frames of the physical event and are time equivalents of the radar returns. They present a 3,000-foot-wide view of the event at a distance of 23,000 yards.

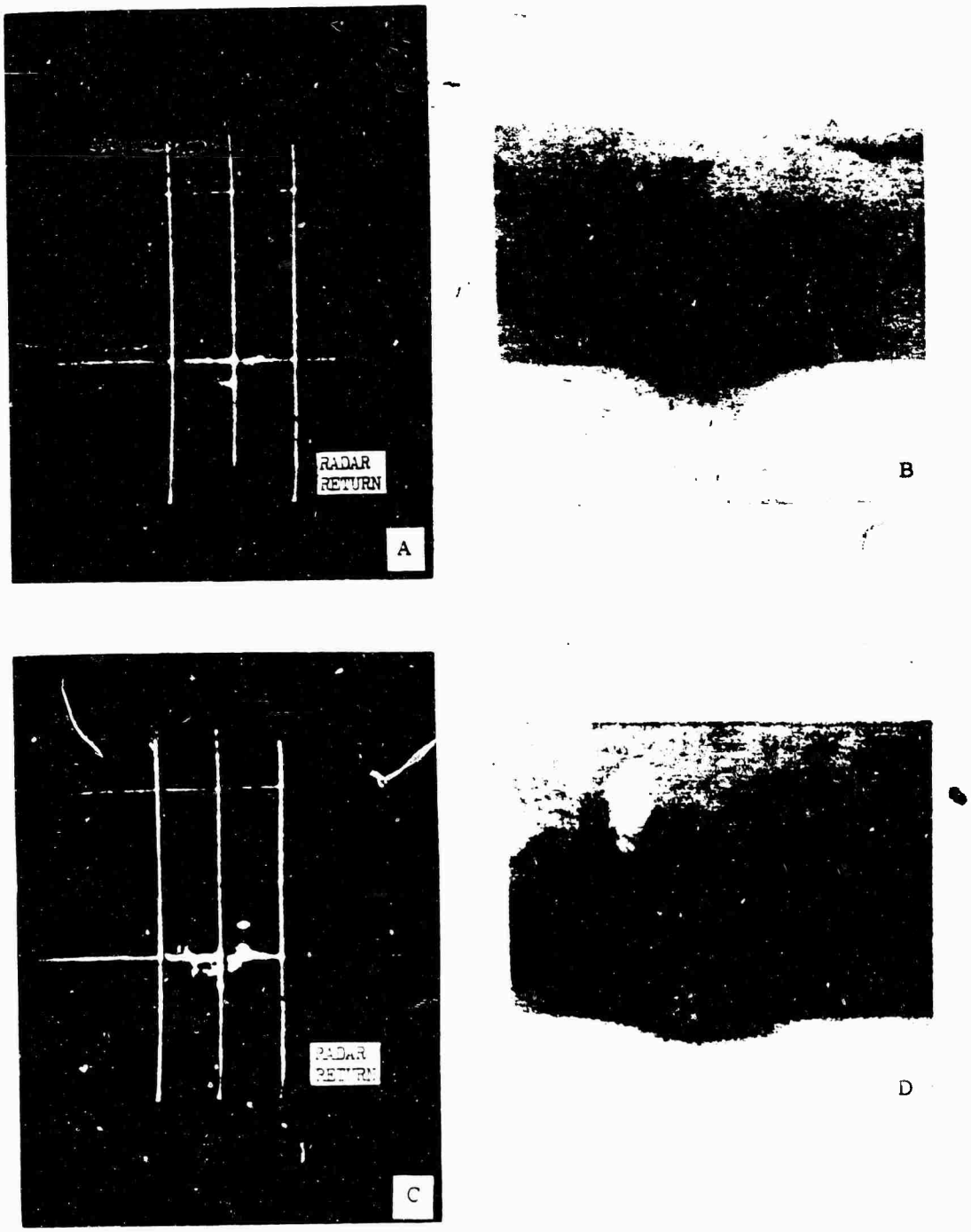

Figure 3.11 Shot Butternut, AN/MPG-1 B-scope returns, Fred radar site. The area covered by the photos is explained in Figure 3.9. Photos A and C show the radar returns changing from semicircular to annular shapes at times H + 3.87 seconds and H + 4.37 seconds, respectively, with a center of curvature closely approximating the shot barge of Figure 3.9. The measurement of the radar returns are commensurate with those of a fireball of this particular yield. Photos B and D are motion-picture frames of the physical event and are equivalent in time to the radar returns.

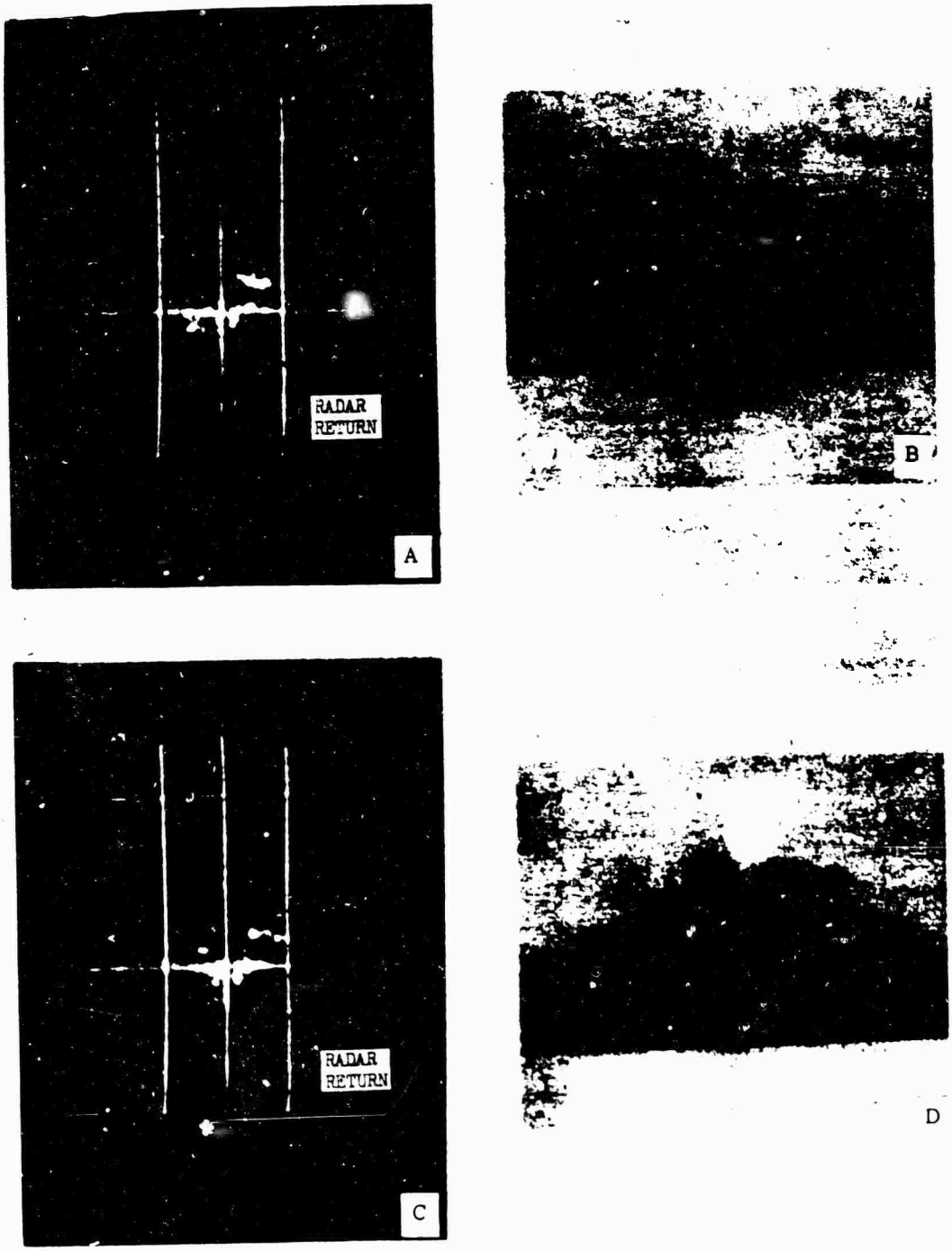

Figure 3.12 Shot Butternut, AN/MPG-1 B-scope returns, Fred radar site. The area covered by the photos is explained in Figure 3.9. Photos A and C display the annular radar return at H + 5.31 seconds and H + 6.5 seconds, respectively. The annular shape of radar returns is characteristic of nuclear detonations, as observed on B scopes by ground-based radar. Photos B and D are physical views of the event and are time-equivalents of the radar returns.

turn appeared. Both the S band (SCR-584) and the X band (MPG-1) radars received the first return from Shot Butternut at the same time, H + 2 seconds. The target grew in size for 8 seconds, remained at maximum dimensions for 17 seconds, then gradually grew smaller, fading out at H + 2 minutes 25 seconds (Figures 3.15 and 3.16). The 8-second target growth agreed well with the 6.81-second growth of the same target on the X-band radar.

The barge target, acquired at H + 2.0 seconds, remained visible together with the burst target until H + 38 seconds, at which time the barge target disappeared. This effect indicated that

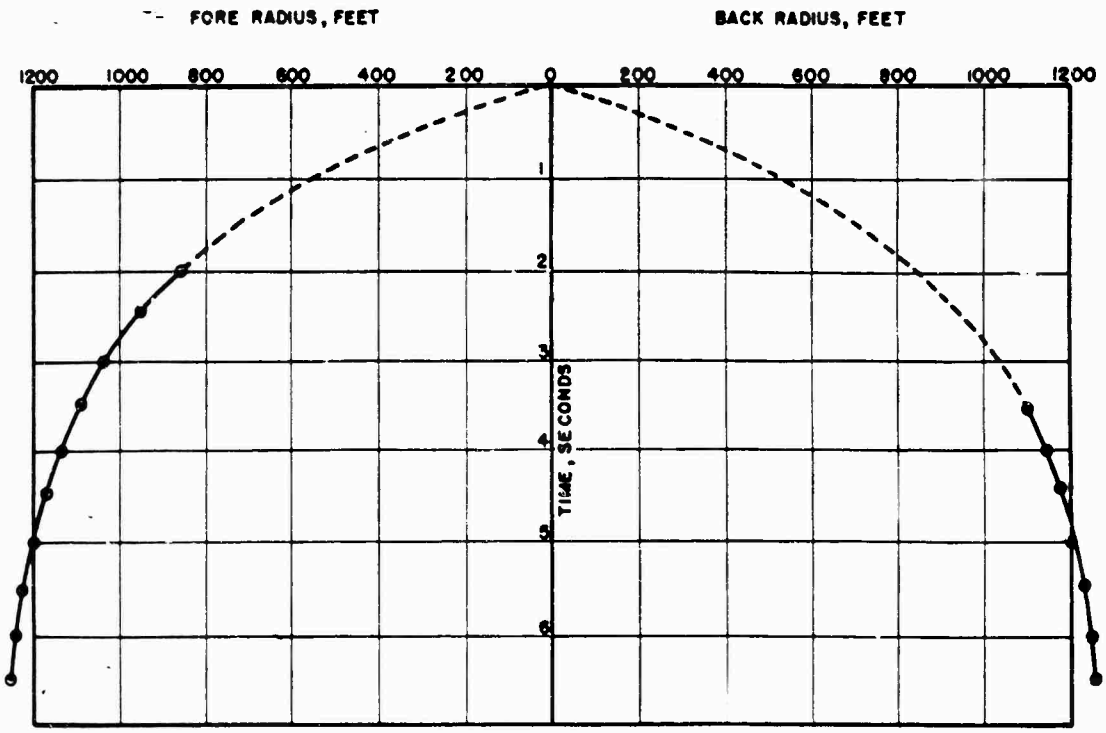

Figure 3.13 Graph of returns from Shot Butternut, B scope, showing fore and back radial growth of the annular return with respect to ground zero (see Figures 3.9 through 3.12).

a high water wave approached the barge from ground zero and finally hid it from radar view. The barge appeared periodically as a radar target affording a count of the water waves passing under it. The maximum size of the burst target revealed that the yield of Shot Butternut was

3.5 SHOT KOA

3.5.1 Radar Set SCR-584, A Scope, Eniwetok. The SCR-584 A-scope presentations compared favorably with the PPI displays. The high-speed camera film recorded the first return as a faint line rising in amplitude (Figure 3.17A). A count of the $^1/_{120}$-second time markers placed the return at H + 2.2 seconds. The growth of the target to maximum size was revealed by the rising amplitude and intensity of the video return (Figure 3.17). The target lasted for the full length of the film, which had a time equivalence of 2 minutes 40 seconds. The time resolution of the recording was high, being dependent on the speed of the camera and the scope's phosphorescent persistency. The latter did not allow resolution of the individual pulse returns but integrated them in a continuous line presentation. The primary purpose of the A-scope instrumentation was to measure the amplitude of the return in terms of known calibration voltages. The amplitude measurements and the maximum intensity revealed a burst of at its great range of 42,000 yards.

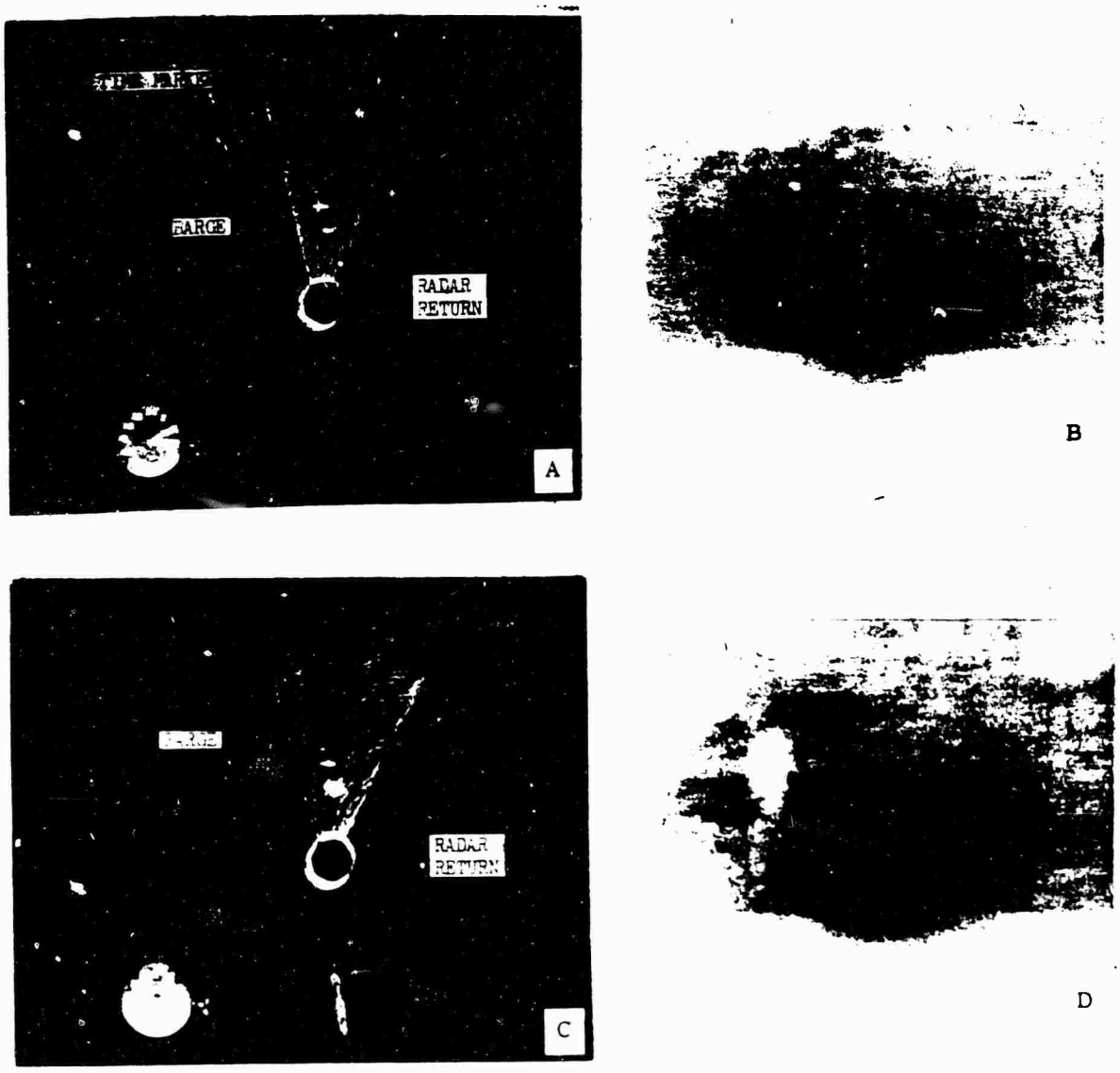

Figure 3.14 Shot Butternut, SCR-584 PPI-scope returns, Fred radar site. Photos A and C show a radar target acquisition within a search area described by a radial 70,000-yard range line sweeping through a 40-degree angle. The radar site is represented by the center of the black dot. A radial line drawn outward from the center through the target geographically locates the radar return at a bearing of N 4° E and at a range of 23,250 yards. Photo A shows a radar bright-point return at approximately time zero. Photo C shows the growth of the return at H + 5 seconds. Photos B and D represent views, 3,000-feet wide and at a distance of 23,000 yards, obtained by the actual filming of the event at the same instances of time as the radar returns.

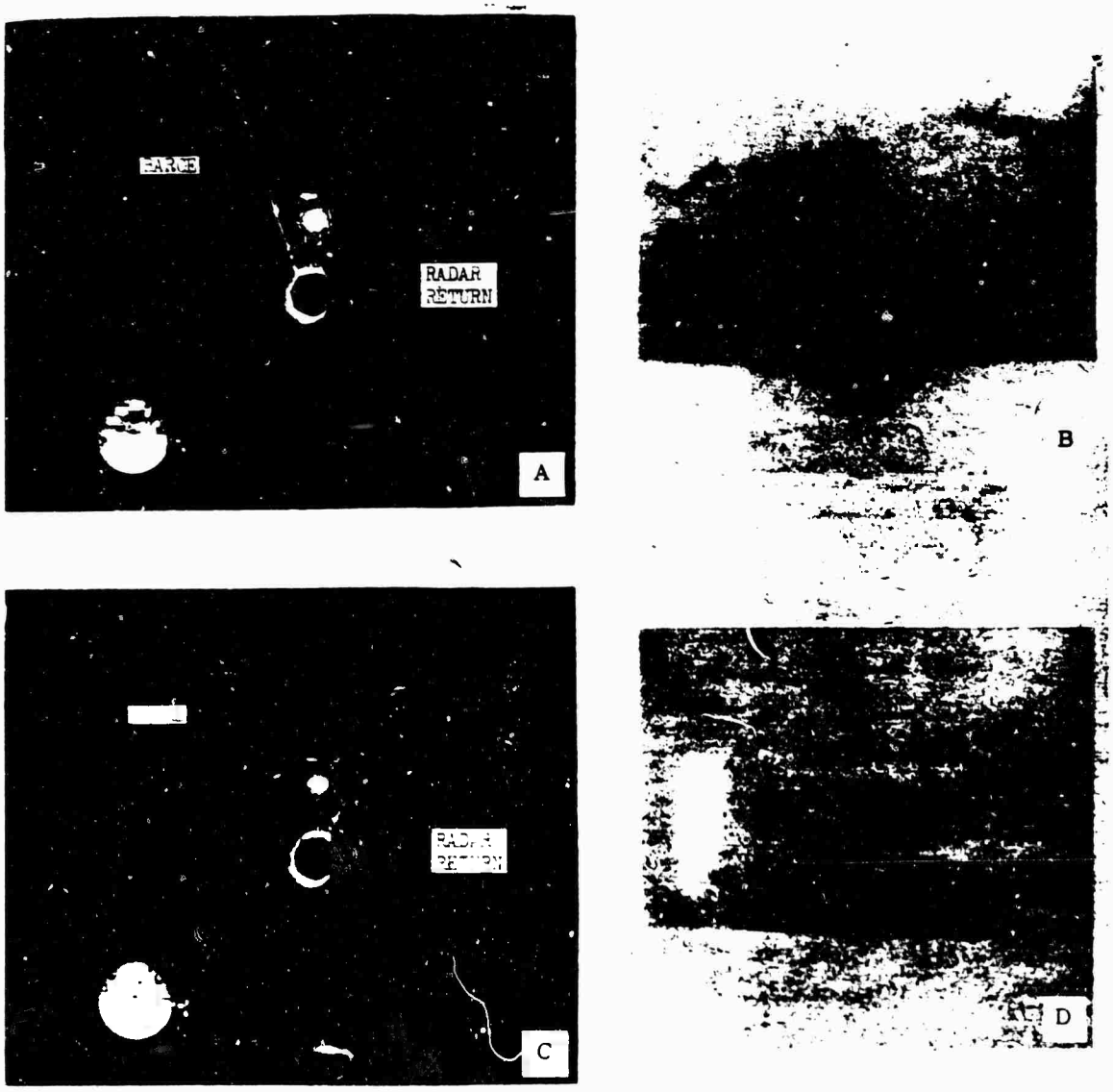

Figure 3.15 Shot Butternut, SCR-584, PPI-scope returns, Fred radar site. The area covered by the photos is explained in Figure 3.14. Photo A shows maximum growth at H + 8 seconds. Photo C shows target persistency at H + 25 seconds. A radar return of abnormal size, intensity, and of relatively short life is characteristic of returns from a nuclear detonation. Comparison may be made between it and a normal radar target such as the barge or ship. Photos B and D are time-equivalent motion-picture frames of the physical event.

3.5.2 Radar Set SCR-584, PPI, Eniwetok. The chronological development of Shot Koa is pictorially illustrated in Figures 3.18 through 3.21. At time zero there was a chance orientation of the antenna directly at ground zero which resulted in a point return (Figure 3.18A). This effect substantiated similar findings by air-borne radar on several previous operations. The small-

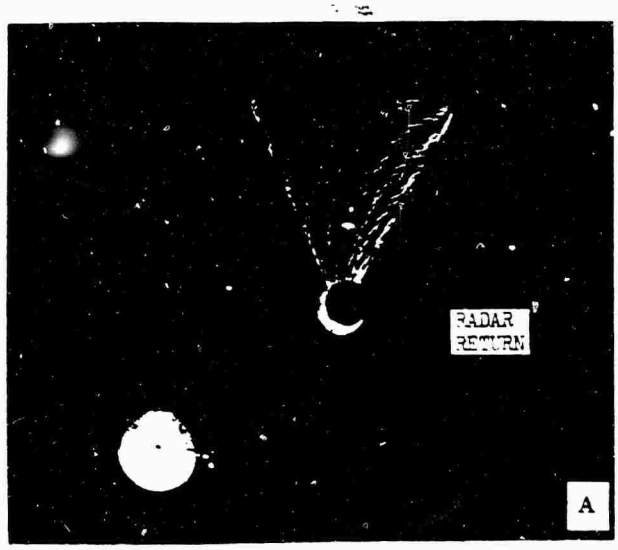

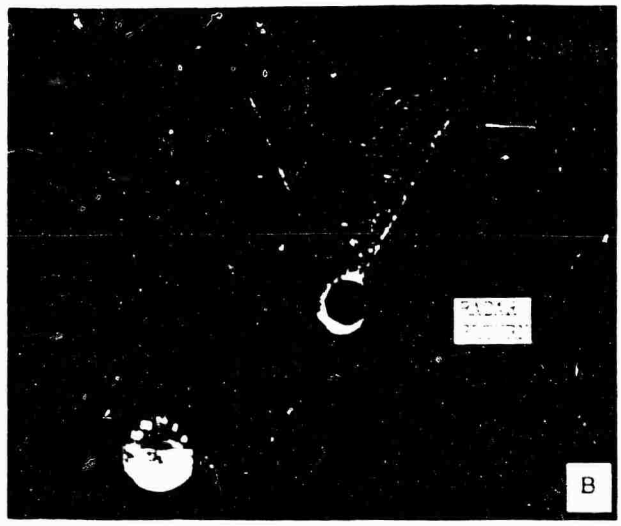

Figure 3.16 Shot Butternut, SCR-584, PPI-scope returns, Eniwetok Site. Photos A and B show target decay at H + 30 seconds and H + 2 minutes, respectively.

point return aided in establishing ground zero to a greater degree of accuracy. On the following sweep the radar beam illuminated the shot area at approximately H + 2 seconds, and revealed a target of abnormal size (Figure 3.18C). A comparison may be made between the barge as a normal radar target at 28,000 yards, and the shot as an unusual target at 42,000 yards. The return grew to maximum dimensions within 15 seconds and remained a large target for 8 minutes 10 seconds (Figures 3.19 through 3.21). Both the maximum target size and the time duration of the return were indicative of high yield. The scope displays possessed no characteristics that could

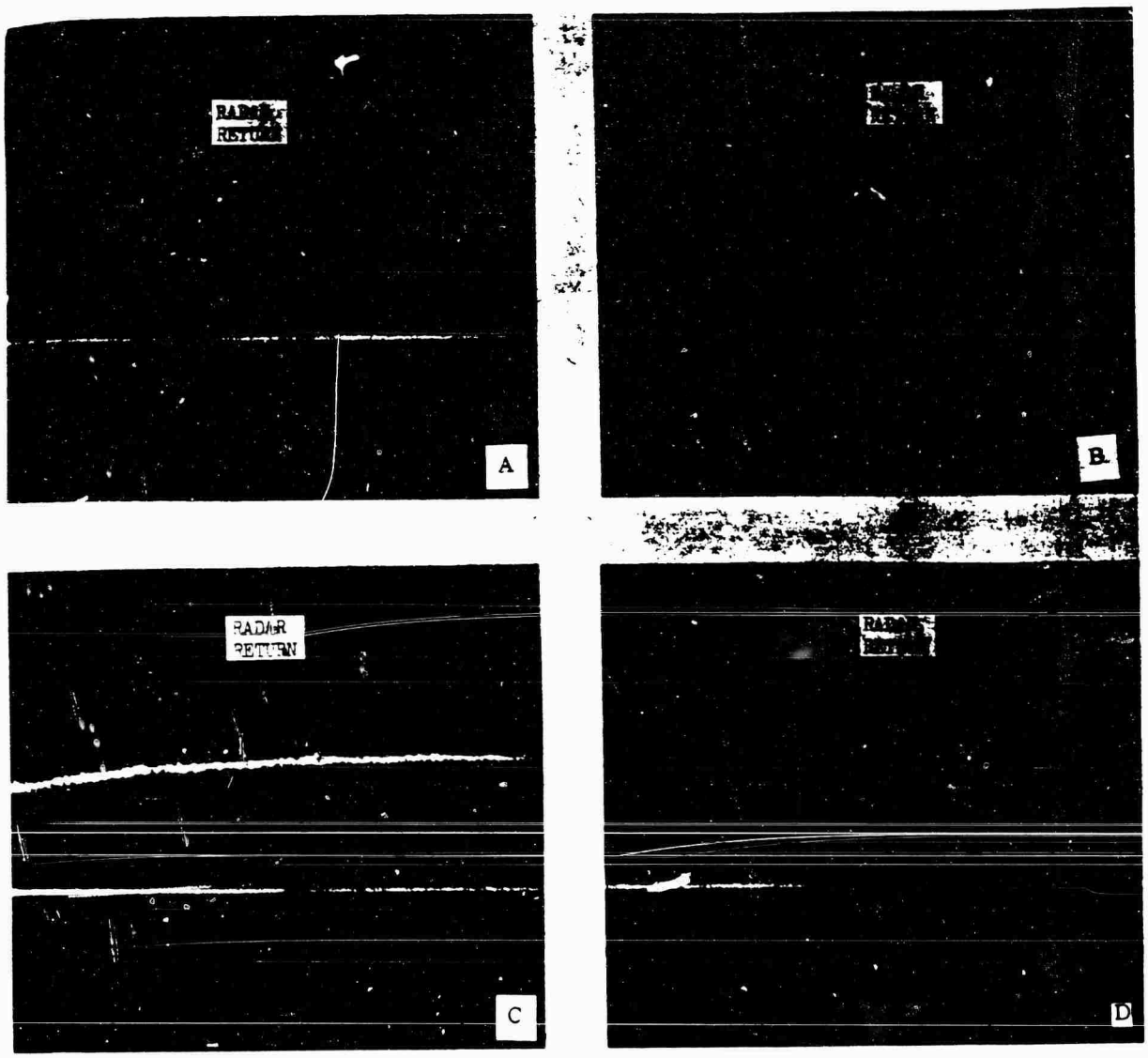

Figure 3.17 Shot Koa, SCR-584 A-scope returns, Eniwetok Site. Photo A shows target acquisition at H + 2.2 seconds. Photo B displays amplitude growth at H + 5.0 seconds. Photo C shows maximum amplitude and intensity at H + 14.8 seconds. Photo D shows persistency of large target at H + 1.4 minutes.

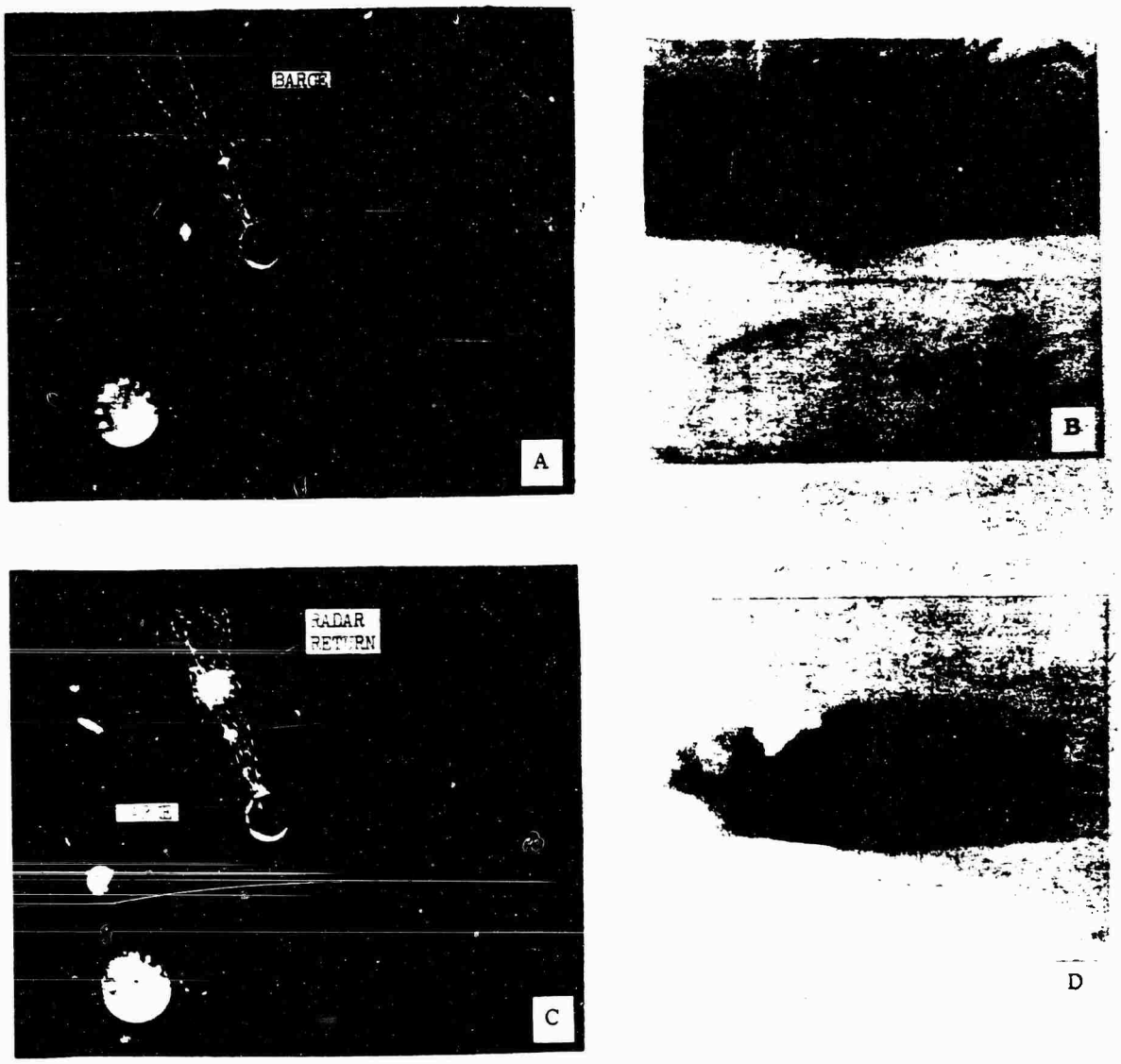

Figure 3.18 Shot Koa, SCR-584, PPI-scope returns, Fred radar site. Photos A and C show a radial 70,000-yard range line sweeping out a small azimuth angle of search. The location of the radar site is represented by the center of the black dot and a radial line drawn from it through the target places the radar return at N 21° W and a range of 42,220 yards from the radar site. Photo A shows a chance orientation of the antenna with a barge in direct line of sight with ground zero. A point return is barely visible along this line of sight above the barge. Photo C shows target growth at H + 2 seconds. Photos B and D are time-equivalent motion-picture frames of the physical event, and represent a view 8,000 feet wide at a distance of 42,200 yards.

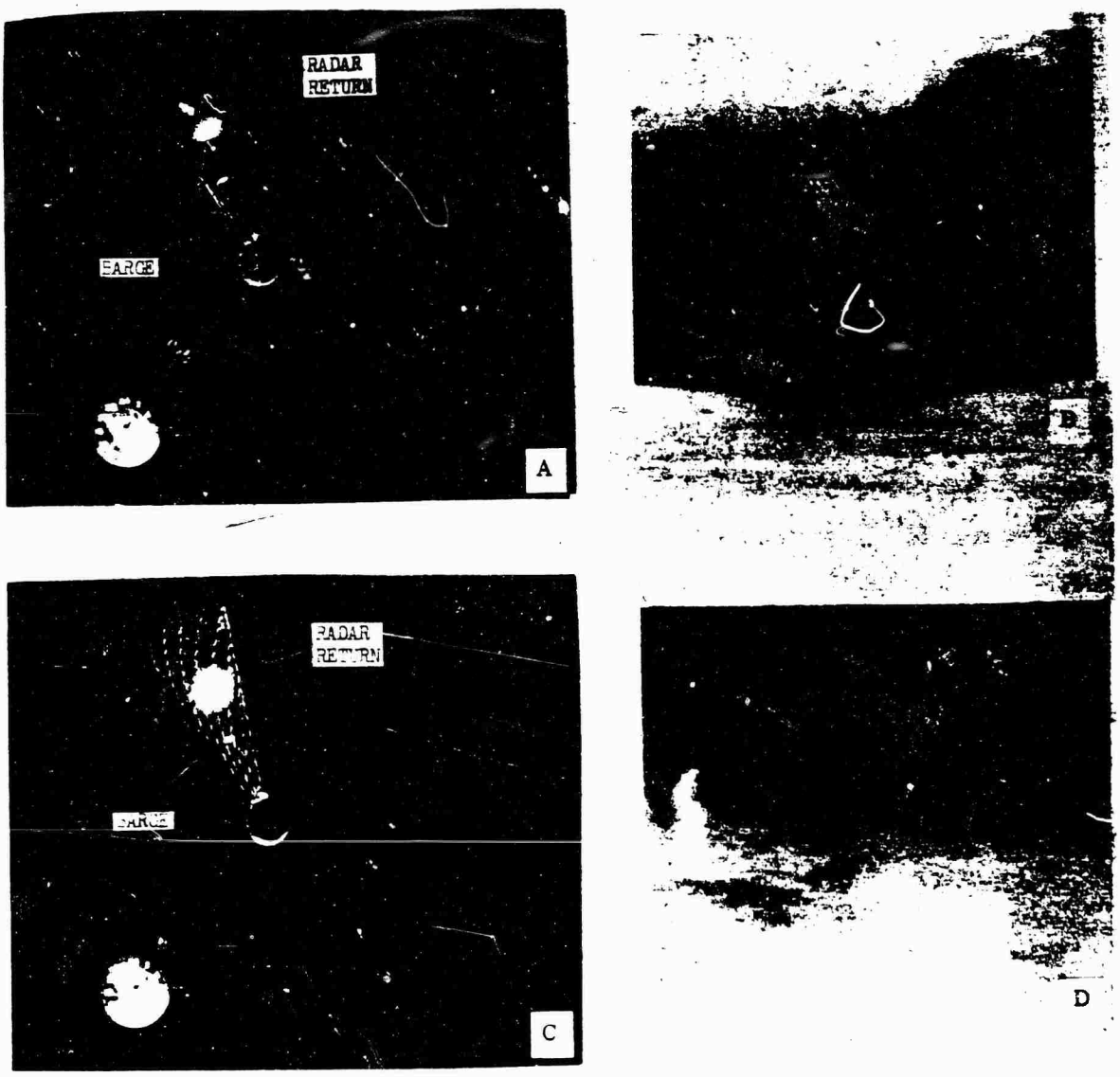

Figure 3.19 Shot Koa, SCR-584, PPI-scope returns, Fred radar site. The area covered by the photos is explained in Figure 3.18. Photos A and C show the chronological growth at H + 5 and H + 7 seconds, respectively. The striated lines in the search area indicate interference from other equipment. Photos B and D, motion-picture frames of the physical event, are the time equivalents of the radar returns.

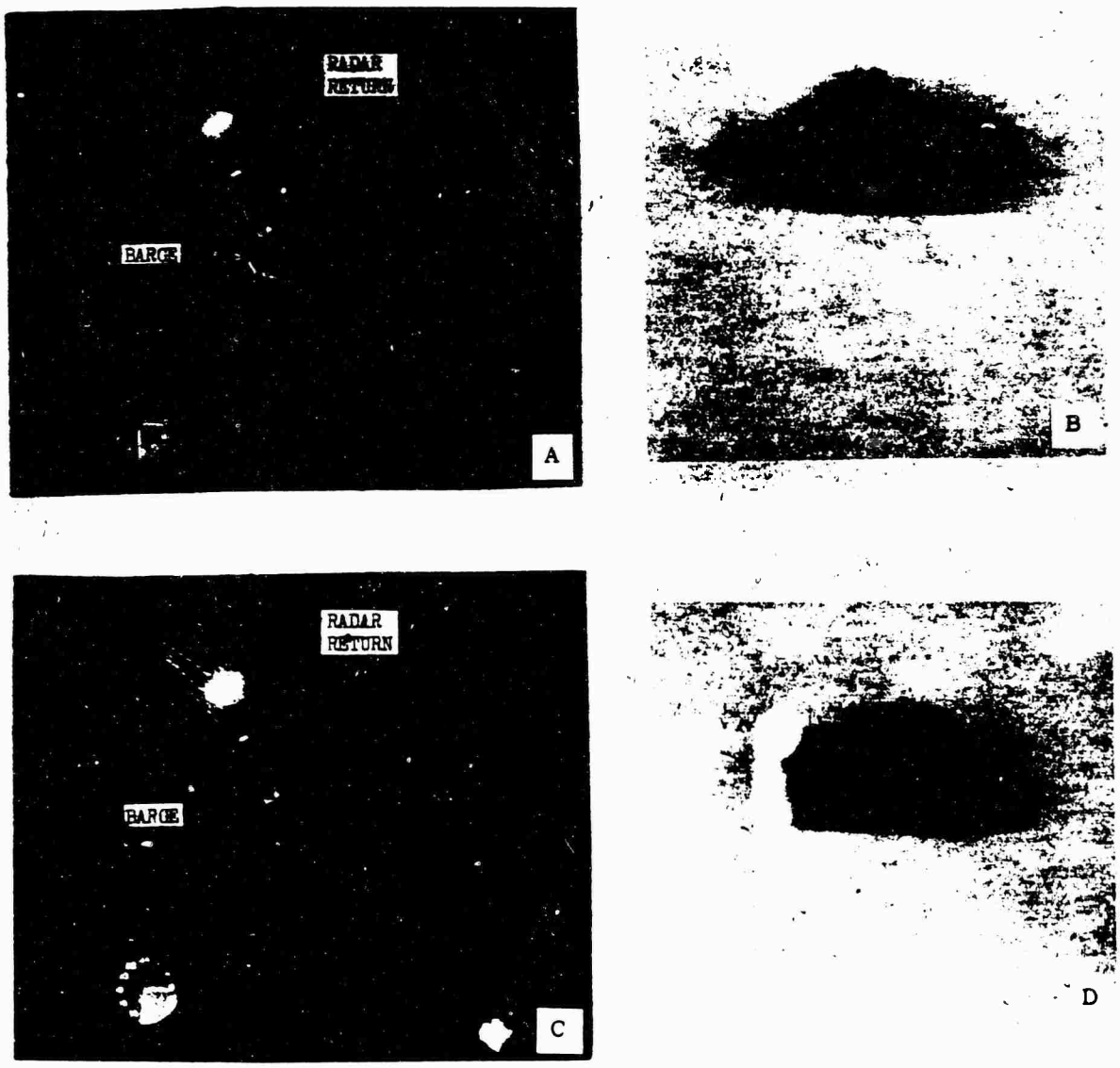

Figure 3.20 Shot Koa, SCR-584, PPI-scope returns, Fred radar site. The area covered by the photos is explained in Figure 3.18. Photos A and C are H + 1 minute and H + 2 minute displays of target persistency. The larger size and intensity at a greater distance than previous shots are indicative of higher yield. Photos B and D are time-equivalent motion-picture frames of the physical event.

differentiate them as returns from the fireball or from the after-effects of the detonation. This condition was largely due to the particular look the radar was taking of the event, a horizontal, line-of-sight view. Air-borne radar takes a downward, slant view that gives a panoramic view which even includes dimensional displays of the shock wave. The particular angle of view aids

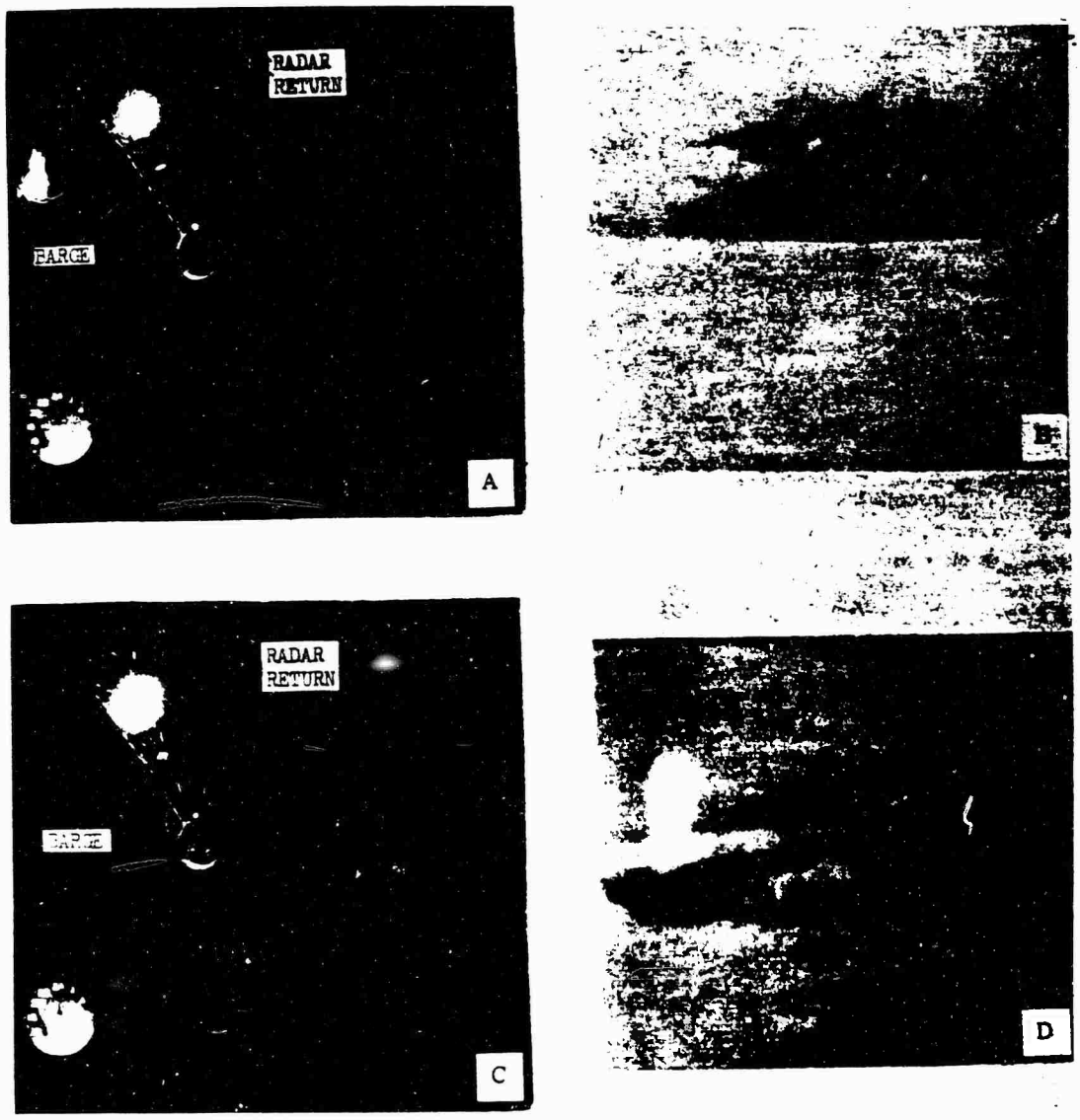

Figure 3.21 Shot Koa, SCR-584, PPI-scope returns, Fred radar site. The area covered by the photos is explained in Figure 3.18. Photos A and C are H + 3 minute and H + 4 minute displays of target persistency. Photos B and D, optical views of the physical event, are the time equivalents of the radar returns.

the PPI resolution of the target. The returns possessed fair approximations of the dimensions of the fireball in the range direction but not in the azimuthal direction.

3.5.3 Radar Set AN/MPG-1. The AN/MPG-1 operated B mode had a maximum range of only 28,000 yards. Shot Koa was at a range of 42,200 yards and, even though the shot afforded a large target, it was not acquired as a second-time-around echo. This failure to acquire the target is

explained by the fact that the return occurred at a time interval when the main bang and clutter were displayed on the B scope.

3.6 SHOT WAHOO

3.6.1 Radar Set AN/MPG-1, B Scope. This was an underwater shot. Since there was no fireball, the sole purpose of Project 6.5's participation was to gather documentary film that would serve as a basis of comparison among shots with and without fireballs. The data proved fruitful because it differed from that of other shots. The return was earlier in time, it lacked the semicircular and annular configuration characteristic of the other returns, and it was more intense and widespread than the other returns. The first return, corresponding to the water dome, appeared at H + 0.81 second (Figure 3.22A). The next radar look presented the water plume at H + 0.94 second (Figure 3.22B). At H + 1.06 seconds the base surge was well depicted on the radar screen (Figure 3.22C). As early as H + 1.75 seconds, waves could be distinguished from the base surge. The 69-second life history of the detonation is pictorially told in Figures 3.22 through 3.24. The barges were seen to appear and disappear as they rode in the crest or trough of the spreading waves. They continued to do this on the film, even after the blast target disappeared from the radar screen.

3.6.2 Radar Set SCR-584, A Scope. The first faint target on the SCR-584 A scope appeared even earlier in time than that on the B scope of the AN/MPG-1. The return was timed at H + 0.60 second (Figure 3.25B). The higher power output of the SCR-584 could easily account for this fact, as there was no question of fireball absorption in this case. The development from first return to maximum growth is shown in Figure 3.25. The amplitude and intensity indicated that this shot presented a large target.

3.7 SHOT HOLLY

3.7.1 Radar Set SCR-584, PPI, Eniwetok. During Shot Holly, ground zero was pinpointed to the actual shot barge in the lagoon. Before time zero, the camera was held open while the antenna made a wide sweep over the target area. This action overexposed the film but revealed three barges in the vicinity of the expected ground zero. Later measurements identified the central barge as the shot barge. Because of the relatively short range of the shot, the PPI range sweep was changed from long range (70,000 yards) to short range (35,000 yards).

The first return was received at approximately time zero and was another case of the bright-point return (Figure 3.26A). The next antenna sweep at H + 2 seconds revealed a target that possessed the familiar characteristics of a nuclear detonation (Figure 3.26C). The target reached maximum dimensions within 7 seconds. The growth of the target and its persistency for 74 seconds are shown in Figures 3.26 through 3.28.

since both shots occurred at approximately the same range. The resolution of the target as depicted on the PPI scope did not allow a study of the nature of the return. The same may be said for all PPI presentations.

3.7.2 Radar Set SCR-584, A Scope. The A-scope presentations of this shot were in good agreement with the PPI views. The immediate appearance and disappearance of the bright-point return within 250 msec after time zero is shown in Figure 3.29. The target again appeared at approximately H + 2 seconds. Its maximum growth was smaller in amplitude than that of Shot Koa despite the fact that the latter was at twice the range. The antenna angle of elevation was slightly less for Shot Holly than for Shot Koa. The lower grazing angle allowed more grass and clutter to appear on the A scope.

If all shots had occurred at the same range, then relative amplitudes of the return would have afforded good measurement of yield, provided that receiver saturation was not reached or calibrated dial settings were not disturbed. In the case of Shot Holly, only a comparative estimate of yield could be made with respect to the known parameters of Shot Koa.

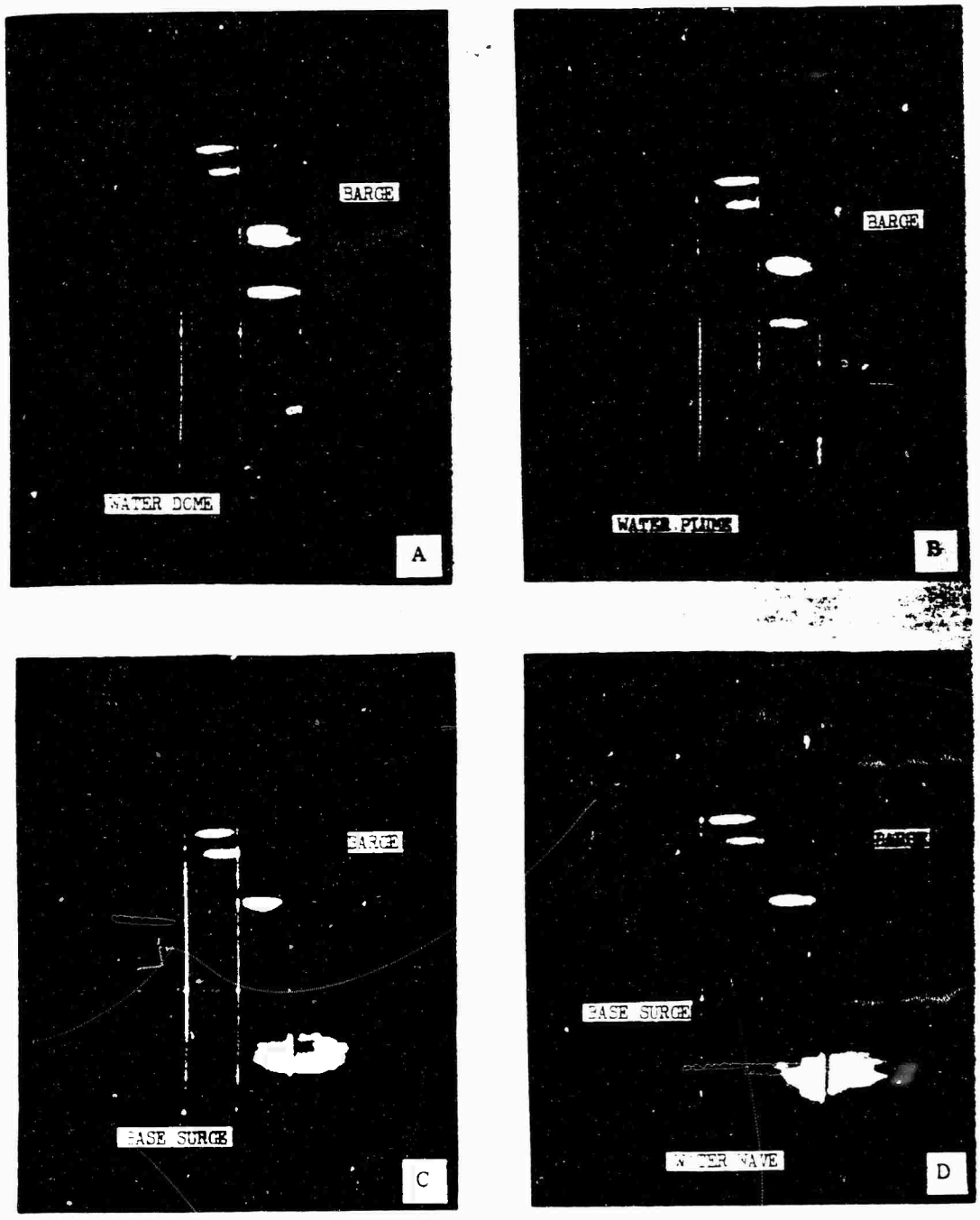

Figure 3.22 Shot Wahoo, AN/MPG-1 B-scope returns, Fred radar site. The horizontal grid lines represent 1,000-yard range markers with the center line at a range of approximately 20,240 yards. The vertical grid lines are 1 degree azimuth markers with the center one located at S 86° W. The water-dome radar return of photo A is located by the radar grid lines at a bearing of S 87° W and a range of 19,743 yards from the radar site. Photo A shows the wager dome as the earliest radar return of an underwater shot at H + 0.81 second. Photo B shows the water plume as a growth of the target at H + 0.94 seconds. Photo C shows the base surge as a radar return at H + 1.06 seconds. Photo D shows the base surge as a water disturbance at H + 1.37 seconds. Note the disappearance of the closest barge in photos C and D.

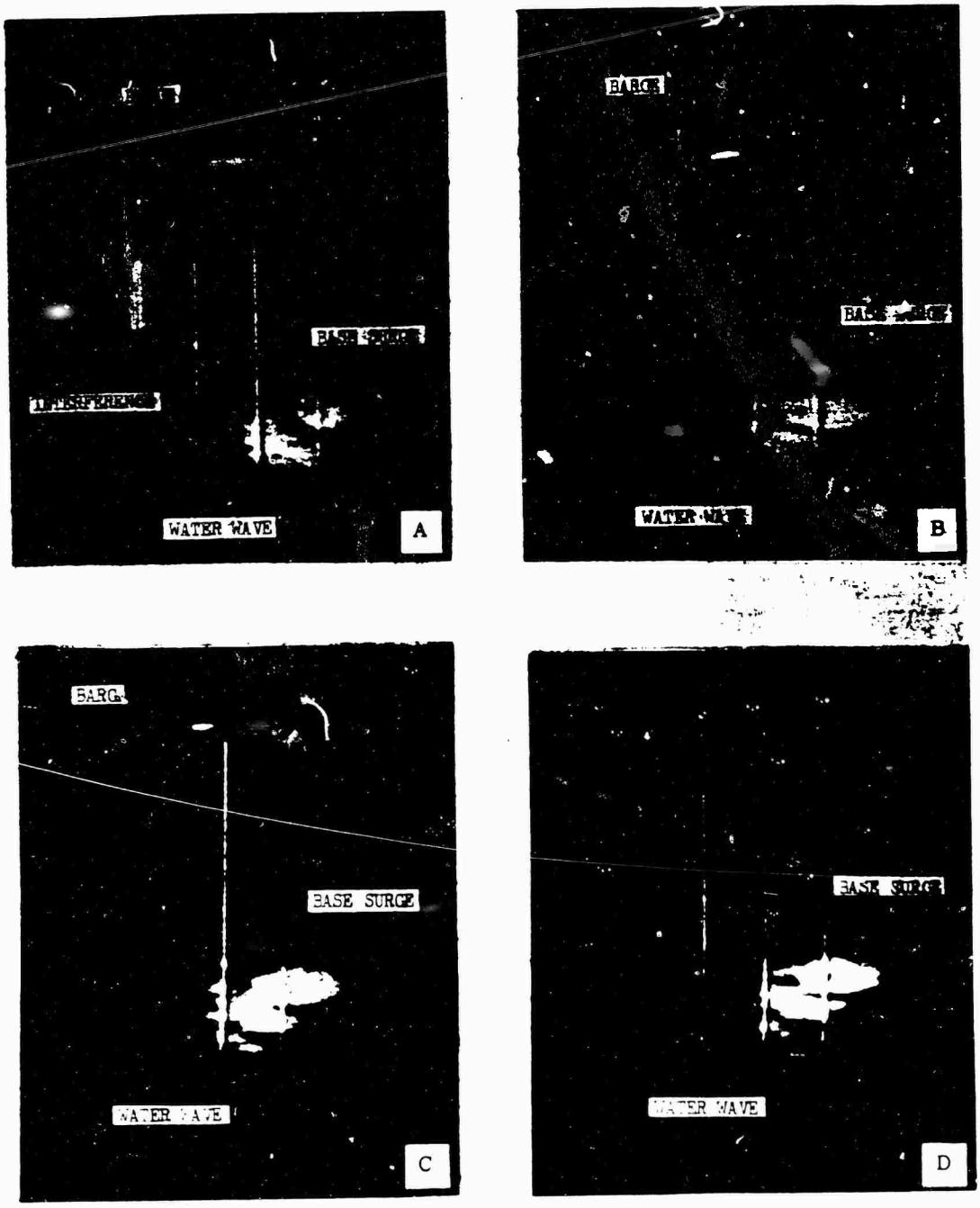

Figure 3.23 Shot Wahoo, AN/MPG-1 B-scope returns, Fred radar site. The area described by the photos is explained in Figure 3.22. Photos A through D show the chronological development of the water disturbance and waves breaking away from it at H + 1.81, H + 2.75, H + 3.0, and H + 3.25 seconds, respectively. Note in photo D the disappearance of the farthest barge, 1,500 yards from ground zero.

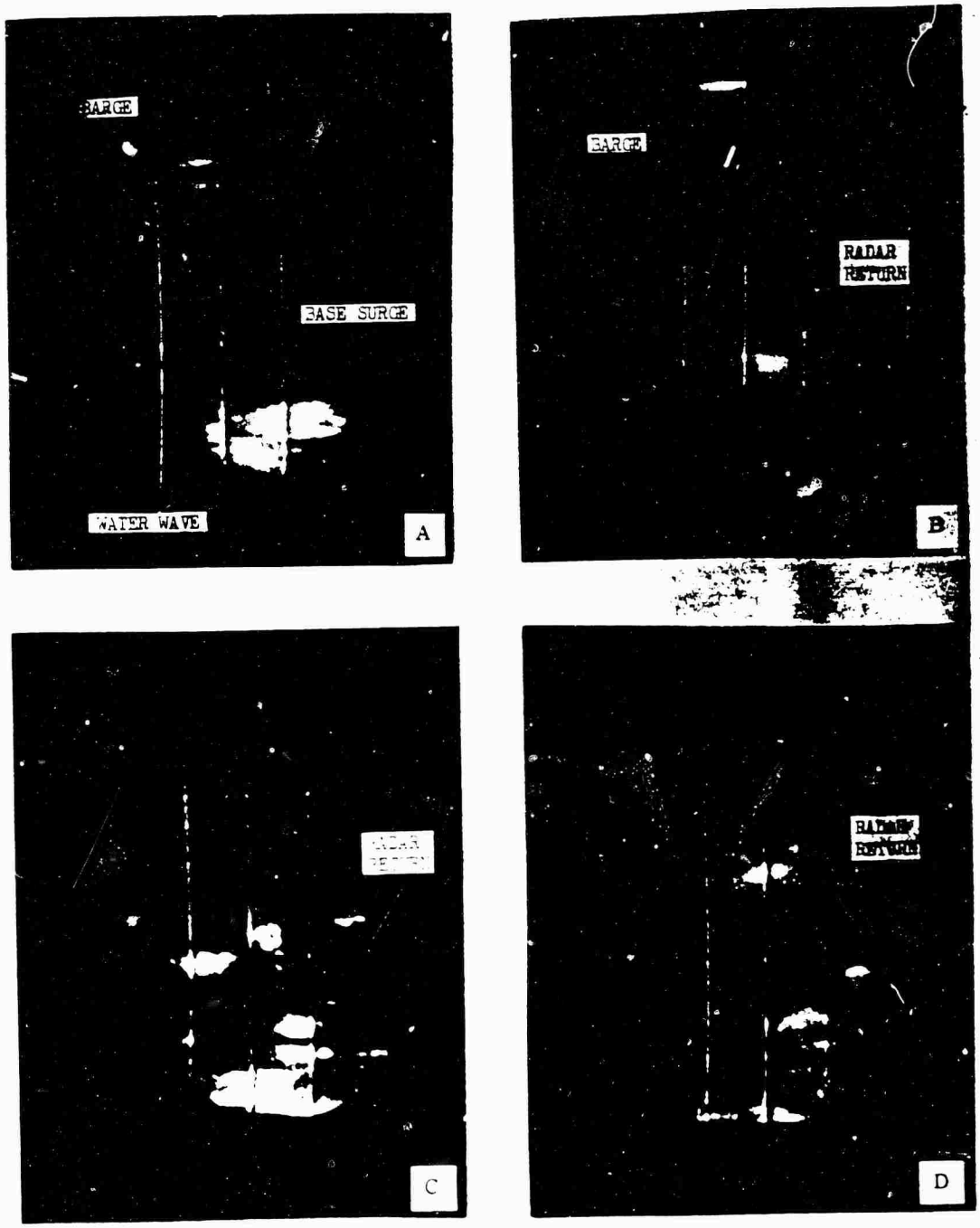

Figure 3.24 Shot Wahoo, AN/MPG-1 B-scope returns, Fred radar site. The area covered by the photos is explained in Figure 3.22. Photos A through D show the chronological development of the water disturbance at H + 3.63, H + 7.56, H + 32.37 and H + 45.25 seconds, respectively. Note the reappearance of some of the barges.

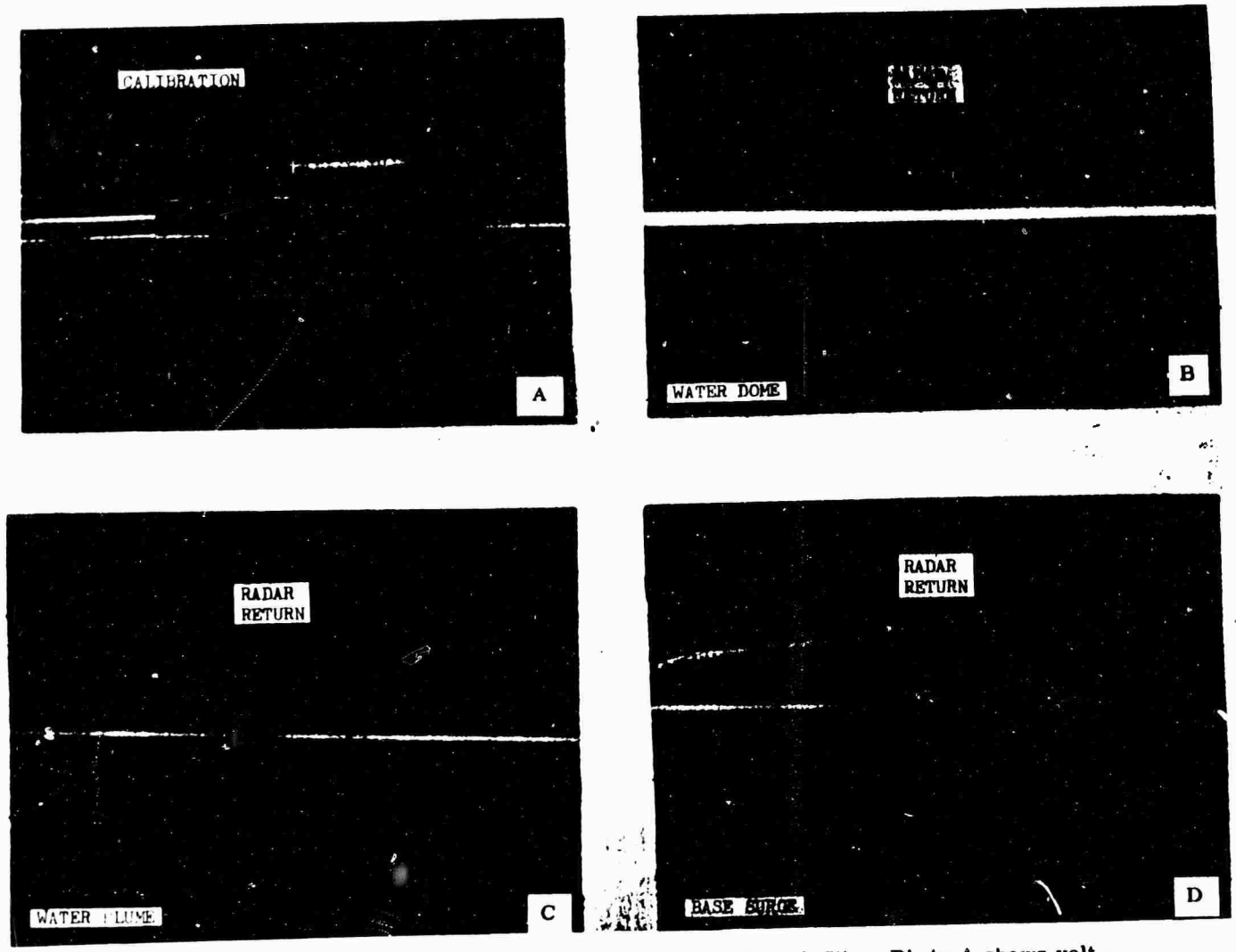

Figure 3.25 Shot Wahoo, SCR-584 A-scope returns, Eniwetok Site. Photo A shows voltage calibration of A scope from 1 to 4 volts. Photo B displays earliest return at H + 0.6 second, photo C shows amplitude growth at H + 0.9 second, and photo D displays maximum amplitude growth at H + 1.1 seconds.

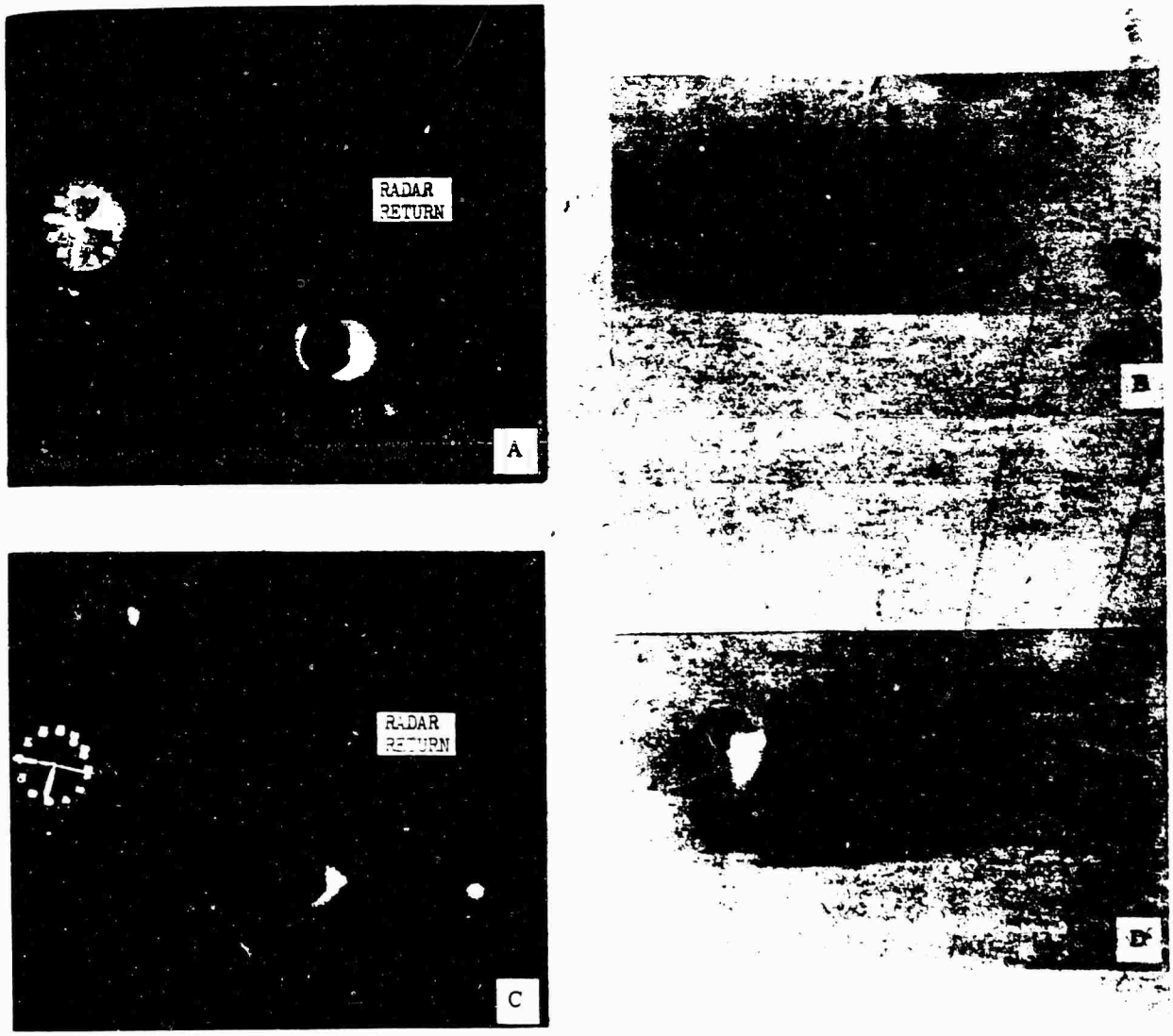

Figure 3.26 Shot Holly, SCR-584, PPI-scope returns, Fred radar site. In photos A and C, the center of the black dot represents the location of the radar site. A radial line drawn from it through the radar return would locate the target at N 5.5° E in azimuth and a range of 23,105 yards from the radar site. Photo A shows a bright-point return at approximately time zero. Photo C shows a 2-second growth of the target, Photos B and D are the time-equivalent motion-picture frames of the physical event, and represent a view 3,600 feet in width at a distance of 23,000 yards.

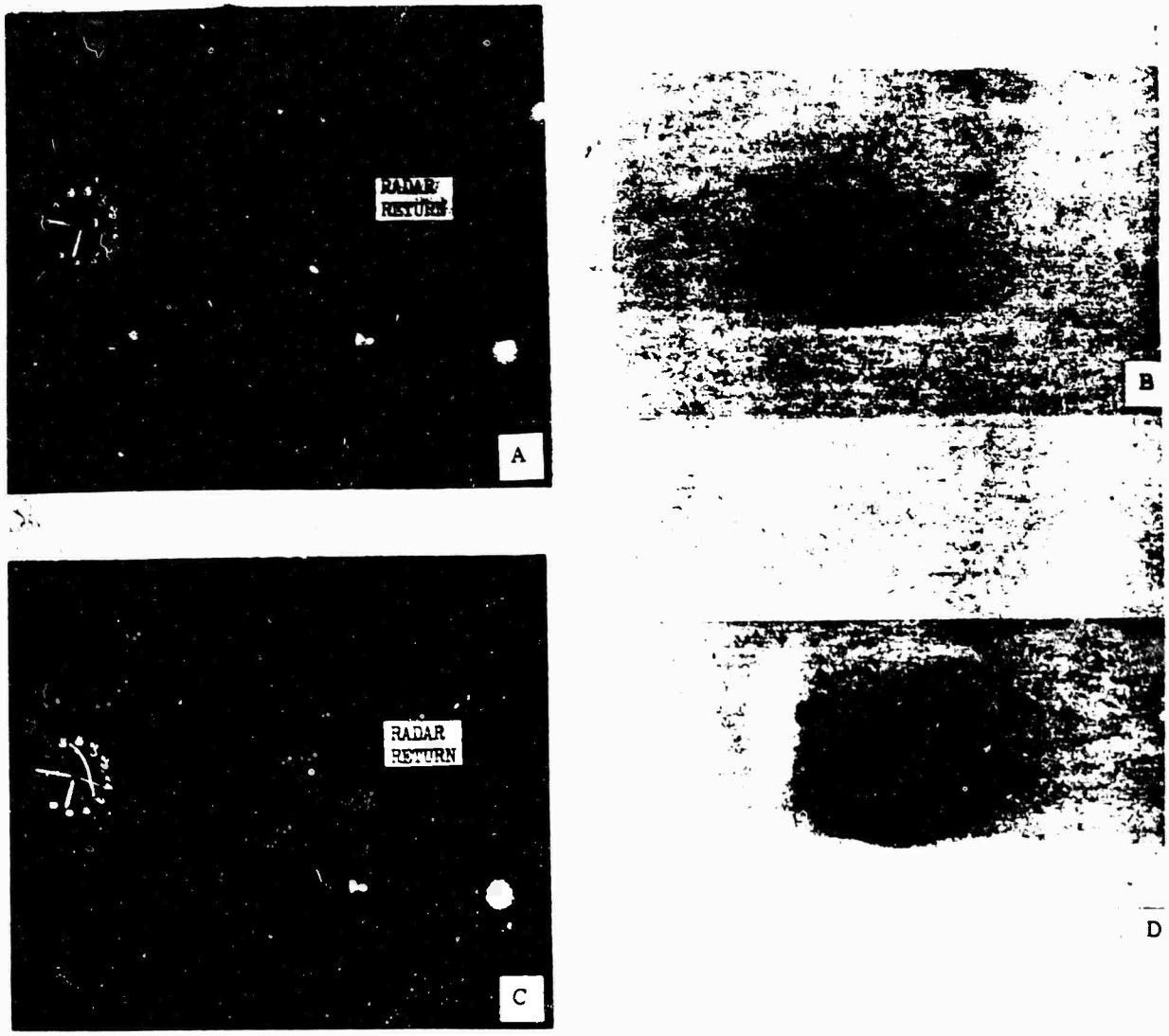

Figure 3.27 Shot Holly, SCR-584, PPI-scope returns, Fred radar site. The area covered in the photos is explained in Figure 3.26. Photo A shows the chronological growth at H + 3 seconds. Photo C displays maximum target growth at H + 3.5 seconds. Photos B and D are optical views of the physical event and time equivalents of the radar returns.

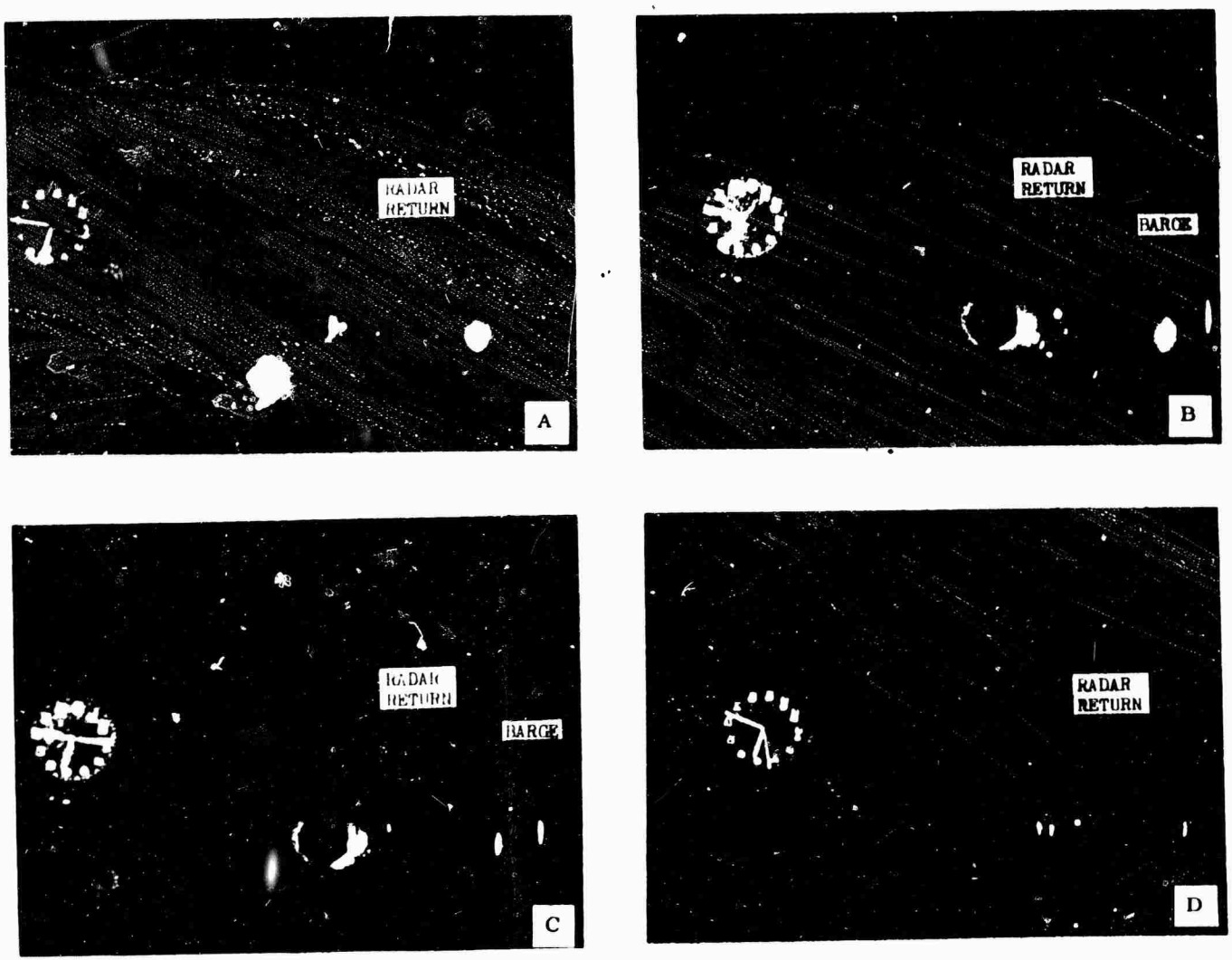

Figure 3.28 Shot Holly, SCR-584 PPI-scope returns, Eniwetok Site. Photos A and B show strong persistency of target at H + 4 and H + 23 seconds, respectively. Photos C and D show decay rate at H + 60 and H + 70 seconds, respectively.

3.7.3 AN/MPG-1, Local B Scope. The early return of Shot Holly as viewed on the local B scope at H + 2 seconds placed ground zero at a range of 23,105 yards from the radar site and at a bearing of 5.5 degrees (Figure 3.30). These measurements were in good agreement with predicted values.

The drift of the target from its

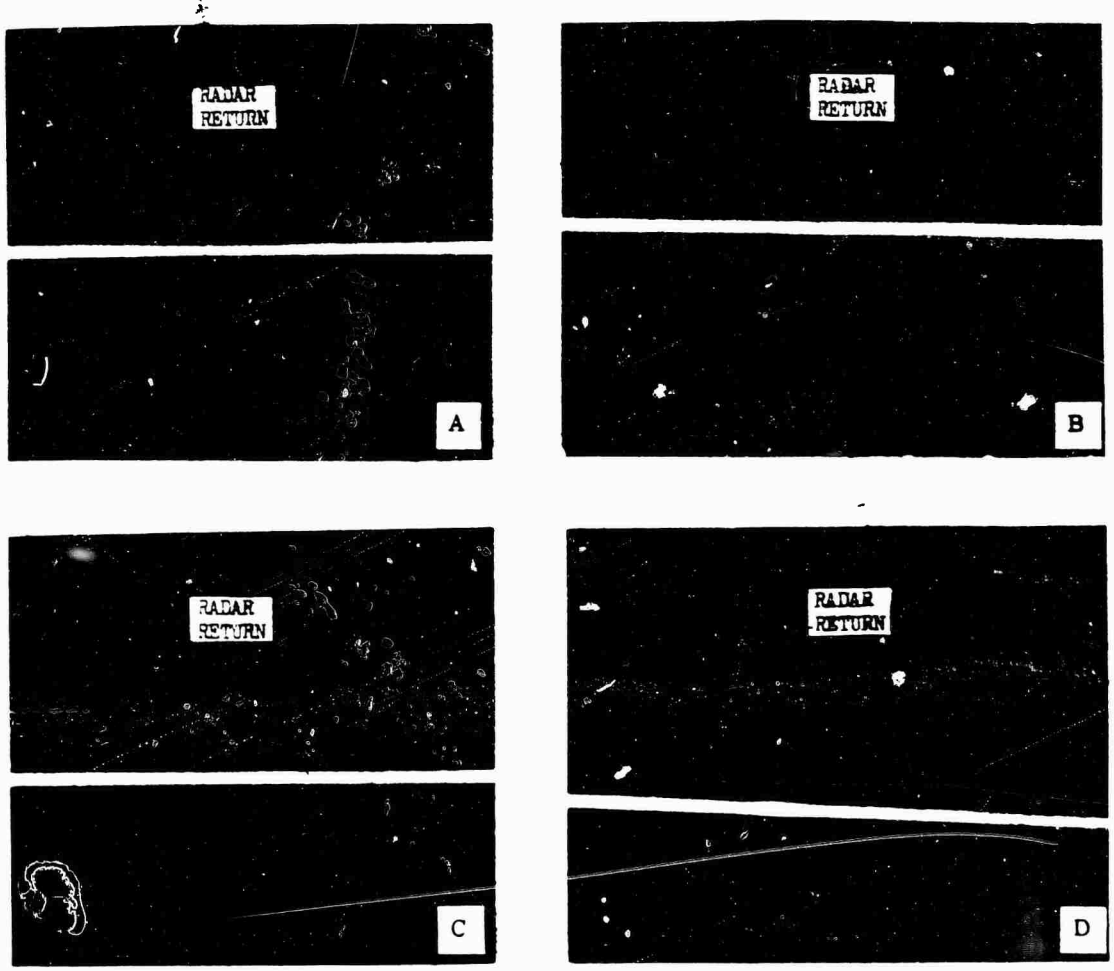

Figure 3.29 Shot Holly, SCR-584 A-scope returns, Eniwetok Site. The four photos represent 250 msec of time and present a bright-point return acquired at approximately time zero. The first faint return is shown in photo A, amplitude growth is shown in photo B, maximum growth and intensity are shown in photo C, and decay is shown in photo D.

original position across the 1-degree azimuth markers of the scope was indicative of the wind velocity on that day (Figures 3.30C and D).

3.8 SHOT TEAK

The radar and the photographic instrumentation on board the USS Cogswell performed well. The radar frequency used was 205 Mc. No useful A-scope recordings were obtained, because of difficulties with the recording equipment. The radar on the USS DeHaven (operating at 220 Mc) performed well, with the exception in intermittent failure of the antenna to follow the manual

scan pattern during the period from H - 30 to H + 30 seconds. This failure appeared to be due to accelerations in the antenna structure caused by the roll of the ship.

At H + 56 seconds, a return at a range of about 192 miles appeared on the PPI scope of the radar on the USS Cogswell. This time delay in receiving a return agreed well with the findings

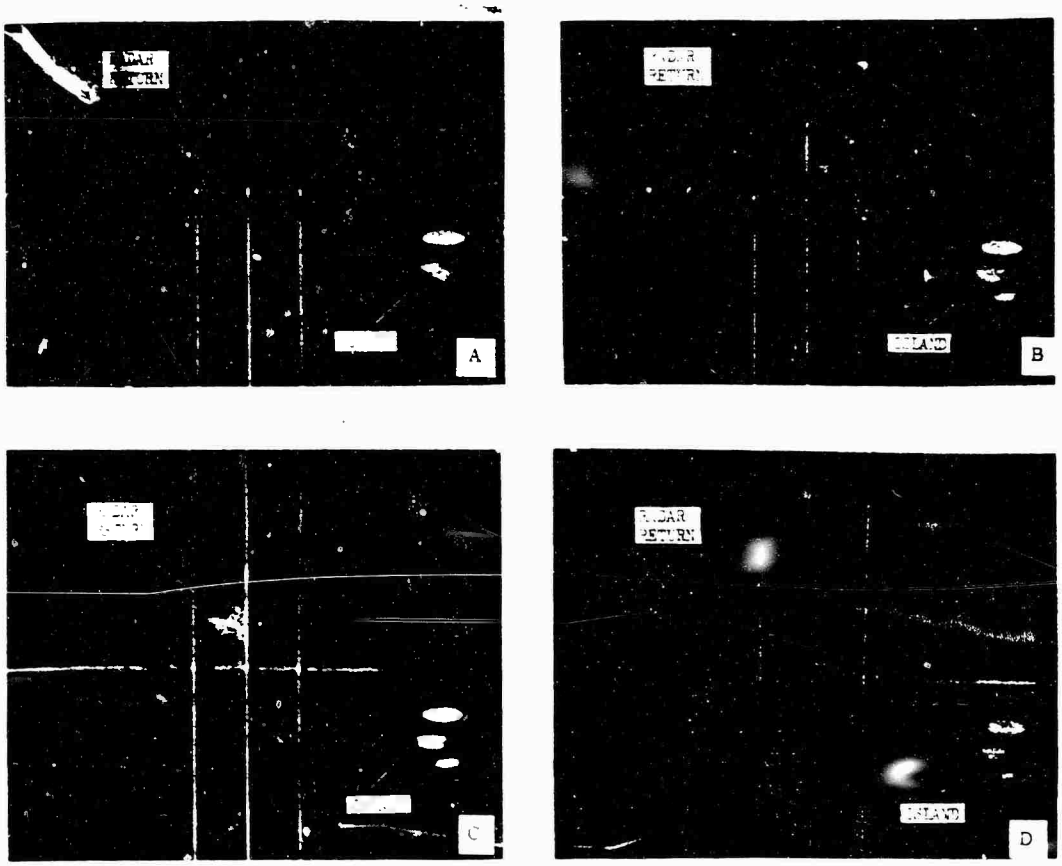

Figure 3.30 Shot Holly, AN/MPG-1 B-scope returns, Fred radar site. The horizontal line is a range marker, representing a range of 22,900 yards from the radar site. The top and bottom of the photos with reference to this line represent ranges of 23,900 yards and 21,900 yards, respectively. The vertical grid lines are 1 degree azimuth markers with the center one located at N 4.9° E. The radar grid lines locate the radar return at N 5.5° E and a range of 23,105 yards from the radar site. Photo A shows the first return at H + 2 seconds (in the central portion, [illegible] the [illegible]age of Site Yvonne (at the lower right). Photo B shows the nondescript cloud pattern that follows the annular return. Photos C and D show dispersion, wind-drift, and fadeout of the return at H + 70 seconds.

of Project 6.11 (Reference 17). This echo appeared as two discrete concentrations of noise centered approximately at bearings of 188 and 199 degrees. (The bearing at which the detonation occurred was 198 degrees, and the slant range to the target at time zero was about 156 naut mi.) On the next scan (beginning at H + 60 seconds) the two discrete returns had moved toward each other and appeared to be less intense. This total mass of signal was centered at about 192 degrees, at a range of about 192 miles. The succeeding scan, beginning at H + 64 seconds, showed a small concentrated target centered at 194½ degrees, at a range of about 204 miles. No further returns were observable. Figures 3.31, 3.32, and 3.33 are photographs of these targets on the PPI display.

A completely satisfactory explanation cannot be given for the Shot Teak returns received on the radar of the USS Cogswell. The returns appeared as large increases in the general back-

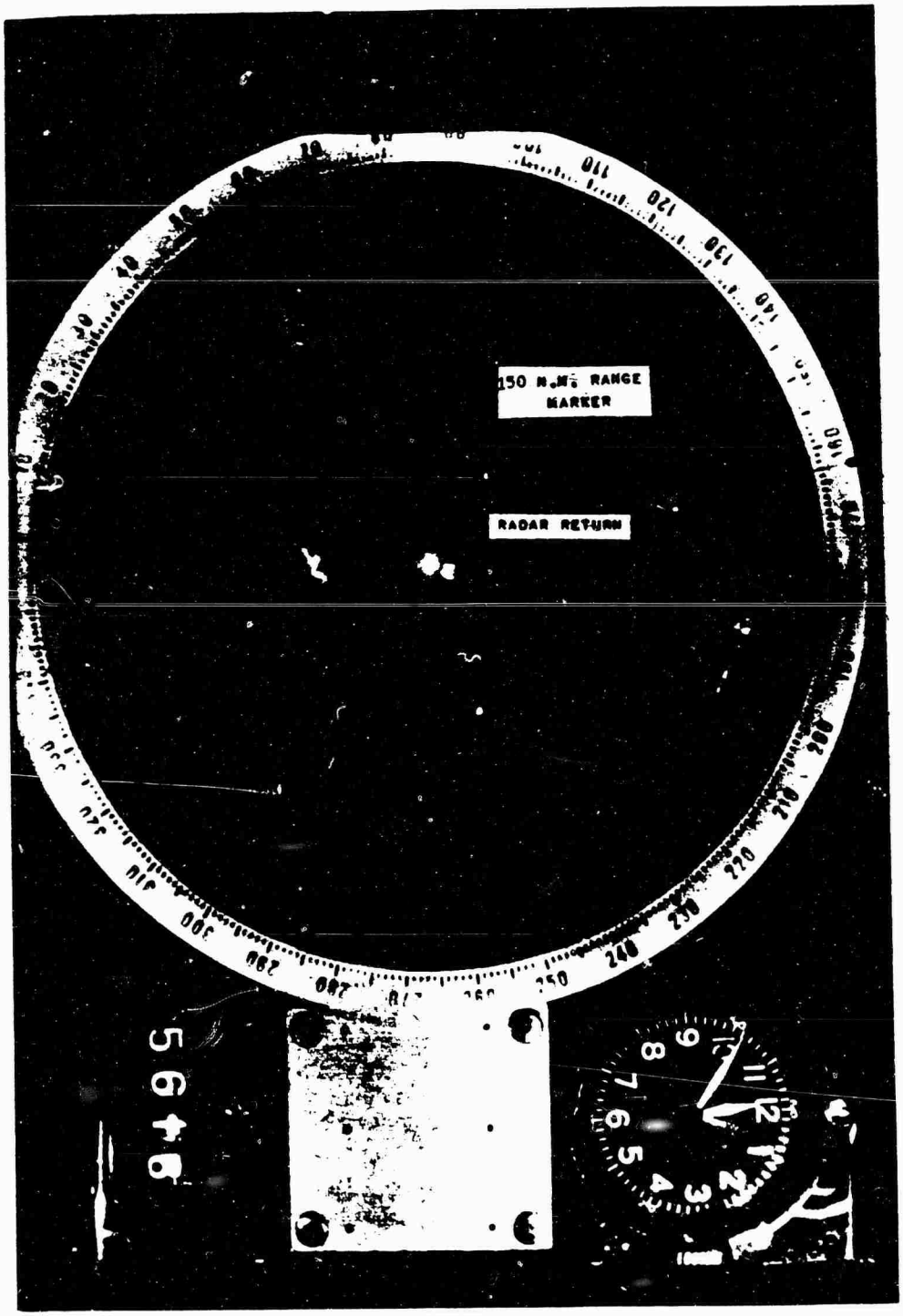

Figure 3.31 Shot Teak, SRb PPI-scope returns, USS Cogswell. The photo shows a wide-azimuth radar return at H + 56 seconds. A 150 nautical-mile range marker is given to facilitate range determination.

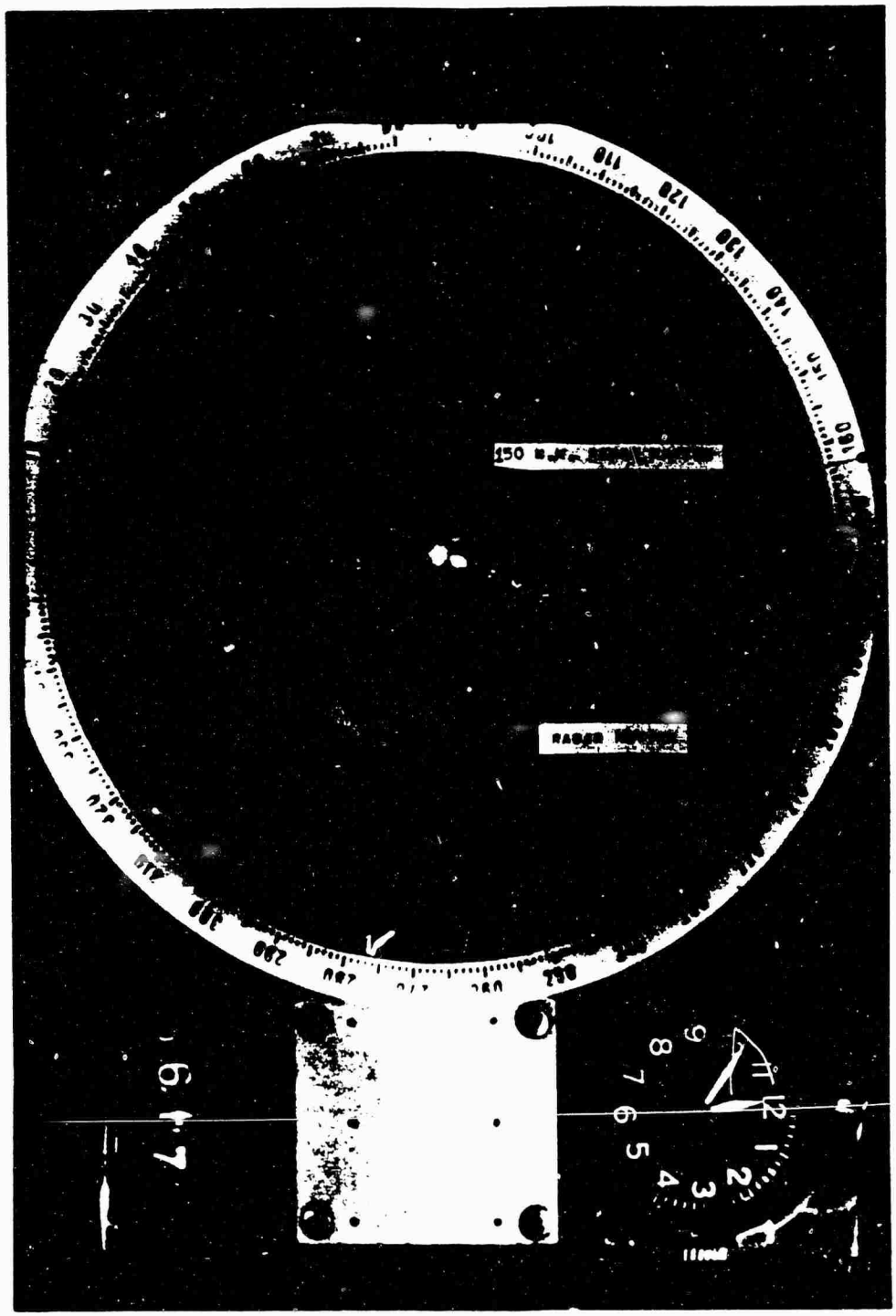

Figure 3.32 Shot Teak, SRb PPI-scope returns, USS Cogswell. The photo shows a wide-azimuth radar return at H + 60 seconds. A 150 nautical-mile range marker is given to facilitate range determination.

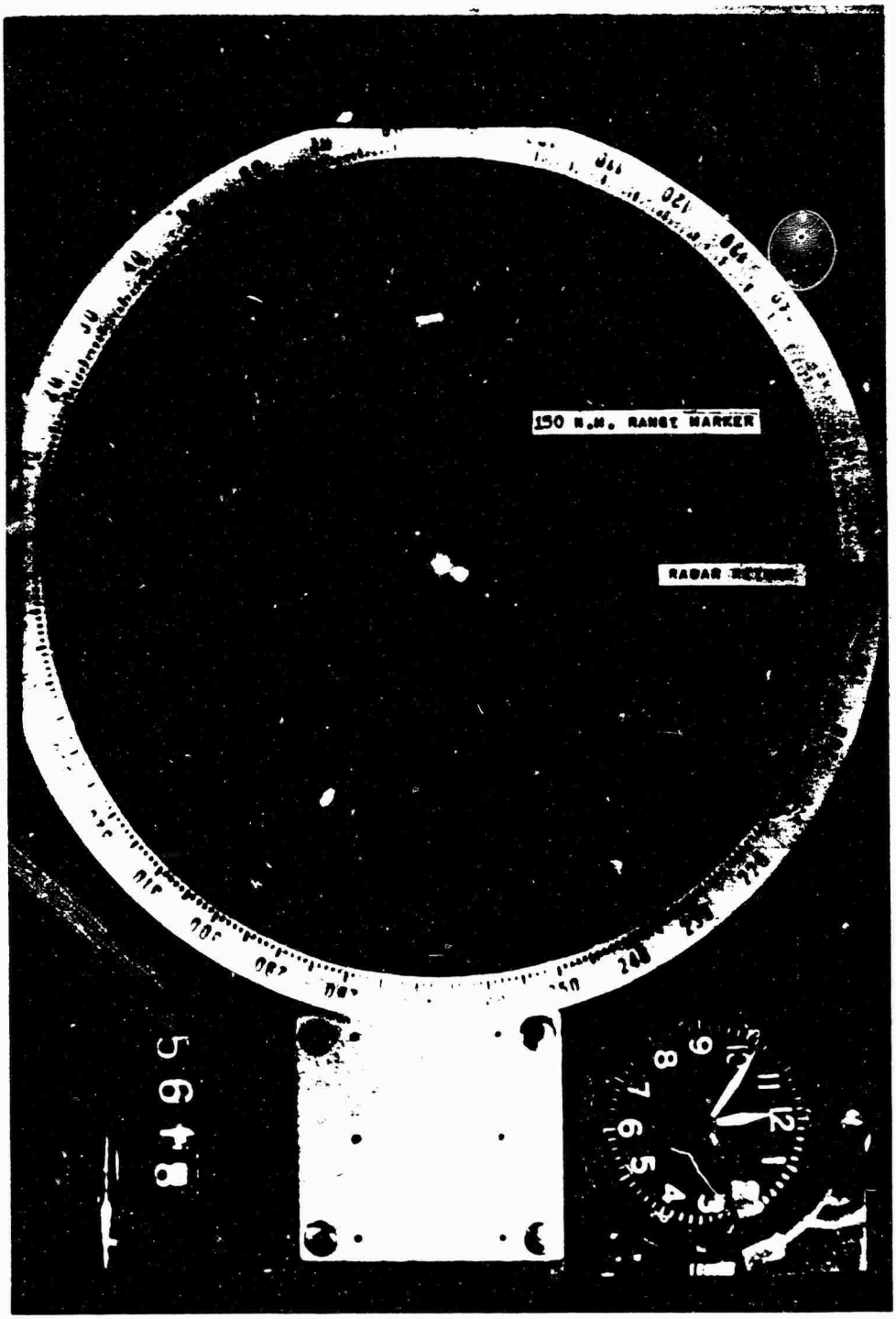

Figure 3.33 Shot Teak, SRb PPI-scope returns, USS Cogswell. The photo shows a radar return at H + 64 seconds. A 150 nautical-mile range marker is given to facilitate range determination.

ground noise. Because of the good azimuth and time correlation and fair range correlation, the returns seemed to be caused by the burst. Since Shot Teak was detonated at a 50-mile height, the returns were probably not caused by water vapor or shock effects. Although missiles were being fired through the burst region both before and after time zero, the rather primitive, low-powered SRb radar was probably incapable of detecting these missiles at the range involved.

It seems reasonable to attribute the Shot Teak returns to reflections from increased ionization in the neighborhood of the burst point. Electron densities of the order of 5×10^8 per cm^3 are needed to reflect 200-Mc energy. At times less than 1-second postshot, electron densities considerably higher than this figure probably existed in the fireball (Figure 3.34). The delay of about 1 minute in receiving an echo was probably due to attenuation by the ionization present in the denser atmosphere between the radar and the burst point (Reference 18). Free electrons disappear more rapidly in the absorbing layer, thus permitting the radar energy to penetrate to

Figure 3.34 Graphs of equal electron density in the upper atmosphere at H + 1 second, Shot Teak. Height (in km) is plotted against range (in km). Electron density is given in electrons/cm^3.

a depth where reflection and return to the radar set is possible. At ranges of less than 10 km from the burst, electron densities of the order 10^8 probably existed between H + 56 and H + 68 seconds, thus permitting the reflection of radar energy from the vicinity of the burst (Figures 3.35 and 3.36). (For the source of these figures, see Section 1.3.2.)

An explanation cannot be given for the apparent discrepancy between the slant range to the burst point and the indicated range of the radar echo. It is possible, although unlikely, that the sweep circuits or range-calibration circuits operated erratically. However, there was no evidence to support this speculation, since the equipment had been carefully checked and adjusted by qualified technical representatives within the 48 hours preceding Shot Teak. The lack of more data from this shot precluded the formulation of definite conclusions.

Page 60 is deleted

No targets were discernible at the station aboard the USS DeHaven. Failure to obtain returns at this station is believed to have been due to the high elevation angle (about 35 degrees) at which the detonation occurred with respect to the USS DeHaven.

At time zero, both destroyers were within 1,000 yards of their assigned stations, proceeding at 10 knots on a course of 108 degrees. This placed Johnston Island at a bearing of 198 degrees true, or at 90 degrees relative to the ship's headings. The ships were proceeding at an angle into moderate swells, which produced rolls of from 3 to 5 degrees. Cloud cover was estimated to be 0.05 to 0.1, with a clear path existing between each of the ships and the point of detonation. By H + 3 minutes an ionization (aurora) trail had traversed the sky in a northerly direction from the point of detonation and appeared (to observers on the USS DeHaven) to extend to within 45

TABLE 3.3 CHRONOLOGICAL DEVELOPMENT OF SIGNIFICANT RETURNS

Shot	Bright-point Return	Earliest Return	Annular Return Appears	Annular Return Disappears	Maximum Growth on PPI	Last Return
		sec	sec	sec	sec	sec
Cactus	—	H + 2.13	H + 3.69	H + 7.94	—	H + 77
Fir	—	H + 84*	--	—	—	H + 104*
	—	H + 22.7†	—	—	—	H + 100†
Butternut	yes	H + 2.0‡	H + 3.75	H + 6.81	H + 8	H + 145‡
	—	H + 2.0§	—	—	—	H + 100.63§
Koa	yes	H + 2.2¶	—	—	H + 15	H + 160¶
	—	H + 2.0‡	—	—	—	H + 490‡
Wahoo	—	H + 81§	—	—	H + 6	H + 69§
	—	H + 0.60‡	—	—	—	—
Holly	yes	H + 2.0¶	H + 3.67	H + 8.03	H + 7	H + 74¶
	—	H + 2.0‡	—	—	—	H + 74‡
	—	H + 2.0§	—	—	—	H + 70§
Teak	—	H + 60‡	—	—	—	H + 72‡

* Enwetok
† Rongelap
‡ PPI-Scope
§ B-Scope
¶ A-Scope

degrees of the northwestern horizon, centered at about 265 degrees azimuth relative to the ship's heading. This phenomenon caused no observable effect on either of the shipborne SRb radars.

The SRb radars used during Shot Teak caused severe interference to beacon receivers located on the destroyers and manned by Project 6.12 personnel. Consequently, Project 6.5 did not participate in Shot Orange.

3.9 DISCUSSION OF RESULTS

3.9.1 Interpretation of the Data. The B- and PPI-scope displays with their symmetrical time-growth patterns, duration, and decay established identifying characteristics of a nuclear detonation. The A-scope presentations possessed no characteristics that could differentiate between various types of targets for the purpose of target identification.

The time history of an atomic explosion as depicted by radar techniques was divided into discrete time intervals (Table 3.3). First, the sporadic occurrence of the bright-point return on several occasions at H + 0.2 second, together with its immediate appearance and disappearance, offered no opportunity for time-resolution studies of this phenomenon. Its appearance, which

depended on the chance orientation of the antenna at time zero, aided in establishing ground zero to a greater degree of accuracy, but the extremely low probability of acquiring this return in a search situation rendered it unreliable for this purpose. Second, there was a 2-second delay of the earliest return for S- and X-band radar (used on surface shots), and a 1-minute delay for VHF radar (used on Shot Teak). The 2-second delay indicated the absence of frequency dependence for S-and X-band returns. Third, maximum growth of the symmetrical scope patterns occurred at 7 to 15 seconds after time zero, which was in good agreement with recorded results of previous tests (References 16 and 19). Furthermore, measurements of maximum diameter were indicative of yield (Figure 3.37). Fourth, the unsymmetrical or nondescript pattern associated with the decay stage remained on the radar screen from 1 to 8 minutes, depending on the yield of the detonation.

3.9.2 Reliability of the Data. Concerning time-resolution studies of the documentary film, the greatest possible error was ±0.03 second for the zero-time marker to score the passing film frame. Sufficient time was allowed for the cameras to reach maximum speed. The error in constant camera speed, by manufacturer's specification, was less than the above-estimated value.

With regard to measurement errors in determining ground zero and slant height, the following points were considered. First, the radar site was surveyed to a geographical point on Site

Fred. This survey established a true north or zero-degree azimuth reference point. The radar azimuth positioning system, which had a 36-to-1 gear ratio, was set to this zero reference with a possible error of 1 mil. All islands of the atoll were viewed on the PPI scope as a check on the zero azimuth setting. Second, the radar elevation system was set to a zero reference by a level that was built into the antenna system. Known tower heights were viewed with a cross-hair telescope, also a built-in feature of the antenna system, as a check on the zero elevation setting. A possible error of 2.5 mils was established for the antenna elevation system. Third, by design the radar range was accurate to 10, 25, and 100 yards for radar sets AN/MPG-1, SCR-584, and SRb, respectively. Fourth, map measurements used to predict the range value of ground zero were correct to 33.3 yards. The accuracy of the map itself was not noted among the map indices. The correlation of map ranges and radar ranges averaged, over all shot participations, to a radar error of 46.8 yards in determining ground zero (Table 2.1). Fifth, a film viewer with movable crosshairs (calibrated to 0.001 inch) was used as a data analyzer and measuring device for determining range, azimuth, diameter, and center of the radar returns. On the PPI-scope films, range was measured from the center of the scope to the center of the return with a maximum readout error of 17.2 yards. On the B-scope films, range was measured perpendicularly from the center of the return to the central horizontal grid line, which was a range marker of known value. The maximum readout error was 5 yards. The azimuth of the PPI presentations was measured by the angular displacement of the center of the return from the zero-degree reference of the viewer's graduated circle. This zero-degree reference was coincident with the zero-degree setting of the PPI-scope film. The maximum readout error was 4.5 mils. The azimuth of the B-scope presentations was measured by the linear displacement of the center of the return from the known azimuth markers scored on the film as vertical grid lines. The maximum readout error was 1 mil. The diameters of the radar returns of the B-scope presentations were measured in the range direction and had the same maximum readout error as the range measurements stated above. The center of the return was determined from the diameter measurements. Sixth, minimum target areas for possible reflections were calculated for discrete ranges that were representative of all shots in which Project 6.5 participated. A summary of these calculations is given in the Appendix.

3.9.3 Correlations With Data From Previous Tests. The following are points of correlation with data from previous tests. First, radar returns from surface shots were not received from the fireball (Reference 11). Second, S- and X-radars detected surface shots of or more (References 1, 2, 5, and 6). Third, bright-point returns were received at approximately H + 0.2 second (Reference 5). Fourth, the semicircular and annular returns of ground radar corresponded in time to the horseshoe and ring patterns of air-borne radar (References 2 and 5). Fifth, the initial 2-second delay of the earliest return agreed with the time of the earliest return by air-borne radar (Reference 9). Sixth, the varying sizes of maximum growths for different shots suggest that maximum diameter might be a measure of yield (References 9 and 11). Seventh, ground zero can be determined to a good degree of accuracy (References 3, 5, and 10). Eighth, indirect bomb damage assessment (IBDA) can be made to a fair degree of accuracy by radar techniques (References 4, 5, 6, 8, 9, 10, and 11). Ninth, height-of-burst measurements can determine if the fireball touched or nearly touched the ground (Reference 5). Tenth, fast scan rate proved effective for time resolution and high information content studies (References 7, 11, and 20).

3.9.4 Estimate of Satisfaction of the Objectives. A study of the data indicated that radar returns were not received from the fireball. For surface shots, ground zero can be determined to an accuracy of ± 140 feet by ground radar. The margin of error is based on both the range accuracy of the radar set and the ability of the radar operator to place a range marker or scope crosshairs on the center of the scope pattern. The proportionality between maximum target size and yield of the device indicated that maximum size might be used as a rough measure of yield (Figure 3.37). If devices of various yields were detonated at the same range, sufficient

sampling would afford data for a more accurate calibration curve of maximum diameter versus yield. Concerning slant height, the data from one high-altitude shot afforded little basis for establishing this objective for high altitudes, but the zero elevation angle of the antenna for known surface shots clearly indicated that the fireball touched the surface.

3.9.5 Effectiveness of the Instrumentation. The effectiveness of the instrumentation is shown by the following considerations. First, the frequencies of the three radar sets were well spread over the radio spectrum to measure frequency-dependent characteristics of the burst as exhibited by the time-arrival of the earliest return, if such occurred. Second, the beam pattern of the antennas afforded ample volumetric coverage of a fast-growing target. Third, the fast antenna scan rate of the AN/MPG-1 was effective in resolving the coordinates of ground zero and in affording a basis for high-information studies. Fourth, the high-speed cameras, together with the $^1/_{120}$-second time markers, allowed for good time-resolution study of each event. Fifth, the magnetic tape recorder for the A scope of the SRb on the USS Cogswell was not adequately monitored. As a result, the radar video could not be satisfactorily distinguished from weak 60-cycle noise which was present on the tape. Sixth, the antenna-positioning circuits were adjusted to give minimum error for azimuth and elevation. Seventh, range dials, range markers, and range sweep circuits of the various scopes were adjusted to give minimum error for range measurements. Eighth, on preshot days, the radars were given peak-performance tests to assure maximum efficiency.

Chapter 4
CONCLUSIONS and RECOMMENDATIONS

4.1 CONCLUSIONS

Based on the data obtained by Project 6.5, it is concluded that no radar echoes were received from the fireballs of any Operation Hardtack detonations. For surface shots, radar techniques can be used to determine ground zero to an accuracy of ± 140 feet. The proportionality between maximum target size and yield of the device indicated that maximum size might be used as a rough measure of yield. Participation by this project in one high-altitude shot (Shot Teak) afforded no basis for a statement relative to the determination of height by radar techniques.

A number of unresolved difficulties should be mentioned. The shock wave was not detected by this project during the Hardtack series. This could be due to the siting of ground radar (as opposed to air-borne radar). Also, the failure to receive an echo for the order of 2 seconds on 10,000 Mc remains unexplained. Although one may be tempted to attribute this failure to absorption, there were no targets within range of the set beyond the detonation point to serve as tests. A completely transparent region would also yield no echo. Moreover, on the occasions when the 2,800-Mc radar received echoes from beyond the burst point prior to time zero, the echoes did not disappear at time zero.

A careful examination of successive photos for a particular shot yields the following conclusions: (1) the signal is received not from a propagating front, but from a forming front; and (2) the target almost completes a ring with no signal received from the space interior to the ring. Conclusion (1) does not exclude the observed slow rate of growth of the radar target; rather, it emphasizes that the echo could not be that which would result from the propagation of some characteristic disturbance in air, as for example, a shock front. Typical average rates of early target growth are indicated by the following:

Shot	Amount of Growth	Time	Rate
Butternut	137 ft	3.06 sec (49 frames)	45 ft/sec
Cactus	40 ft	3.69 sec (68 frames)	11 ft/sec

These findings are totally different from any previous ones, and suggest condensation around the cooler periphery of the detonation. Further, the appearance of the back side of the ring, albeit weak, indicates propagation of radio waves through the fireball region a few seconds after detonation. This phenomenon requires that the region be sufficiently hot to prevent condensation of vaporized materials (dust, bomb materials, or water), and not hot enough to cause attenuation of 10,000 Mc radio waves. This last condition is not compatible with the existence of a shadow pattern at 9,000 Mc (Reference 5) about 10 seconds after detonation. The final pattern before break-up is explainable as due to condensation of cooled materials throughout the region of detonation.

4.2 RECOMMENDATIONS

4.2.1 Surface Shots. It is recommended that, for future tests involving surface shots, a range of frequencies be used (from 30 to 1,500 Mc). The experiment should include provisions for transmitting and receiving through the burst point both before and after time zero. This type of investigation may yield more information about absorption. In addition, tests should be conducted

in dry as well as in humid areas, and at several altitudes (some with the fireball touching, and others with the fireball not touching the ground.

4.2.2 High-Altitude Shots. Tests like that of Shot Teak should be repeated so that radar observations could be made at various frequencies (from 50 to 700 Mc) in order to try to learn more about the distribution of electron densities with time. The radars used should have fast-scan antenna systems in both azimuth and elevation.

REFERENCES

1. W.J. Merchant; "Radar Photography of Atomic Bomb Explosions"; Working paper No. 19, September 1951; Operations Analysis Division, DCS/O, Hq USAF, Washington, D.C.; Secret Restricted Data.

2. "Scientific Director's Report of Atomic Weapon Tests at Eniwetok, 1951"; Annex 8.3, Operation Greenhouse, WT-33, October 1951; Wright Air Development Center, Headquarters, Joint Task Force Three, Los Alamos Scientific Laboratory; Secret Formerly Restricted Data.

3. J.M. Towey; "Bomb Scoring from Radar-Scope Photos"; August 1951; WADC, Wright-Patterson Air Force Base, Dayton, Ohio; Secret Restricted Data.

4. P.E. Hockman; "A Method for Obtaining IBDA Parameters by Radar"; April 1952; WADC, Wright-Patterson Air Force Base, Dayton, Ohio; Secret Restricted Data.

5. H.F. Boone; "Operational Tests of Radar and Photographic Techniques for IBDA"; Project 6.4, Operation Snapper, WT-534, August 1951; Weapons Components Division, Wright Air Development Center, Wright-Patterson Air Force Base, Ohio; Secret Restricted Data.

6. Frank E. James; "Operational Tests of Techniques for Accomplishing Indirect Bomb Damage Assessment"; Projects 6.5 and 6.4, Operation Buster-Jangle, WT-344, March 1952; Aircraft Radiation Laboratory, Weapons Components Division, Wright Air Development Center, Wright-Patterson Air Force Base, Ohio; Secret Restricted Data.

7. D. Levine; "Application of High-Information-Content Study to Radar-Scope Photography in Operation Upshot-Knothole"; Technical Note WCLR, September 1954; WADC, Wright-Patterson Air Force Base, Dayton, Ohio; Secret Restricted Data.

8. R. Zirkind; "Test of Airborne Naval Radars for IBDA"; Project 6.5, Operation Teapot, ITR-1142, May 1955; Bureau of Aeronautics, Department of Navy, Washington, D.C.; Secret Restricted Data.

9. R. Triantafellu; "Test of Interim IBDA Procedures"; Project 6.1, Operation Castle, WT-924, January 1956; Headquarters Strategic Air Command, Offutt Air Force Base, Nebraska; Secret Restricted Data.

10. G.G. Keeling; "Interim IBDA Capabilities of Strategic Air Command"; Project 6.3, Operation Upshot-Knothole, WT-752, January 1955; Strategic Air Command, Offutt Air Force Base, Omaha, Nebraska; Secret Restricted Data.

11. F.E. James; " IBDA Phenomena and Techniques"; Project 6.2, Operation Upshot-Knothole, WT-751, September 1955; Aircraft Radiation Laboratory, Wright Air Development Center, Wright-Patterson Air Force Base, Ohio; Secret Restricted Data.

12. R. Latter and R.E. Le Levier; "The Effects of Nuclear Explosions on the Propagation of Electromagnetic Waves"; USAF Project Rand Research Memorandum RM-2168; 1 May 1958; Rand Corporation, Santa Monica, California; Secret Restricted Data.

12a. J.A. Kane; "Artic Measurements of Electron Collision Frequencies in the D-Region of the Ionosphere"; Journal of Geophysical Research, 64, 133, 1959; Unclassified.

12b. R.H. Fowler; "Statistical Mechanics"; Cambridge University Press, 1936, Chapters 14 and 15; Unclassified.

13. Department of the Army Technical Manual, Radar Set AN/MPG-1, TM 11-1566; Unclassified.

14. Department of the Army Technical Manual, Radar Set SCR-584, TM 11-1524; Unclassified.

15. Department of the Navy Technical Manual, Radar Set SRb, Navships 900, 946, and 92524; Unclassified.

16. "The Effects of Nuclear Weapons"; Samuel Glasstone, Editor; U.S. Department of Defense; Published by the US Atomic Energy Commission, June 1957; Unclassified.

17. L.T. Dolphin, R.B. Dyce, and R.E. Winkelman; "Effects of Very-High-Altitude Bursts on Radio-Wave Reflection and Attenuation"; Project 6.11, Operation Hardtack, ITR-1645, October 1958; Stanford Research Institute, Menlo Park, California; Secret Restricted Data.

18. "Technical Summary of Military Effects Programs 1-9"; Operation Hardtack Preliminary Report, ITR-1660, September 1959; Deputy Chief of Staff, Weapons Effects Tests, Field Command, AFSWP, Sandia Base, Albuquerque, New Mexico; Secret Restricted Data.

19. "Capabilities of Atomic Weapons"; TM 23-200, Revised Edition, November 1957; Armed Forces Special Weapons Project, Washington, D.C.; Confidential.

20. "Effectiveness of Fast Scan Radar for Fireball Studies and Weapons Tracking"; Project 6.13, Operation Upshot-Knothole, WT-761, June 1955; U.S. Naval Electronics Laboratory, San Diego 52, California; Secret.

Appendix
MINIMUM DETECTABLE TARGET AREA

The effective area of the target which gives the minimum detectable signal for a particular radar set at a given range may be determined by use of the radar equation. The minimum detectable signal is given by:

$$P_{min} = NkT\Delta\nu \qquad (A.1)$$

if receiver noise is the limiting factor. In Equation A.1:

N = receiver noise factor
k = Boltzmann's constant
T = absolute temperature
$\Delta\nu$ = receiver bandwidth.

The presence of a hot radiating noise source may require a considerably higher signal for detection. If the propagation path traverses an absorbing region, the power received back at the transmitter is given by:

$$P_r = \frac{GP_t}{4\pi R^2} \cdot \frac{\sigma}{4\pi R^2} \cdot A_r f^2 \cdot e^{-4\int\kappa(s)ds} \qquad (A.2)$$

In Equation A.2:

P_t = peak (pulse) power of the radar transmitter
G = antenna gain
σ = radar cross section of target
R = distance to target
A_r = receiving-antenna aperture
f = illumination factor (taken to be ≈ 0.6).

Since the same antenna is used on transmitting and receiving,

$$G = 4\pi A/\lambda^2$$

where $A = A_t = A_r$. Equation A.2 is written for optimum bandwidth of the receiver, hence, modulation loss is ignored. If one sets $P_r = P_{min}$, then one may determine the minimum target area which can be detected at a given range by a given radar set. From Equation A.2 one finds:

$$\sigma_{min} = \frac{4\pi R^4\lambda^2}{A^2 f^2} \cdot \frac{P_{min}}{P_t} \cdot e^{4\int\kappa(s)ds} \qquad (A.3)$$

The minimum detectable areas are easily determined from the last row of the table for the sets used in the series of tests reported here. For example, if one considers a range of 100 km, the marginally detectable targets have areas as follows:

AN/MPG-1 $\sigma_{min} = 2{,}380\ e^{4\int\kappa ds}\ m^2$
SCR-584 $\sigma_{min} = 2.05\ e^{4\int\kappa ds}\ m^2$
SRb $\sigma_{min} = 95.5\ e^{4\int\kappa ds}\ m^2$.

TABLE A.1 CHARACTERISTICS OF THE RADARS USED IN PROJECT 6.5

	AN/MPG-1	SCR-584	SRb
λ	3.3 cm	10.73 cm	146 cm
$\Delta\nu$	10 Mc	2 Mc	1.5 Mc
N	16	10	6.3
P_{min}	6.6×10^{-13}w	8.3×10^{-14}w	3.9×10^{-14}w
P_t	35 kw	210 kw	200 kw
A	1.73 m^2	2.8 m^2	3.9 m^2
$\frac{10^{18}\sigma_{min}}{R^4 e^{4\int\kappa ds}}$	238 m^{-2}	0.205 m^{-2}	9.55 m^{-2}

Pages 71 & 72 deleted